

the micro and nanotechnology center of  
Politecnico di Milano

# ANNUAL REPORT 2022

February 2023 - Copyright © Polifab, unless otherwise stated.

Frontpage picture: The “Cremlino” building (istituto G. Ronzoni), where Polifab is located.

The image is an AFM reading of a  $12 \times 16 \mu\text{m}^2$  area, patterned by the staff on a 40 nm PPA film on a silicon chip via thermal scanning probe lithography, creating a micro-grayscale version of the original picture.

Polifab - Politecnico di Milano  
Via Giuseppe Colombo, 81  
20133 Milano – Italy  
<https://www.polifab.polimi.it/>  
[infopolifab@polimi.it](mailto:infopolifab@polimi.it)



## Foreword

Polifab is the place where brilliant scientific ideas meet cutting-edge technologies. A definition borrowed from someone who knows well one of the top research labs of our university.

These are the words used by its Director a few years ago when Polifab entered the 2.0 phase with the expansion of the clean room, at the very core of its activities. When, together with STMicroelectronics, Politecnico di Milano gave birth to a leading center for studies and applications on advanced materials and MEMS.

The history of Polifab has deep roots firmly planted in the ground. Since July 3, 2015, the date of its opening alongside Pirelli, for almost a decade this "21st century workshop" has represented the contact point between advanced research and business as a central topic for the development of our country. As a key element for the growth of human capital and career advancement of young researchers. As an attractive value to increase investments, increase competitiveness and operate in an international perspective.

This description fits perfectly into the overall mission and vision of Politecnico di Milano: a university that is open and dynamic, that is based on long-term cooperation agreements with innovative companies, that looks to the future. In fact, our goal is to further focus on joint initiatives, on recruiting talent programs, on increasing spaces and modern equipment that let us compete with the best European research institutes.

Polifab's first Annual Report matches the goals for the upcoming years, which are increasingly aimed at converging and multidisciplinary research areas, such as those represented by electronics and digital, micro and nano technologies, photonics and materials science. An essential step for a technical university that intends to anticipate change.

Prof. Donatella Sciuto  
Rector of Politecnico di Milano





# Table of contents

- Introduction..... i
- Polifab at a Glance..... ii
- Mission & Vision..... iii
- Polifab timeline..... iv
- Organization..... vi
- Polifab Staff..... vii
- Cleanroom equipment..... viii
- Polifab cleanroom map..... ix
- Access and training..... x
- JRC with STMicroelectronics..... xii
- Polifab's national and international position..... xiii
- Users contributions..... 1-56
- Publications citing Polifab..... 57
- Patents..... 60



## Users Contributions

B. J. Green et al., "PillarX: A Microfluidic Device to Profile Circulating Tumor Cell Clusters Based on Geometry, Deformability and Epithelial State".....	1
P. Piedimonte et al., Differential Impedance Sensing platform for high selectivity antibody detection down to few counts: a case study on Dengue Virus.....	3
C. Viola et al., "MEMNONE - Micro Electro Mechanical System Nonlinearities Exploitation for Filtering and Sensing Applications".....	5
G. Barbalace et al., "Innovative D.O.D. printing for high-conductivity micrometric inductor manufacturing".....	7
S. Cuccurullo et al., "Integration of magnetic materials on MEMS and power devices".....	9
F. Telesca et al., "From front-side to back-side illumination of InGaAs/InP SPADs for photon detection efficiency enhancement".....	11
L. Nessi et al., "Epitaxial chalcogenides for non-volatile, spin-based and ultralow power computing".....	13
A. Cordiale et al., "Intestinal epithelium on chip for absorption studies".....	15
C. Palma et al., "A compartmentalized microfluidic device to model the proprioceptive".....	17
E. Ferrari et al., "LivHeart: a platform for liver and heart compartmentalized culture".....	19
E. Ferrari et al., "3D Liver-on-Chip with a perfusable physiologic-like vascular channel".....	21
R. Visone et al., "Predicting human cardiac QT alterations and pro-arrhythmic effects of compounds with a 3D beating heart-on-chip platform".....	23
E. Bianchi et al., "3D PDMS micropatterned substrates to observe the cellular response to substrate stiffness".....	25

E. Bianchi et al., "PDMS Microstructures For Capillarity-Driven Filling In Open Microfluidic – Matrigel® and 3D cell cultures".....	27
A. Kyndiah et al., "Organic Biosensors".....	29
A. Luzio et al., "Patterning of microelectrodes for organic field-effect transistors".....	31
C. De Vita et al., "Integrated in-line visible light detector on Silicon nitride".....	33
C. De Vita et al., "Antireflection coating in LWIR for TMOS performance improvement".....	35
S. Ricci et al., "Development of crosspoint memory arrays for neuromorphic computing".....	37
M. Farronato et al., "Memtransistor devices based on MoS2 for memory and neuromorphic applications".....	39
C. Barri et al., "SPOON – Silicon hyperuniform microfluidic channels".....	41
G. Tavani et al., "Fabrication and optical characterization of erbium-doped SOI nanodiode for few photon emission at telecom wavelength" .....	43
R. Giani et al., "Impact of substrate doping on the performance of vertically illuminated Ge-on-Si photodetectors".....	45
J. Frigerio et al., "SiGe waveguides for mid-infrared nonlinear photonics".....	47
M. Gardina et al., "Thermal phase shifters for femtosecond-laser-written universal photonic processors".....	49
M. Almeida De Oliveira et al., "Flat optics for light engineering".....	51
G. G. Gentili et al., "Characterization of ferroelectric and state-change tunable materials for mm-wave applications".....	53
D. Girardi et al., "Research Activity of PhyND group".....	55



# Introduction

It is a great pleasure and honor for me to present the first annual report of Polifab. I can hardly believe these words and the contents of the report. While preparing the annual report, I realized how much work has been done during this year and how much Polifab is an opportunity for a considerable number of groups at the Politecnico, research institutes and companies.

Polifab was originally conceived as a multidisciplinary center dedicated to both research and education, capable of acting as a catalyst and support for existing realities. A kind of melting pot where different knowledge comes together to create new knowledge. A technology center capable of mastering the emerging technologies and achieving international leadership. A moral commitment to our students and to Italy. Mastering these technologies means being at the forefront of managing the transition to a low-carbon, knowledge-based economy. They play an important role in the R&D, innovation and cluster strategies of research groups and industries and are considered crucial to ensure competitiveness in an international scenario.

I am proud to be the director of an infrastructure that has turned these ambitions into reality.

The thoughts go back to the early days of Polifab and to the visionary directors of the Department of Electronics and Information, Prof. Gianantonio Magnani, and of the Department of Physics, Prof. Rinaldo Cubeddu. Without their contribution, together with that of the entire Rectorate, the realization of such a dream would have been impossible.

Special mention goes to STMicroelectronics for financial and visionary support, bridging the gap between basic academic research and microsystems, adopting a "rapid technology transfer model" compatible with wafer-scale integration.

I hope this annual report can serve as an inspiring source for new projects and a sustainable and long-term scientific relationship.

I wish you all the best for a successful future and fruitful collaboration.

Prof. Andrea Melloni  
Polifab Director



# Polifab at a Glance

Polifab is one of the four major infrastructures of the Politecnico di Milano, the open access reference facility for micro- and nanofabrication. It was created to provide the highest technological standards for a wide range of applications, including micro- and nanoelectronics, photonics, spintronics, MEMS, biotechnologies, advanced materials and nanotechnologies in general.

Since its creation in 2015, we have established clear access policies in terms of users and access costs, technical training on equipment and safety courses. In Polifab, Masters and PhD students, scientists and researchers, and even industrial personnel can enter and work, supported by staff who can also work on a service model. Our unique user access model makes it possible to attract talented researchers and students, satisfy their passion for technology and science and contribute to forge a class of young researchers that will boost micro and nanotechnologies in the territory.

In Polifab, almost 25 research groups working in different fields are conducting research on forty fundamental, EU and industrial research projects, and Principal Investigators of 5 ERC grants are generating world-leading research with their groups in an international environment. It is worth mentioning that the accountability of access costs for research groups is accepted by the European Commission in Horizon Europe and ERC programs.

This year, more than 35 publications, including Nature Materials, Nature Photonics, Small and Scientific Reports Journals and 4 patents, have acknowledged Polifab, demonstrating that Polifab is an enabling factor for both basic research and industrial collaboration.

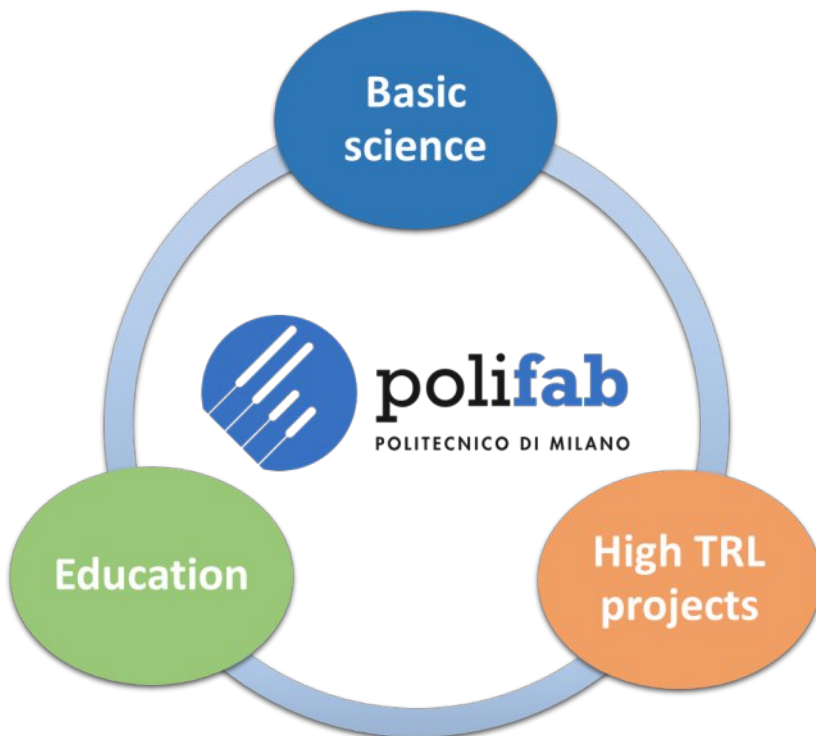
The community of Polifab users grows in synergy and contributes to enrich the portfolio of materials and processes available. The list of available equipment, continuously improved and enriched, is detailed in our website and ranges from lithography to thin film deposition, from metrology to back-end, able to operate from small samples to 8" wafers, with processes often compatible with industrial requirements.

Polifab is becoming the reference facility for micro-nanofabrication in the Lombardy region, with a growing user community and increasing interest from high-tech industries such as STMicroelectronics, Technoprobe, Huawei, AFR, Luxottica, etc.

## Mission & Vision

*The main mission of Polifab is to provide technology infrastructure, high-tech tools and know-how to support research from proof-of-concept in materials science and devices to rapid prototyping for industrial applications.*

*We envision Polifab as an aggregation center for scientists from universities, research centers and industries, promoting world-leading interdisciplinary research and education, as well as the development and transfer of key enabling technologies.*



# Polifab Timeline

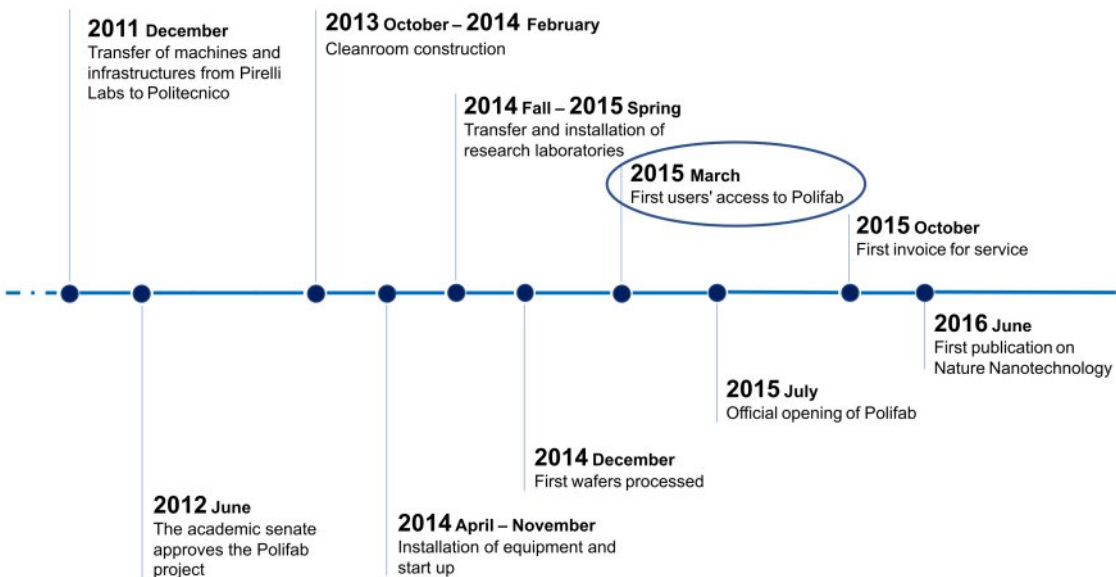
## Prof. Andrea L. Lacaita

*Polifab Director 2013-2018*



Over the past decade, sensors and microsystems have begun to spread in objects and everywhere, making the world "smarter" and more "interactive" with people. This trend is accelerating, and these devices are profoundly changing our lives and opening a wide range of new applications. Nanoscale manufacturing technologies are key drivers of these advances, and the use of nanotechnologies and microsystems will be increasingly important for future engineers. In this perspective, Polifab has been established to (i) provide researchers and students with access to micro- and nanoscale prototyping tools; (ii) create a multidisciplinary environment that promotes "knowledge convergence" from different engineering fields on microsystems; (iii) support, with a sound technological platform, advanced collaborative research programs with industrial partners and research centers.

It has been very exciting to contribute to the birth of Polifab. It is equally gratifying to see today how the community of researchers around this center has progressively grown together with the involvement of major industrial partners. I look forward to achieving more great things together.



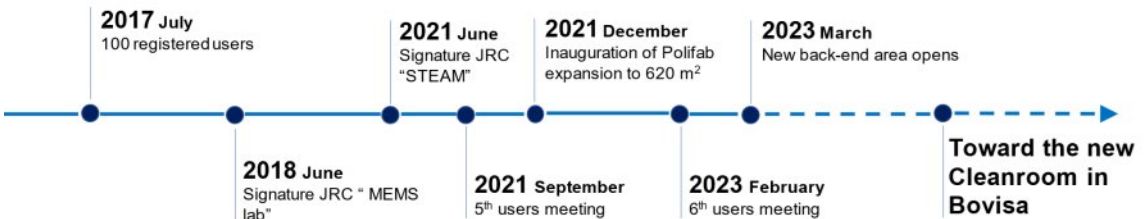
## Prof. Riccardo Bertacco

*Polifab Director 2019-2021*



When I entered the Pirelli Labs for the first time, I had the feeling that, in one way or another, I would have to deal with those machines that were then abandoned. It was then that I realized that this was a unique opportunity to provide the Politecnico di Milano with an infrastructure for micro- and nanofabrication. And so it was. We put passion and commitment into it, overcoming obstacles and epic moments in the infrastructure construction phase, with a limited budget, "recycled" machines, and in a historic building in Milan. But the results were not long in coming, and I think they are well represented in this publication. In my mandate as director, I have tried to define a development perspective that will be realized in the Parco dei Gasometri in Bovisa, where Polifab will take on a dimension that meets the needs of our users and will constitute the aggregation center of a scientific-technological pole of national importance.

I wish the new director and the staff, who are now realizing this perspective, every success in their work.



# Organization



## **Director**

Prof. Andrea Melloni  
*Department of Electronics,  
Information and  
Bioengineering*



## **Deputy Director**

Prof. Giovanni Isella  
*Department of Physics*

## **Scientific Committee**



Prof. Marco Bocciolone  
*Director of the  
Department of  
Mechanical Engineering*



Prof. Luca Magagnin  
*Department of  
Chemistry, Materials and  
Chemical Engineering*



Prof. Stefano Mariani  
*Department of Civil  
and Environmental  
Engineering*

Dr. Laura Castoldi  
*External Member  
(ST Microelectronics)*



Prof. Giorgio Rossi  
*External Member  
(IOM-CNR, UniMi)*



Dr. Claudio Somaschini  
*Cleanroom Manager*



Dr. Andrea Scaccabarozzi  
*Technologist*



Chiara Nava  
*Process Engineer*



Stefano Fasoli  
*Technician*



Dr. Marco Asa  
*Technologist*



Dr. Elisa Sogne  
*Process Engineer*



Stefano Bigoni  
*Backend processist*



Gianluca Cannetti  
*Process Engineer*

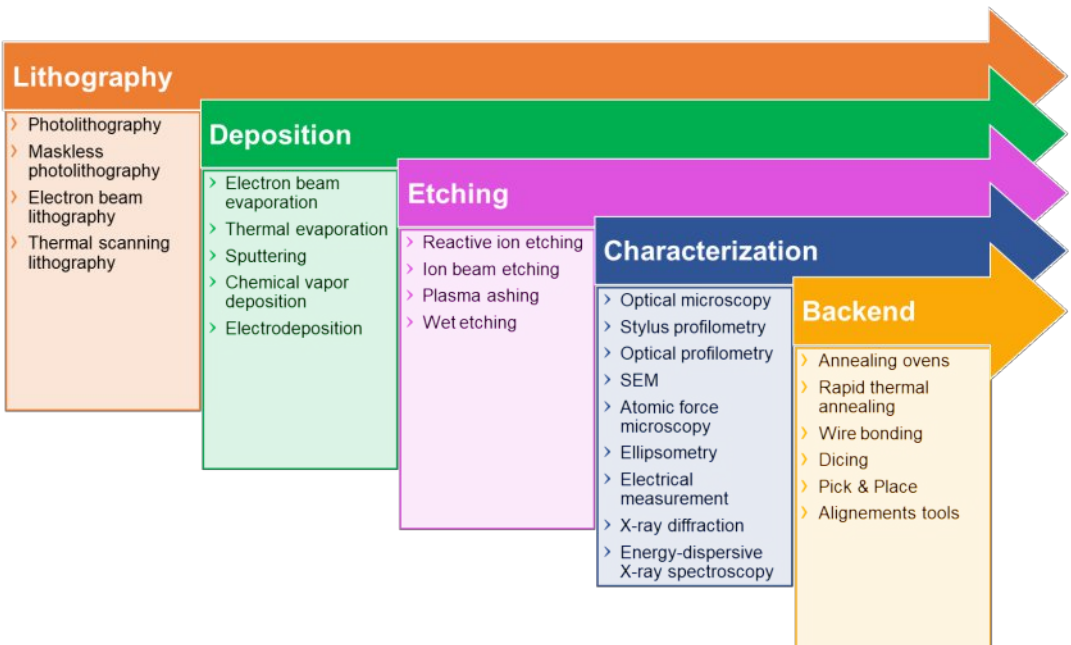


# Cleanroom Equipment

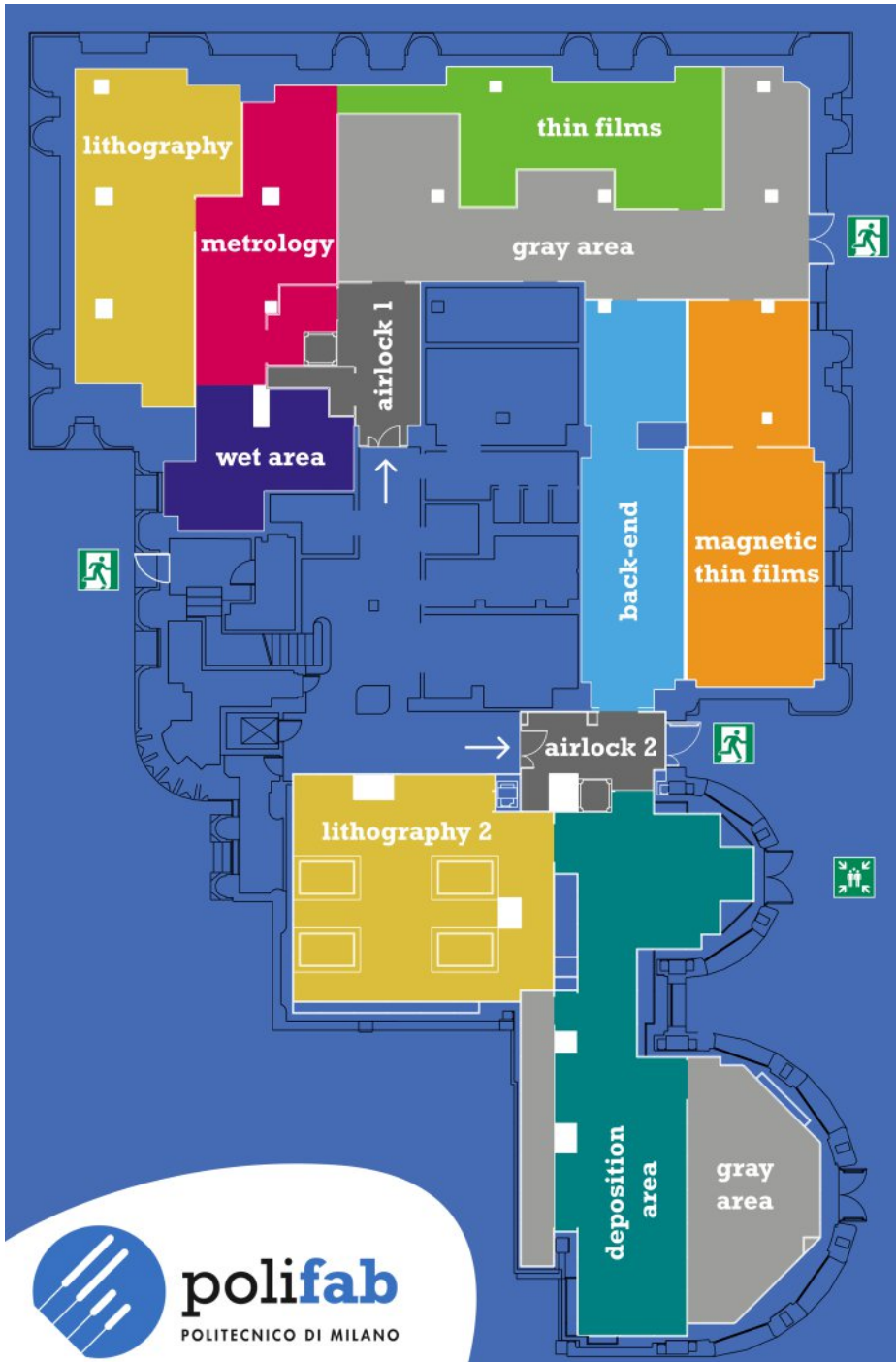
Polifab is based on a 620 m<sup>2</sup> cleanroom (330 m<sup>2</sup> ISO06 and 290 m<sup>2</sup> ISO08) plus annexed laboratories for materials and device characterisation.

The core of Polifab is a pilot line for micro- and nano-fabrication capable of processing different formats from small samples to 200 mm wafers. It includes facilities for lithography (mask aligner, laser writer, e-beam lithography, thermal scanning probe lithography), thin films deposition (e-beam and thermal evaporation, PECVD, sputtering, electroplating, MBE and PLD), direct printing (ink aerosol jet printer), etching (wet, RIE, IBE), metrology (stylus and optical profilometer, SEM+EDX, AFM, probe station, spectroscopic ellipsometry, XRD) and back-end (thermal treatments, dicing saw, ball bonder, automatic alignment, packaging machines).

More information on our facility and equipment can be found on our website: <https://www.polifab.polimi.it/equipments>



# Polifab cleanroom map



# Access and training

Claudio Somaschini has been Polifab's Cleanroom Manager since the very beginning. With a Ph.D. in Materials Science and a background in semiconductor epitaxy, Claudio has been at Polifab since 2014 and focuses his work both on the infrastructure and on staff management and administration.

## ***Claudio, Polifab is an open access infrastructure, what does that mean?***

In the world of semiconductor technology, a manufacturer that produces chips for third parties is called a "foundry" or "fab". These facilities do not allow the customer to operate the tools, and we could define them as closed. The case of Polifab is very different: we are a university infrastructure, and one of our main goals is to create a community of users with hands-on experience with the technologies. We have a quite unique access policy: any student, graduate student, and researcher can access the fab, get proper training from the staff, and then become independent in the development of their projects.

## ***But advanced technologies are complicated, how difficult and how long is it for a student to learn how to work in Polifab?***

The first step is, of course, a safety course on the general risks associated with working in our cleanroom. In order to carry out our processes, we often have to deal with dangerous chemicals, gases, lasers, high voltages, etc. We have to make sure that even an inexperienced student remains safe during his first access to the cleanroom. After that, specific training is required for each tool, and then it takes some time to become independent on a fabrication run, which usually consists of several processes. It usually takes three to six months to learn how to work in a cleanroom, a time that is fully compatible with a Ph.D. or thesis.

## ***Can students enter in Polifab also during the thesis period? And the companies?***

Of course, they do! That's part of our mission as an open access infrastructure. We organize specific lab experiences and support master courses. Students get a clear understanding of how to work in a cleanroom and which technologies are available. In terms of companies, direct access is also possible in their case, but in our experience, they most often outsource the work to the staff, as in the foundry model.

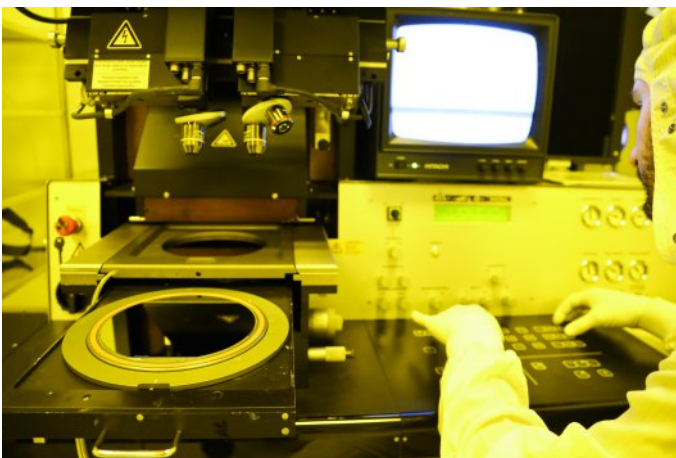
### ***Who are the typical users of Polifab?***

As an infrastructure of the Politecnico di Milano, our typical users are academic researchers. However, over the years we have clearly seen a growing interest from private institutions for different purposes, from simple characterization to complex development of novel devices. We work with many start-ups and small companies, as it is convenient for them to test new ideas in an external laboratory, but large industries have also shown great interest in the infrastructure. Successful technology transfer is not uncommon in our collaborations.

### ***The plan for the future is to grow even more. Polifab seems to be strategic for the technologies in PoliMi & Milano.***

When we started about ten years ago, I thought we would focus mainly on students and research groups because industry seemed so far away in Italy. But that was absolutely wrong! The truth is that the area around Milan is rich in different realities and an infrastructure like Polifab opens up different possibilities for many of them and of course for us.

*Thank you Claudio and good luck for the future!*



# JRC with STMicroelectronics



life.augmented

Polifab represents a unique opportunity for STMicroelectronics, it is the place where new disrupting R&D initiatives can quickly find their materialization into real prototypes. This approach has been conceived few years ago to speed-up both fundamental academic research and its potential technology transfer at an industrial level and it is turning day after day into an Italian excellence in the field of semiconductor technologies.

The year 2022 has represented another fruitful key step along the evolution and the growth of the overall PoliFab initiative. The realization of the cleanroom expansion and the installation of new process and characterization equipment has enabled the push of many running research projects in the fields of Micro Electro-Mechanical Systems (MEMS).

The tight cooperation that has been established between the R&D MEMS team located in Agrate and Polifab staff is driving day after day the strengthening of an excellent partnership on advanced materials and technologies for MEMS. Nowadays the topics of interests are various and span from design and manufacturing of innovative devices, advanced additive manufacturing, photonics, micro and nanoelectronics, biotechnologies, advanced materials, and nanotechnology.

ST believes that this collaboration can have a disruptive contribution in paving the way for a leadership in advanced research in multiple innovative MEMS sensors and actuators applications. The successful collaboration with Politecnico is part of a global innovation strategy that has also the target to foster high-quality fresh talents and facilitate the transfer of highly skilled personnel from academia straight into high tech industry.

Dr. Laura Castoldi  
STMicroelectronics

## Polifab's national and international position

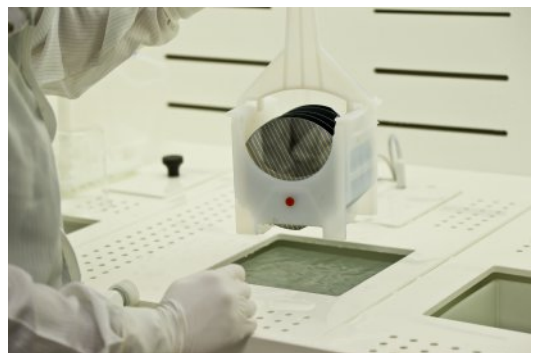
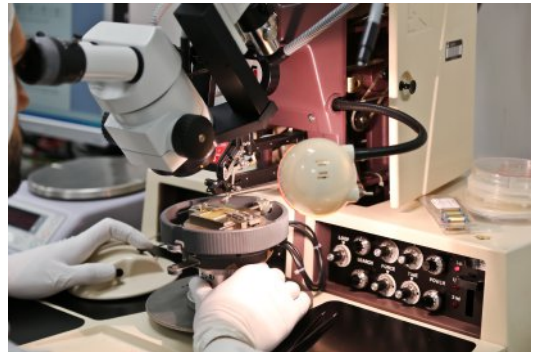
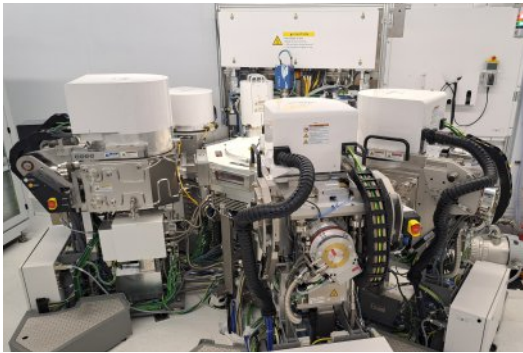
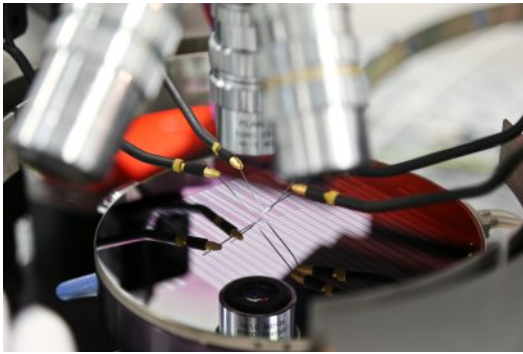
Even during the construction of Polifab, when we were still immersed in the typical start-up problems, it was clear to us that the development of the infrastructure could not proceed without its correct placement in the networks of national and international research infrastructures.

Therefore, in 2017, two years after the inauguration, we started a dialog with other Italian cleanrooms for the creation of a national network.

In 2018, It-FAB, the Italian Network for Micro- and Nanofabrication, was officially born; its founding members were CNR, Politecnico di Milano, and Bruno Kessler Foundation. It-Fab was initially set up as the Italian node of a European initiative (Euronanolab) to establish a pan-European distributed research infrastructure in the field of nanofabrication under the ESFRI program, with the aim of consolidating Europe's national nanofabrication centers, services and core resources into a single, coordinated nanofabrication research infrastructure at European level.

In 2021, Polifab joined the European network 'Nanoscience Foundries and Fine Analysis (NFFA) - Europe PILOT' - 'NEP' as a third-party, providing access to facilities and services to users. The collaboration with the NFFA has been consolidated in the last year with the participation of Polifab in a research infrastructure project (NFFA-DI) financed by the PNRR, which provides for a significant enhancement of Polifab's research capabilities in the field of innovative materials and the creation of a distributed infrastructure capable of offering users a wide portfolio of materials, processes, analysis and modeling techniques.

The challenge for the coming years will be to make these networks accessible and effective for users, as the complexity of research can only be addressed by sharing state-of-the-art instrumentation within efficient research infrastructures.



**Users  
contributions**

# PillarX: A Microfluidic Device to Profile Circulating Tumor Cell Clusters Based on Geometry, Deformability and Epithelial State

B. J. Green<sup>1\*</sup>, M. Marazzini<sup>1</sup>, B. Hershey<sup>1</sup>, A. Fardin<sup>2</sup>, Q. Li<sup>1</sup>, Z. Wang<sup>5</sup>, G. Giangreco<sup>2,7</sup>, F. Pisati<sup>1</sup>, S. Marchesi<sup>1</sup>, A. Disanza<sup>3</sup>, E. Frittoli<sup>1</sup>, E. Martini<sup>1</sup>, S. Magni<sup>1</sup>, G. V. Beznoussenko<sup>1</sup>, C. Vernieri<sup>1,3</sup>, R. Lobefaro<sup>1,3</sup>, D. Parazzoli<sup>1</sup>, P. Maiuri<sup>1</sup>, K. Havas<sup>1</sup>, M. Labib<sup>4</sup>, S. Sigismund<sup>2,6</sup>, P. P. Di Fiore<sup>2,6</sup>, R. H. Gunby<sup>2</sup>, S. O. Kelley<sup>4,5</sup>, G. Scita<sup>1,6</sup>

<sup>1</sup>FOM-FIRC Istituto Fondazione di Oncologia Molecolare, via Adamello 16, 20139 Milano, Italy.

<sup>2</sup>IEO, Istituto Europeo di Oncologia IRCCS, Via Giuseppe Ripamonti 435, 20141 Milano, Italy.

<sup>3</sup>Fondazione IRCCS Istituto Nazionale dei Tumori, Via Giacomo Venezian 1, 20133 Milano, Italy.

<sup>4</sup>Department of Chemistry, Northwestern University, Evanston, USA.

<sup>5</sup>University of Toronto, Toronto, Canada.

<sup>6</sup>Università degli Studi di Milano, Milano, Italy.

<sup>7</sup>The Francis Crick Institute, London, UK.

Metastasis begins with invasion of primary tumor cells into the surrounding tissues. Cells that successfully intravasate into the vasculature become circulating tumor cells (CTCs) that can exist either as single cells or as clusters.<sup>[1]</sup> Cancer cells belonging to the same cluster can be highly heterogeneous, however they typically express epithelial cell-cell adhesion proteins.

CTC clusters are usually small (2-50 cells) and rare in circulation but they possess up to 50-fold increased metastatic potential compared to individual CTCs.<sup>[2]</sup> Several groups have used different technologies to detect CTC clusters in patients with early and metastatic epithelial cancers.<sup>[3]</sup>

The continuous presence of elevated counts of CTC clusters in the blood of patients with metastatic breast and prostate cancer are shown to correlate with poor prognosis and shorter progression-free survival, relative to patients with fewer circulating clusters.<sup>[2]</sup> In the hostile environment of the blood vessels, clustering of cancer cells may protect against fluid shear stress, oxidative stress or immune attack. Clustering facilitates multiclonal interactions between cells displaying different epithelial-to-mesenchymal transition states, ultimately increasing their potential for colonization at biologically and mechanically diverse distant sites.<sup>[4]</sup>

Mechanical adaptability of tumor cells to various environmental conditions has been

linked to metastatic potential.<sup>[5]</sup> Clustering of cancer cells has been further implicated in mechanical protection against hostile hemodynamic forces.

The PillarX device is a bimodular microfluidic device (Pillar-device and an X-magnetic device, Figure 1) that is developed to profile single CTCs and clusters from whole blood based on their size, deformability and epithelial marker expression. Larger, less deformable clusters and large single cells are captured in the Pillar-device and sorted according to pillar gap sizes. Smaller, deformable clusters and single cells are subsequently captured in the X-device and separated based on epithelial marker expression using functionalized magnetic nanoparticles. Clusters of established and primary breast cancer cells with variable degrees of cohesion driven by different cell-cell adhesion protein expression are profiled in the device. Cohesive clusters exhibit a lower deformability as they travelled through the pillar array, relative to less cohesive clusters, and have greater collective invasive behavior. The ability of the PillarX device to capture clusters is validated in mouse models and patients of metastatic breast cancer (Figure 2). Thus, this device effectively enumerates and profiles CTC clusters based on their geometrical, physical and biochemical properties, and could form the basis of a novel prognostic clinical tool.

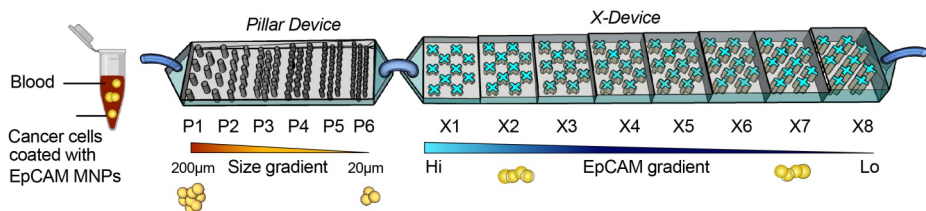
[1] C. Alix-Panabieres et al., *Clinical Chemistry*, 59(1), 110 (2013).

[2] N. Aceto et al., *Cell*, 158(5), 1110 (2014).

[3] S. L. Stott et al., *Proceedings of the National Academy of Sciences of the United States of America*, 107(43), 18392 (2010).

[4] K. J. Cheung et al., *Cell*, 155(7), 1639 (2013).

[5] V. Gensbittel et al., *Developmental cell*, 56(2), 164 (2021).



### Comsol Fluid Modeling

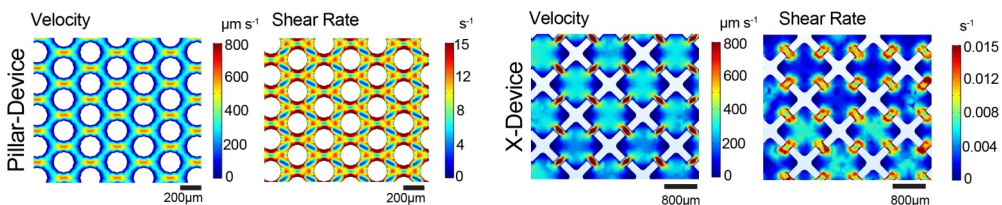


**Figure 1** Overview of the PillarX device and Comsol fluid modeling showing velocity and shear rate profiles between micro-pillars and X structures. Epithelial cell adhesion molecule (EpCAM) antibodies were conjugated to magnetic nanoparticles (MNPs).

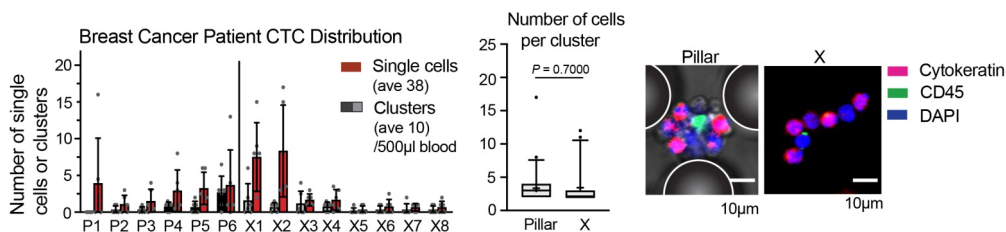


**Figure 2** PillarX profiles of breast cancer patient CTCs. Blood samples (500 mL) were incubated with EpCAM-MNPs before loading in the PillarX device at 750 mL/h. Mean CTC counts are determined by immuno-staining and quantification by applying a semi-automated counting method. Number of cells per cluster were determined using a semi-automated imaging approach. Representative immuno-staining images of patient CTCs in the Pillar- and X-device obtained by confocal microscopy (63X). CTCs were identified as cytokeratin+/DAPI+/CD45-, based on the epithelial phenotype of breast cancer cells. Human patient data are mean  $\pm$  s.d. of biological replicates ( $n = 6$ ). Dots represent experimental repeats. Data plotted as box and whiskers display 5-95 percentile, with + indicating the mean.  $p$ -values were calculated with an unpaired two-tailed Student's  $t$ -test.  $p < 0.05$  is considered significant.

# Differential Impedance Sensing platform for high selectivity antibody detection down to few counts: a case study on Dengue Virus

P. Piedimonte<sup>1</sup>, A. A. Maurina<sup>1</sup>, C. de Oliveira Figares<sup>1</sup>, F. Zanetto<sup>1</sup>, G. Ferrari<sup>1</sup> and M. Sampietro<sup>1</sup>  
L. Sola<sup>2</sup>, F. Damin<sup>2</sup>, M. Cretich<sup>2</sup>, M. Chiari<sup>2</sup>

<sup>1</sup>Dipartimento di Elettronica, Informazione e Bioingegneria, Politecnico di Milano, Via Ponzio 34/5, 20133 Milano, Italy.

<sup>2</sup>Istituto di Scienze e Tecnologie Chimiche SCITEC, CNR, Via Mario Bianco 9, 20131 Milano, Italy.

The technological facility of Polifab has been essential for the successful development of a new biosensing system for serological detection of viruses. The biosensor merges a sophisticated biochemistry recognition mechanism into an advanced miniaturized platform based on Differential Impedance Sensing (DIS). The system indeed is based on measuring the impedance variation between interdigitated microelectrodes upon the capture of the target antibodies on the surface of an insulating borosilicate chip, hybridized with nanobeads for signal amplification.

The interdigitated gold microelectrodes have fingers of 3  $\mu\text{m}$  width, 90  $\mu\text{m}$  length, and 3  $\mu\text{m}$  spacing. Dimensions were optimized using numerical simulations (COMSOL Multiphysics) of the impedance response to a bead of 800 nm. The overall area of the microelectrodes is 90x90  $\mu\text{m}^2$  to match the minimum spotting size of the machine used to functionalize the chip surface, resulting in a dynamic range of about 1 part over  $1.3 \times 10^4$  given by the full coverage of the sensing area by a layer of beads. The sensors were fabricated on a 3-inch borosilicate wafer (MicroChemicals GmbH) using conventional microfabrication techniques and lithography process.

The impedance measurement in DIS is actually performed as the impedance difference between an active sensor, where the probes are present, and a reference sensor, identical but with no probes and placed in close vicinity to the previous. This setting ensures to be insensitive to temperature fluctuations and to variation of the liquid medium of the assay in terms both of its salinity and its molecular composition that would alter both sensors

in the same way, thus allowing high stability of DIS results over time and sensitivity. The electrodes for DIS are not active/reactive as required in ES and therefore do not call for special elemental compositions as Ag/AgCl or carbon used in recent reports

The platform therefore has proven to reach nanoparticle resolution of few tens, and therefore antibody resolution of few tens.

To this aim the biosensor was functionalized with a copoly layer housing a synthetic peptide designed and synthesized to mimic the antigenic determinant of Dengue full envelope protein forming the outermost layer of the virion particle. It has been chemo-selectively grafted over the biosensor surface to target anti-Dengue Virus antibodies. The immunodiagnostic performance of the peptide in discriminating Dengue infected individuals from healthy controls is comparable with that of the full protein E with advantages in terms of preparation, manipulation, and cost. A limit of detection (LOD) below 100 pg/ml has been demonstrated, yet with the system operating in a real clinical setting using human serum samples from Dengue positive individuals.

The system is perfectly suited to be easily reconfigured for including novel probes by simply modifying the preparation of the biosensor chip, thus addressing a wide range of pathogens and diseases with clinically relevant concentrations for rapid immunoassays in a point of care setting.

[1] P. Piedimonte et al, *Biosensors and Bioelectronics*, Vol.202, 113996, ISSN 0956-5663 (2022).

[2] P. Borgia et al., *Sensors*, 22(9), 3292 (2022).

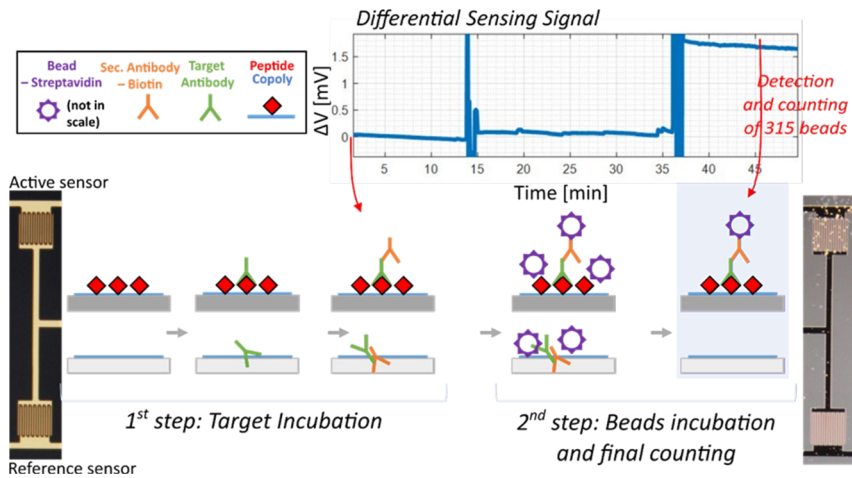


**Figure 1** Scheme of the protocol of the assay, subdivided into an Incubation phase followed by beads counting phase. On the top right the Differential Sensing Signal as obtained after the lock-in. On both lower sides, pictures of the biosensors before and after the full protocol. On the right the active sensor with the bound polystyrene beads as compared to the clean reference sensor.

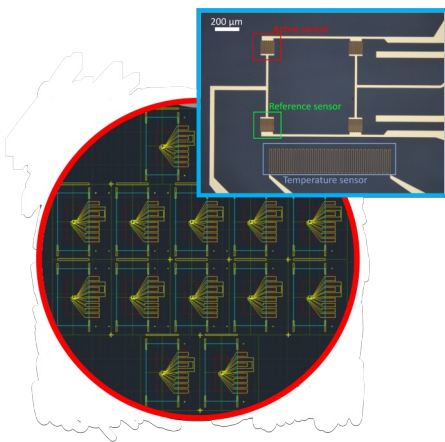


**Figure 2** Borosilicate wafer with 14 sensor chips whose close-up is in the inlet.

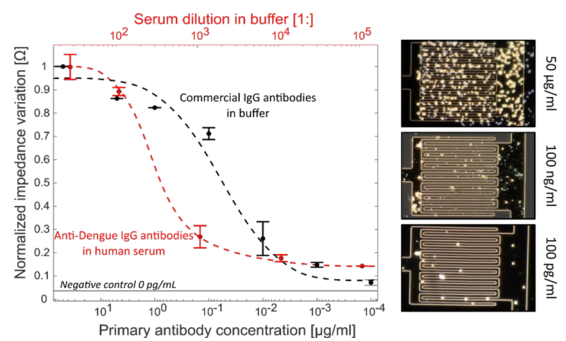


**Figure 3** Differential Impedance amplitude variation vs. dilution in a buffer of human serum positive to anti-DENGUE antibody. On the right, microphotographs of active sensors after the final wash for four exemplary cases.

# MEMNONE - Micro Electro Mechanical System

## Nonlinearities Exploitation for Filtering and Sensing Applications

*C. Viola, M. Furlan, F. Maspero, G. Gobat, V. Zega*

Dipartimento di Ingegneria Civile e Ambientale (DICA), Politecnico di Milano, Piazza Leonardo da Vinci 32, 20133 Milano, Italy.

Nonlinear phenomena in MEMS devices have been largely investigated, nevertheless exploiting nonlinearities for practical applications is still a major challenge. Within this setting, we leverage innovative Model Order Reduction (MOR) techniques we developed to design and optimize MEMS structures to operate in a fully nonlinear regime. The outcome of this project is to design and model an innovative class of resonators that exploits nonlinear phenomena for enhanced performance.

During the last year, the MEMNONE group designed and tested MEMS design able to display a nonlinearity content predicted by design. To achieve this goal, our group started with simple structures (Figure 1). Furthermore, during the design we accounted for the fabrication uncertainties e.g., overetch by producing different versions of the same design able to compensate for these effects. We designed five kinds of structures: a cantilever (Figure 1a)), a rigid mass actuated with combs or parallel plates (Figure 1b)), two types of arch resonators susceptible to 1:2 internal resonance (Figure 1c-d)) and clamped beam susceptible to 1:3 internal resonance (Figure 1e)). The latter designs aim to exploit nonlinear modal coupling for filtering purposes. All these structures have been fabricated using dry etching (Figure 2a)) and examined by looking for defects and fabrication faults using the Scanning Electron Microscope (SEM) (Figure 2b)). From our experiences, a good quality of the fabrication process has been observed, see (Figure 2c)). As a result, we were able to test two different nonlinear designs, a cantilever, and a double arch resonator using the vacuum chamber in (Figure 2d)).

Starting from estimates of the actual values of the overetch and the material properties,

we built nonlinear reduced-order models able to predict the system behaviour. In particular, the cantilever structure from a mechanical standpoint is a hardening structure. Nevertheless, due to its compliance and the electrostatic contributions, the overall behaviour is softening with strong frequency shifts, as measured experimentally (Figure 2e)). Our reduced order models can capture these behaviours in a non-intrusive way. On the other hand, the arch resonator is a stiff structure with a strong nonlinear softening behaviour induced by its curvature. Here the electrostatics contribution is limited and mainly induces shifts in the eigenfrequency. This behaviour is predicted by our models

In conclusion, the present work gives first promising results paving the way for more exciting and complex applications. Thanks to the modelling technique used by our group, the device's nonlinear behaviour can be predicted with high accuracy. Furthermore, the lean prototyping guaranteed by the PoliFAB process allows for testing fully functional MEMS designs within weeks. The MEMS fabrication process is robust i.e., fabrication uncertainties spread is limited, allowing for the exploitation of the previous knowledge in the new runs. Our group plans to design more complex MEMS e.g. Disk Resonating Gyroscopes and internally resonant MEMS for filtering purposes.

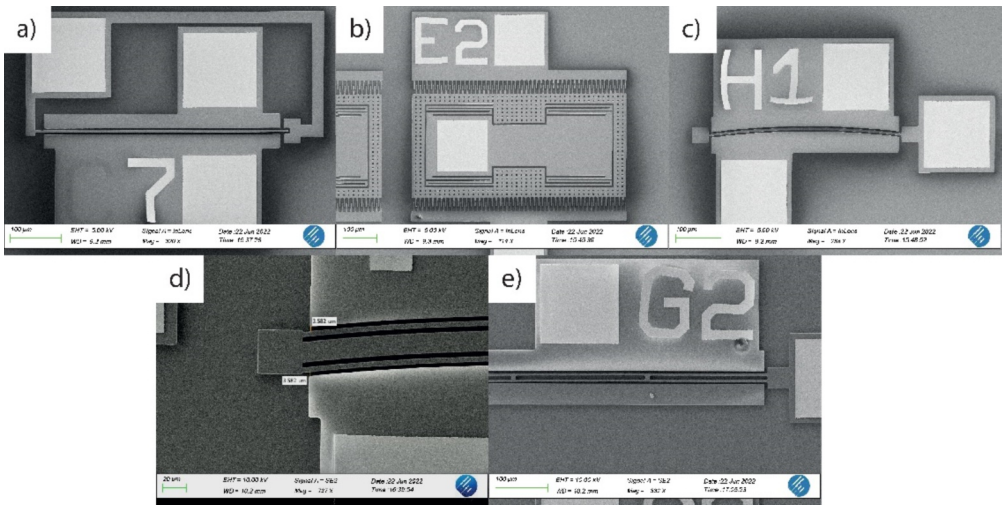


**Figure 1** Scheme MEMS design fabricated by the MEMNONE group. a) cantilever b) rigid mass with combs c) arch resonator d) double arch resonator e) doubly clamped tunable beam.

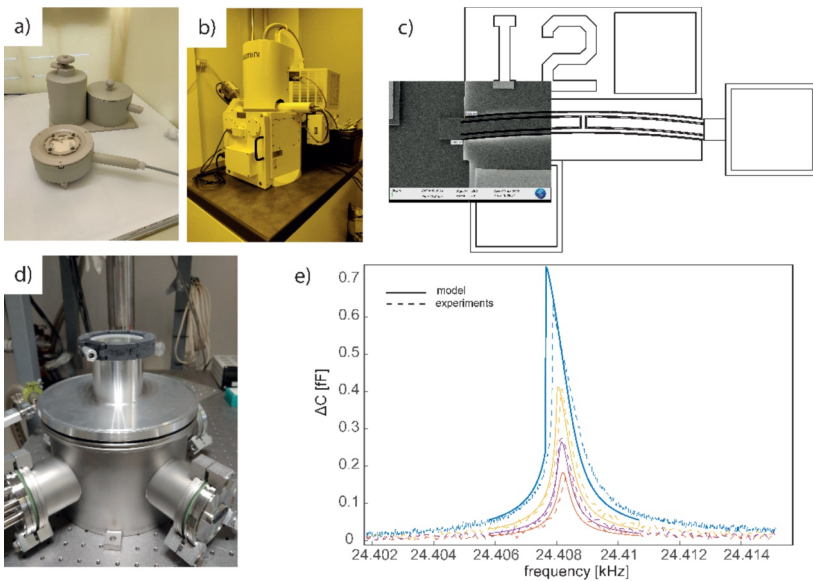


**Figure 2** Outline of the lean prototyping and testing. a) after the model-based design stage the devices are fabricated. Dry etching is here considered. b) After fabrication the devices are inspected through Scanning Electron Microscope (SEM) looking for defects and information related to the fabrication process e.g. overetch. c) the SEM images confirm the quality of the fabrication w.r.t. the original design d) the devices are tested in a vacuum chamber to enhance the nonlinear properties and response e) finally the experiments are compared with our predictive models.

# Innovative D.O.D. printing for high-conductivity micrometric inductor manufacturing

G. Barbalace<sup>1</sup>, D. Natali<sup>1</sup>, M. Salina<sup>2</sup>

<sup>1</sup>Dipartimento di Elettronica, Informazione e Bioingegneria, Politecnico di Milano, Via Ponzio 34/5, 20133 Milano, Italy.

<sup>2</sup>STMicronics, Via Camillo Olivetti 2, 20864 Agrate Brianza, Italy.

In the recent years additive manufacturing techniques are gaining a increasing interest in electronic components manufacturing<sup>[1]</sup>. Among these techniques inkjet printing is the most widespread and the simplest one, it is characterized by low costs and the highest accuracy in drops placement<sup>[2]</sup>. Ad-hoc designed inks are employed, according to their composition they can act as conductors, semiconductors and insulators<sup>[3]</sup>.

With Drop on Demand (D.O.D) printing the ejection of individual drops is controlled, with sizes and ejection frequency limited by the type of utilized cartridge. Usually D.O.D. printing is unsuitable for high-conductivity micrometric components manufacturing, because of more prominent impact of printing-related coalescence flaws in this size scale and of limited conductor thickness increase implemented with the usually available number of printed layers (up to 10).

With Ceraprinter F-serie printer, installed in Poifab in 2019, a innovative printing strategy was successfully implemented in order to manufacture high-conductivity micrometric inductors. This “all-in-one state-of-art” device integrates inkjet printing, aerosol printing, thermal control of chuck and cartridge, positioning of cartridge-chuck distance, video cameras for ejected drops and substrate, IR and UV lamps (Figure 1). A silver nano-particles commercial ink was printed with DMC-Samba cartridges thanks to piezoelectric D.O.D. inkjet, individual drops ejected with a customized voltage waveform had a diameter about 21  $\mu\text{m}$  (Figure 2).

Instead of typical filling strategy, in which

geometry to be printed is an area filled by a drops distribution set with an automatic algorithm and implemented with deposition along a single printing direction, a innovative strategy was implemented, in which geometry to be printed is a path joining points defined by the user and implemented with deposition along more printing directions thanks to synchronized movements of cartridge and substrate (Figure 3).

Thickness increase and printing-related width variabilities limitation were more effective by letting the previous layer left to dry at a fixed temperature before depositing the next layer. After printer parameters optimization, the deposition of new layers onto printings present on the substrate was implemented with micrometric precision, enabling to exceed the number of layers usually deposited in a individual printing session (up to 15). In order to make the printing conductive a annealing treatment was implemented in a oven heated with a maximum temperature of 250 °C.

Printed micrometric inductors had track-widths smaller than 100  $\mu\text{m}$ , thicknesses bigger than 1  $\mu\text{m}$  and a sheet resistance down to 40  $\text{m}\Omega/\square$  (Figure 4).

[1] Suganuma K., Brief of Electrical and Computer Engineering, Springer, Vol. 75 (2014).

[2] Z. Cui, Printed electronics: materials, technologies and applications, Wiley, pp. 1-19, 54-64, 106-111, 129-131, 143-136, 316-337 (2016).

[3] Lu. B et al., Engineering, 1(1), 85-89 (2015).

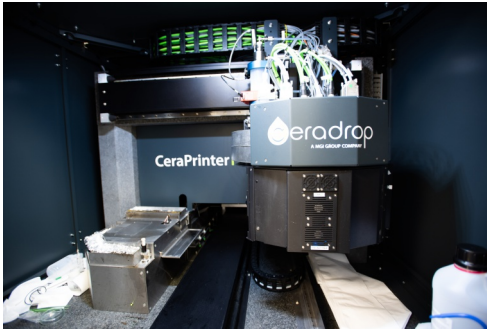


**Figure 1** CeraPrinter F-serie inkjet part.

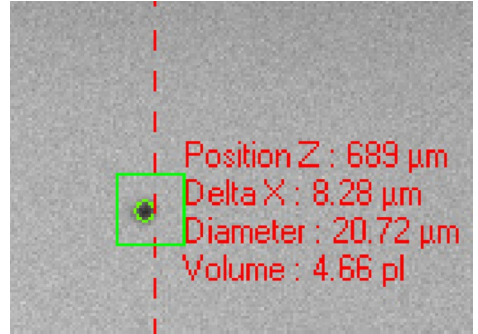


**Figure 2** Ejected drop by a single nozzle.

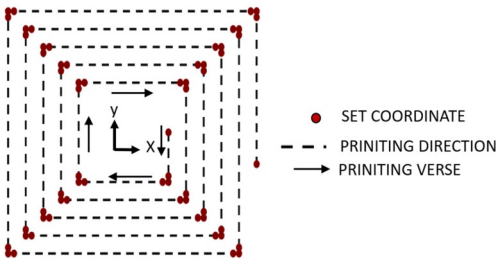


**Figure 3** Implemented printing strategy.

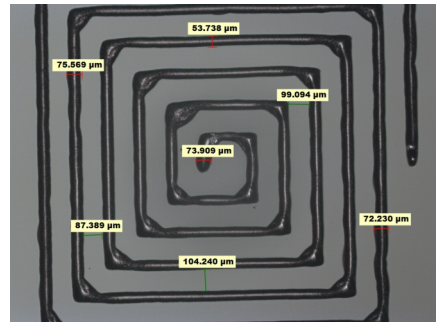


**Figure 4** Multi-layers micrometric spiral.

# Integration of magnetic materials on MEMS and power devices

S. Cuccurullo<sup>1</sup>, G. Pavese<sup>1</sup>, F. Marson<sup>1</sup>, A. Plaza<sup>1</sup>, O. Koplak<sup>1</sup>, J.M. De Ponti<sup>2</sup>, L. Iorio<sup>2</sup>, M. Rosso<sup>2</sup>, F.P. Perli<sup>2</sup>, F. Maspero<sup>2</sup>, R. Ardito<sup>2</sup>, R. Bertacco<sup>1</sup>

<sup>1</sup>Dipartimento di Fisica, Politecnico di Milano, Piazza Leonardo da Vinci, 32, 20133 Milano, Italy.

<sup>2</sup>Dipartimento di Ingegneria Civile e Ambientale (DICA), Politecnico di Milano, Piazza Leonardo da Vinci 32, 20133 Milano, Italy.

The integration of soft and hard magnetic materials can open new scenarios in several integrated technologies such as power devices and micro-electro-mechanical systems (MEMS). The current research activity on this topic at PoliFAB focuses on both these aspects, with the aim of integrating relatively thick magnetic layers (hundreds of nm) in a micro-electronic fabrication process.

New generation of power devices require integrated inductors able to carry high values of current and provide large inductance. Such devices would lead to a strong size reduction of the power supply thanks to the removal of discrete bulky inductors. Integration of magnetic layers on planar coils can lead to high performance inductors reaching this goal. For this reason, we have developed a process to integrate thick permalloy layers (up to 1 $\mu$ m) to planar coils in order to boost their inductance value (X10). Figure 1 reports a cross-section of the multilayer of Permalloy (Py)-Polyimide-Copper used in this process and a schematic representation of the fabricated devices. As can be seen in Figure 1b, these inductors have larger inductance with respect to the non-magnetic ones, however the value of inductance is current-dependent as the magnetic materials saturate for large currents. This type of phenomena was studied and modeled in a recently submitted work showing the impact of the non-linear magnetic behavior on the inductor performance<sup>[1]</sup>.

The second research activity regards the integration of magnetic layers with MEMS and the fabrication of new meta-MEMS devices for acoustic wave harvesting and permanent magnets can have different roles when coupled to micro-mechanical

systems. For instance, they can be used to sense magnetic fields or to harvest energy from the surroundings. Indeed, our activity on this topic has first focused on the fabrication of MEMS magnetometers integrating permanent magnets made of cobalt and magnetic flux concentrators made of Py<sup>[2]</sup>. Such MEMS magnetometers can sense the magnetic field through the change of their resonance frequency leading to a low-power magnetic sensor with potential integration with existing inertial MEMS sensors. Figure 2 reports a close-up view of suspended MEMS structure integrating magnetic materials. The second focus of magnetic MEMS developed at PoliFAB is to harvest vibrational energy. For this type of application large volumes of magnetic materials are necessary. For this reason, we have been working on the deposition of thick layers of permanent magnets such as SmCo-based magnets, which have large magnetic energy product (Figure 3). This magnetic film can be patterned and integrated into MEMS where they act as non-linear transducers of the external mechanical stimulus enhancing the vibration energy transfer from the surroundings to the harvesting element. This technique is known as frequency up-conversion and it is used to match the frequency of environmental vibrations to the one of the harvesting elements. Finally, to further enhance the transduction efficiency of the harvester, we have been developing meta-structures able to slow down and amplify acoustic waves such as the one reported in Figure 4. This concept was demonstrated at the macro-scale<sup>[3]</sup>, but it is now being studied also at the microscale.

[1] S. Cuccurullo et al., Applied Physics Letters (under review).

[2] F. Maspero et al., 2021 IEEE 34th International Conference on Micro Electro Mechanical Systems (MEMS), Gainesville, FL, USA (2021).

[3] J.M. De Ponti et al., EPJ Applied Metamaterials, 9, 6 (2022).

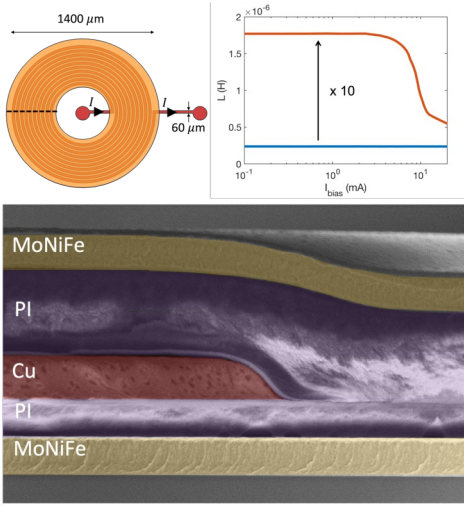


**Figure 1** a) Schematic image of the integrated inductor b) Inductance versus bias currents of the inductor c) SEM cross-section of the multi-layer process.

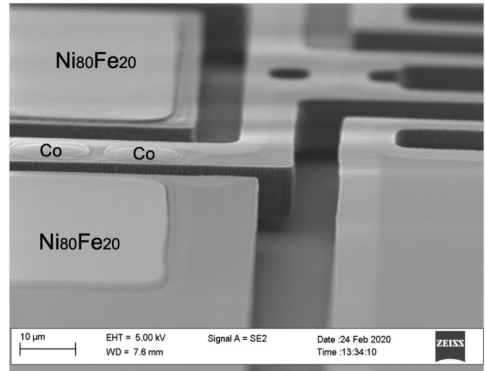


**Figure 2** SEM image of a suspended silicon element with cobalt magnets and permalloy magnetic flux concentrators [2].

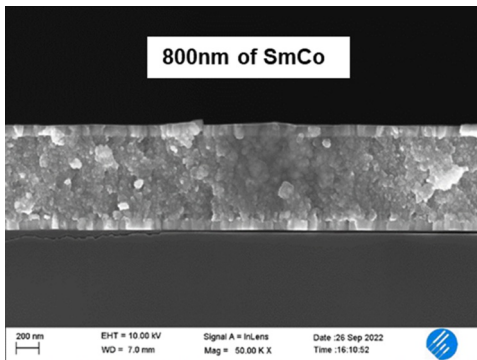


**Figure 3** Thick layer of SmCo on silicon. This compound can reach coercive fields larger than 1 Tesla.

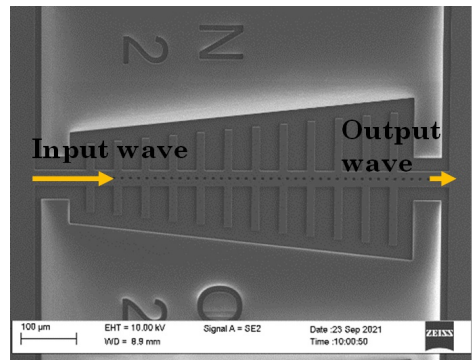


**Figure 4** MEMS meta-structure for acoustic waves filtering and harvesting. This structure can slow down and amplify elastic waves depending on their frequency.

# From front-side to back-side illumination of InGaAs/InP SPADs for photon detection efficiency enhancement

*F. Telesca, F. Signorelli, K. Herrera, A. Tosi*

Dipartimento di Elettronica, Informazione e Bioingegneria (DEIB), Politecnico di Milano, Via Ponzio 34/5, 20133 Milano, Italy.

Single-photon detection in the short-wavelength infrared range is an enabling technology for quantum optics applications (e.g., QKD – Quantum Key Distribution) as well as remote sensing techniques, such as LIDAR. Among the available detectors, InGaAs/InP Single-Photon Avalanche Diodes (SPADs) are often the best choice, since they can be operated with moderate cooling in compact and portable systems. For a thin InGaAs/InP SPAD, the photon detection efficiency (PDE) at 1550 nm is ~ 25%, with a dark count rate (DCR) of ~ 1 kcps. The PDE can be pushed towards 50% if the thickness of the absorber is doubled, but this comes at the expenses of a tenfold increase of DCR, due to the larger total volume. To overcome this trade-off, we envision converting our front-side illuminated (FSI) devices to backside-illuminated (BSI) detectors, so that the photons crossing the active area of the device may be reflected by the frontside metal contact and cross the absorption region a second time. In this way, the optical path is doubled without increasing the absorber thickness, thus leading to a PDE boost without compromising DCR. Moreover, this would also enable the 3D stacking of flipped InGaAs/InP SPADs over a CMOS readout circuit.

For the first prototype, we employed a 8x8 mm<sup>2</sup> chip, which includes different SPADs sharing the same cathode contact on the back-side, while the anodes are each independently contacted to metal pads. Among such SPADs, 20 devices were targeted to be converted to back-side illumination.

On the front-side, a 50 nm thick Al reflective layer was deposited on the active areas of the selected devices. To this aim, the whole chip was spin-coated with a ~1- $\mu$ m-thick layer of AZ 5214E photoresist

using the Sawatec SM-150 and was patterned with negative polarity using the Heidelberg MLA100 to expose the active areas. The metal was sputtered on the chip with the Moorfield MINILAB-080 thermal evaporator, and the excess material was removed by lift-off using acetone. Next, the chip surface was passivated by depositing a 200 nm thick layer of SiO<sub>2</sub> via CVD. This layer was then patterned using photolithography and subsequently wet etched (using BOE) to open vias on the selected anode contact pads. With a further photolithography step, the chip surface was prepared for a metal deposition aimed at creating 1- $\mu$ m-thick Cu bonding pads in correspondence of the selected SPAD anodes, with a diameter of 200  $\mu$ m. The final BSI chip will be bump-bonded to the test carrier board.

Regarding the back-side, the first step was to remove the common-cathode contact, which consists of a 500 nm thick Ti/Pt/Au multilayer. The chosen technique was ion milling, carried out using the Ion Beam Etching System – Kenosistec VS80. A Kapton mask was used for defining the etching region (the central part of the 8x8 mm<sup>2</sup> chip, i.e., where the chosen SPADs are housed). The final step was the deposition of a 250 nm SiO<sub>2</sub> anti-reflection coating using CVD.

All of the above-mentioned processes were successfully performed on two separate test chips. The front-side processing did not worsen the SPAD performance after mounting it on the PCB carrier. Instead, the effect of the back-side operations is not verified yet.

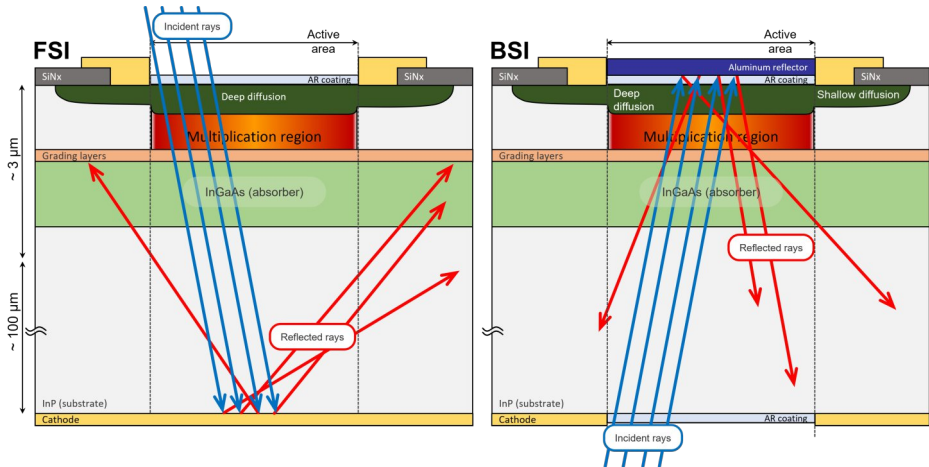


**Figure 1** Schematic representation of the conversion of a FSI InGaAs/InP SPAD into a BSI InGaAs/InP SPAD. The shorter optical path after reflection on the p-contact metallization increases the probability that the reflected photon would pass again through the absorption layer below the active area, rather than being scattered away.

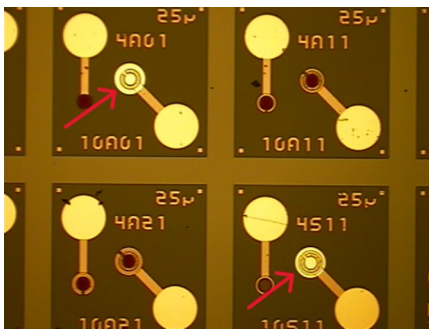


**Figure 2** Micrograph of the Al reflective layer deposited on the active areas of selected devices.

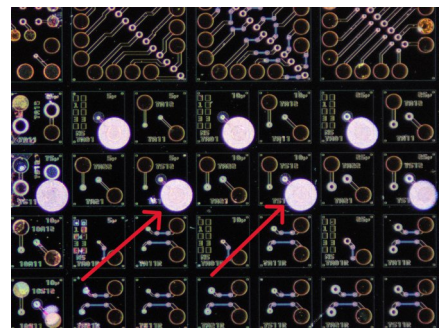


**Figure 3** Micrograph of the Cu bonding pads deposited in correspondence of selected devices.

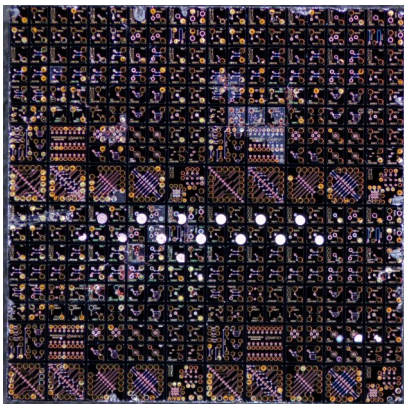


**Figure 4** Micrograph of the finished front-side of the 8x8 mm<sup>2</sup> chip.

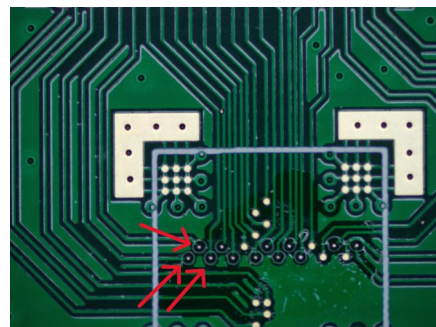


**Figure 5** Detail of the prototype PCB designed for readout. The Sn/Pb solder spheres are already deposited on the pads.

# Epitaxial chalcogenides for non-volatile, spin-based and ultralow power computing

L. Nessi, F. Fagiani, G. Gandini, M. Cantoni, R. Bertacco, C. Rinaldi

Dipartimento di Fisica, Politecnico di Milano, c/o via G. Colombo 81, Edificio 30, 20133 Milano, Italy.

Information and communication technology is going to use 20% of the yearly electricity production by 2030. This unsustainable trend requires architectures beyond the well-established complementary metal oxide semiconductor (CMOS) platform. In 2016, Intel proposed a conceptual architecture exploiting the spin of electrons that holds huge potential for ultra-low power electronics<sup>[1]</sup>, to minimize environmental impact while fulfilling consumer demand. The so-called Magneto-Electric Spin-Orbit (MESO) device comprises two distinct functional units (memory and read-out), each one requiring non-trivial interfaces and materials stacks. The complexity of the original concept is the reason why a prototype has not appeared yet, while the scientific community is struggling against material issues.

In this context, epitaxial films of chalcogenides belonging to the class of ferroelectric Rashba semiconductors (FERSC) have gained a growing attention. Those materials are characterized by a one-to-one relation between the direction of ferroelectric polarization and the spin-to-charge current conversion. As so, when a spin current is injected into such semiconductors by means of a ferromagnet, an “output” charge current proportional to the ferroelectric polarization is generated. A fully upward (downward) polarization state produces a positive (negative) current, thus allowing for non-volatile digital logic (Figure 1). Intermediate ferroelectric states would instead allow for analog and neuromorphic computing.

Our experimental work is mostly focused on germanium telluride (GeTe) and related compounds, with In or Sn doping, all robust ferroelectrics at room temperature and endowed by monolithic integrability on

silicon<sup>[2, 3]</sup>. We have recently shown that the ferroelectric polarization of epitaxial thin films of GeTe can be reliably switched back and forth by electrical gating and used to effectively control a sizeable spin-to-charge conversion by spin Hall effect<sup>[4]</sup>. GeTe thus allows for logic-in-memory devices, where the information is conveniently stored in the ferroelectric state and the read-out is provided by spin-to-charge conversion.

In Polifab, we can exploit a cluster tool operating in ultra-high vacuum (LASSE) for the growth of epitaxial thin films by molecular beam epitaxy. *In-situ* X-ray and ultraviolet photoemission spectroscopies enable the chemical analysis of the heterostructures with surface sensitivity, while electron diffraction provides insights about the crystallinity of the films (Figure 2) which is also studied *ex-situ* by X-ray diffraction. The ferroelectric properties are investigated by piezo-response force microscopy at the facility. By combining electron beam, thermally assisted scanning probe and optical lithography (Figure 3), we finally fabricated the target devices and nanostructures.

The research activity will continue investigating the figures of merit and the scaling laws of the proposed architecture (Figure 4), along a realistic pathway towards ultralow power electronics.

[1] S. Manipatruni et al., *Nature*, 565, 35 (2019).

[2] D. Di Sante et al., *Advanced Materials*, 25, 509 (2013).

[3] C. Rinaldi et al., *Nano Letters*, 18, 2751 (2018).

[4] S. Varotto et al., *Nature Electronics* 4, 740 (2021).

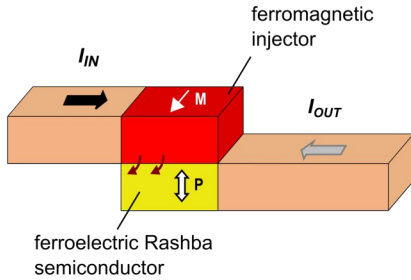


**Figure 1** Ferroelectric spin-orbit logic devices allow for the realization of transfer functions that are controlled by the ferroelectric polarization in a non-volatile way. Intel demonstrated that the approach holds potential for ultralow power electronics.

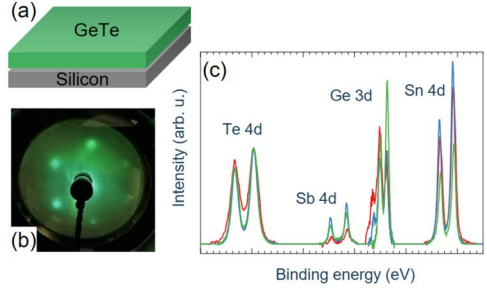


**Figure 2** Our cluster tool in ultra-high vacuum enables the growth of chalcogenides on top of silicon (a). It also allows for a complete structural (b) and chemical (c) characterization by electron diffraction (LEED, RHEED, XPD) and X-ray photoemission spectroscopy.

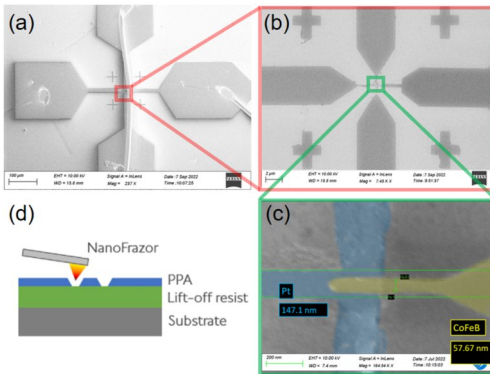


**Figure 3** Nanofabrication of spintronic devices is performed at Polifab using a combination of optical (a), e-beam (b) and thermally assisted scanning probe lithography (c). The NanoFrazor Explore was optimized to achieve below 60 nm resolution with a bilayer lift-off process (d).

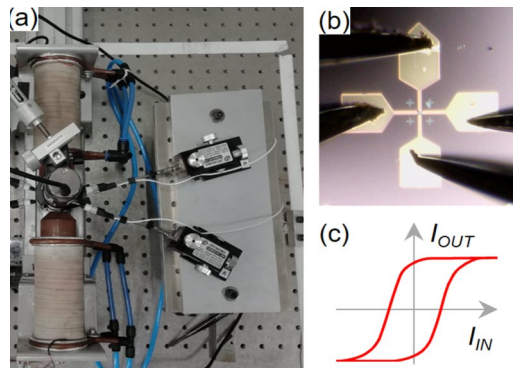


**Figure 4** (a) Experimental setup for transport measurements within a magnetic field. (b) Micrograph of a spin-orbit device under test, measured with four probes and within a uniform magnetic field. (c) Input-output characteristic of a ferroelectric spin-orbit device.

# Intestinal epithelium on chip for absorption studies

A. Cordiale<sup>1</sup>, M. Ballerini<sup>2</sup>, A. Pigazzini<sup>1</sup>, P. Occhetta<sup>1,3</sup>, M. Rasponi<sup>1</sup>

<sup>1</sup>Dipartimento di Elettronica, Informazione e Bioingegneria (DEIB), Politecnico di Milano, Via Ponzio 34/5, 20133 Milano, Italy.

<sup>2</sup>Dipartimento di Oncologia Sperimentale, Istituto Europeo di Oncologia - IRCCS, Via Ripamonti 435, 20141 Milano, Italy.

<sup>3</sup>BiomimX Srl, Via Giovanni Durando 38/A, 20158 Milano, Italy.

Discovery of new therapeutics is an expensive and risky process: success rate of candidate drugs is lower than 0.1% with severe waste of investments, in terms of money, time and human safety<sup>[1]</sup>.

In this scenario, the study of absorption, distribution, metabolism and excretion (ADME) is crucial, moreover the absorption efficiency of orally administered therapeutics occurring at the gastrointestinal tract (GUT) level is paramount for their success<sup>[2]</sup>.

Current methods used to assess GUT absorption lack in recapitulating 3D and dynamically active microenvironment of intestinal epithelium and Organ on chips (OoC) models have been lately proposed to overcome this limitation<sup>[3]</sup>.

We developed an *in-vitro* model of intestinal epithelial barrier in an OoC (uBeat® patented technology<sup>[4]</sup>) able to provide for mechanical stimulation mimicking the peristaltic motion.

The barrier was recapitulated by culturing CACO2 and HT29 cells mixed in a 9:1 ratio (8 10<sup>6</sup> cells/mL) adhered to a fibrin hydrogel matrix. 10% uniaxial strain stimulation at 0.2 Hz was exerted for 9 days to induce tissue maturation. In particular, the effects of impulse-wave stimulation and sine-wave stimulation were compared to the cells cultured in static conditions.

As readouts, brightfield and fluorescence microscopy analyses were performed in order to compare cell proliferation (Ki-67), epithelial integrity (ZO-1), and specific protein production (villin, mucin) among groups. Moreover, fluorescent dextran (4

kDa) diffusion studies were performed to assess the integrity of the epithelial barrier.

Brightfield microscopy images showed the presence of cells proliferating and self-assembling in 3D villi-like structures. The amount of such structure is higher in both stimulated groups while the static control mainly showed a 2D cells monolayer.

Mechanically stimulated tissues feature a higher ZO-1 level than static ones. Sine-wave stimulation is also responsible for an increase in villin-positive zones and larger areas hosting 3D-structures, with a statistical difference with respect to both other experimental conditions.

The on-chip epithelial barrier developed with sine-wave stimulation was shown to be impermeable to Dextran even after 1 hour of incubation, therefore proving the functionality of the *in-vitro* model.

The system has shown that the mechanical stimulation is a fundamental cue that guides cell behaviour: physiological-like stimulation leads to a massive generation of three-dimensional villi-like structures and improves the stability of the epithelium.

The developed gut-on-chip model represents a powerful tool for drug development that can provide for more accuracy and physiological relevance when it comes to ADME profiling.

[1] J. A. DiMasi et al., *Journal of Health Economics*, 47, 20-33 (2016).

[2] A. Fedi et al., *Journal of Controlled Release*, 335, 247-268 (2021).

[3] A. Bein et al., *Cellular and Molecular Gastroenterology and Hepatology*, 24, 5(4), 659-668 (2018).

[4] M. Rasponi, P. Occhetta and A. Redaelli, *A microfluidic device for controlled generation and/or culture and/or maturation of three-dimensional cells and/or tissue constructs*. (2015).

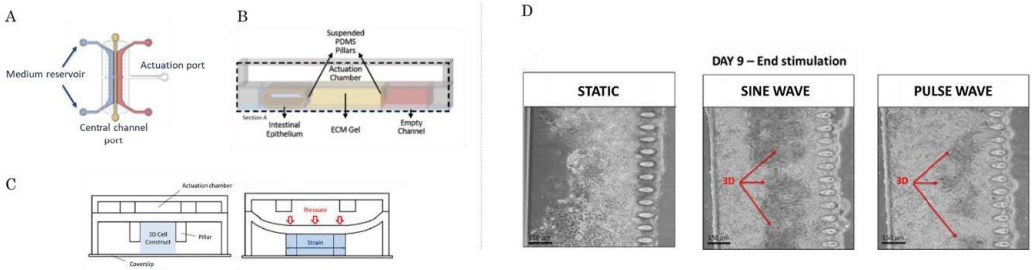


**Figure 1** Gut on chip model. (A) Top view of the chip showing the ports for medium change and cell seeding, and for ECM (fibrin hydrogel) injection. (B) cross-section of the device showing the biological experiments configuration. (C) Stimulation on the gut on chip through the pressurisation of the pneumatic chamber located on top of the cell culture compartment. (D) Comparison of the intestinal epithelium on chip after 9 days of culture. Cells subjected to two different pattern of stimulation were compared to unstimulated constructs showing that physiological mechanical cues are able to generate 3D villi-like structures (red arrows).

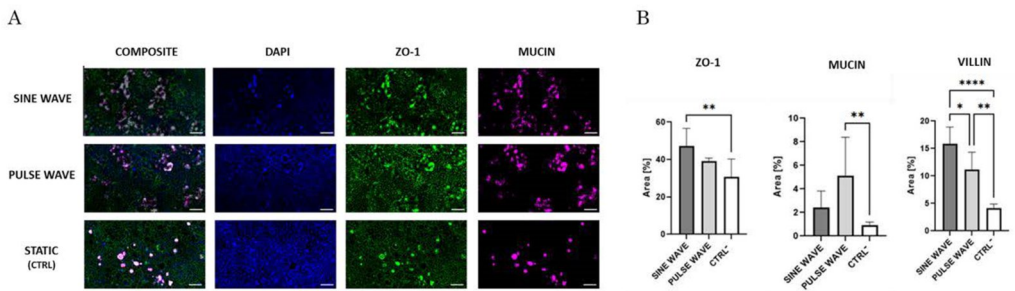


**Figure 2** Immunofluorescence analysis. (A) Immunofluorescence microscopy images of the epithelial barrier cultured on chip with sine stimulation, pulse stimulation and no stimulation. Nuclei (blue) were counted to evaluate cells proliferation while the morphology of the tight junction between cells (ZO-1, green) and the amount of produced mucin (magenta) were considered to assess the physiological reliability of the model. (B) Quantitative analysis of the immunofluorescence images. The expressions of villin, a protein related to the brush border of epithelial cells, mucin and ZO-1 were proved to be enhanced when stimulation was applied.

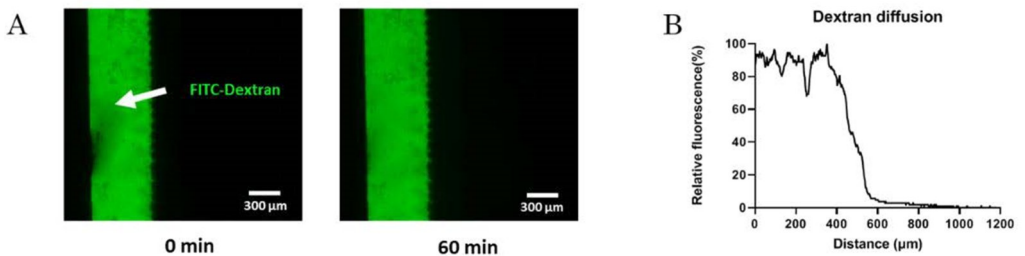


**Figure 3** Barrier integrity analysis. (A) FITC-Dextran was inoculated in the compartment hosting the epithelial barrier and pictures were acquired over 60 minutes to assess its passage through the in-vitro epithelium. (B) Distribution curve of dextran across the OoC channels: the barrier was shown to completely hinder the diffusion of dextran, proving the tightness of cell-cell junctions and the physiological relevance of the model.

# A compartmentalized microfluidic device to model the proprioceptive

C. Palma<sup>1</sup>, A. Cacioppo<sup>1</sup>, E. Melacini<sup>2</sup>, P. G. Mazzara<sup>2,3</sup>, A. Iannielli<sup>2</sup>, V. Broccoli<sup>2</sup>, M. Rasponi<sup>1</sup>

<sup>1</sup>Dipartimento di Elettronica, Informazione e Bioingegneria (DEIB), Politecnico di Milano, Via Ponzio 34/5, 20133 Milano, Italy.

<sup>2</sup>Divisione di Neuroscienze, Istituto Scientifico San Raffaele, 20132 Milano, Italy.

<sup>3</sup>Department of Neuroscience, The Scripps Research Institute, 92037 La Jolla, CA, US.

Friedreich's ataxia (FRDA) is an autosomalrecessive neurodegenerative and cardiac disorder, which leads to limb and gait ataxia, dysarthria, dysphagia, loss of deep tendon reflexes, oculomotor dysfunction and cardiomyopathy.<sup>[1]</sup> Loss of postural balance and ataxia are caused by the degeneration of dorsal root ganglia (DRG) and peripheral nerves, that together with their peripheral targets, i.e. muscle spindles, constitute the proprioceptive sensory circuit.<sup>[2]</sup> At present, there is no effective treatment for FRDA which can either ameliorate the symptoms or modify its pathological progression, mainly due to the lack of robust FRDA cellular or animal models.<sup>[3,4]</sup> In this scenario, organs-on-chip are promising candidates for disease modeling, as they can replicate essential functions of human tissues and organs into micro-scaled systems and allow the co-culture of multiple cell types. Here, we developed a microfluidic compartmentalized device, allowing the co-culture of organoids recapitulating dorsal root ganglia (DRGOs)<sup>4</sup> and intrafusal muscle fibers, aiming at recapitulating the proprioceptive sensory circuit.

Microfluidic devices were fabricated through photolithography and soft-lithography. The design (Figure 1) features two lateral channels intended to host muscle fibers, and a central chamber to house a DRGO. The chambers are 150  $\mu\text{m}$  high and are connected through an array of 5 $\mu\text{m}$ -high microgrooves to guide axonal growth and fluidically isolate the compartments. Firstly, master molds were fabricated through standard two-layer photolithography of SU-8 on silicon wafers.

Microfluidic devices were then produced by soft lithography of PDMS on master molds. Briefly, PDMS was poured on silicon wafers at a pre-polymer to curing agent mixing ratio of 10:1 (w/w) and cured at 65 °C for 3h. Cast PDMS was peeled-off the molds, trimmed and through-holes were punched to obtain muscle culture chamber access ports (6 mm diameter) and DRGO seeding site (2 mm diameter). Finally, PDMS microfluidic layers were plasma bonded to glass cover slides and stored until use.

The microfluidic platform was successfully used to culture human primary myoblasts on a Matrigel coating for up to 15 days (Figure 2) and to induce their maturation into intrafusal muscle fibers. Moreover, a protocol was optimized to seed DRGOs in the corresponding chamber (Figure 3) and to provide axonal guidance through the microgrooves, by using a gradient of neurotrophins. Proper axonal growth from the DRGO chamber through microgrooves towards muscle chambers was assessed through immunofluorescence staining (Figure 4).

Next steps will include the co-culture of myoblasts and DRGOs in the microfluidic platform to recapitulate a functional proprioception sensory circuit, followed by the comparison between wild-type DRGOs and diseased DRGOs, aiming at elucidating the molecular features of FRDA pathology.

[1] A. Harding et al., *Brain*, 104(3), 589–620 (1981).

[2] A. H. Koeppen et al., *Journal of Neuropathology and Experimental Neurology*, 72(2), 78–90 (2013).

[3] S. Schmucker et al., *Human Molecular Genetics*, 19(R1), R103–R110 (2010).

[4] P. G. Mazzara et al., *Nature communications*, 11, 4178 (2020).

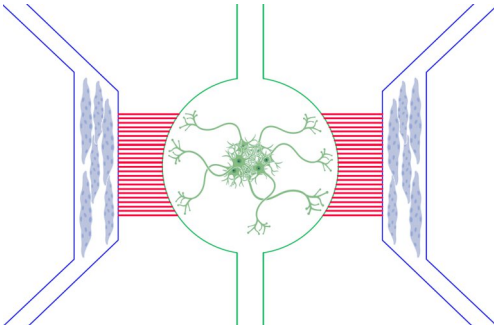


**Figure 1** Illustration of the microfluidic device with two lateral chambers hosting intrafusal muscle fibers (in blue) and a central chamber hosting a dorsal root ganglia organoid (in green). The chambers are connected through arrays of microgrooves (in red).

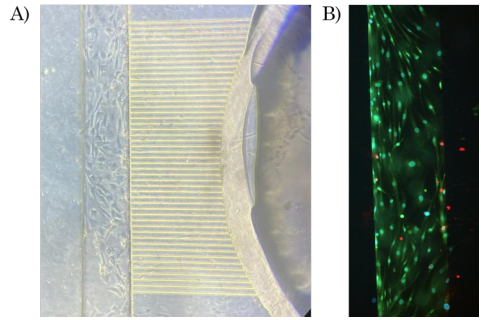


**Figure 2** A) Brightfield image of human primary myoblasts cultured inside the microfluidic device. B) Live/Dead image showing live (in green) and dead (in red) myoblasts in the chip.

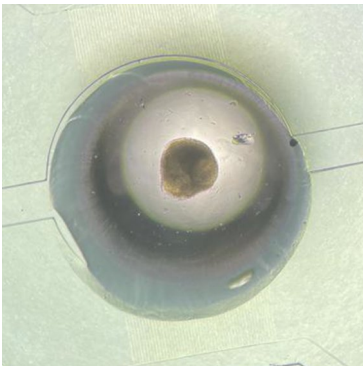


**Figure 3** Brightfield image showing a dorsal root ganglia organoid seeded in the corresponding chamber of the microfluidic device.

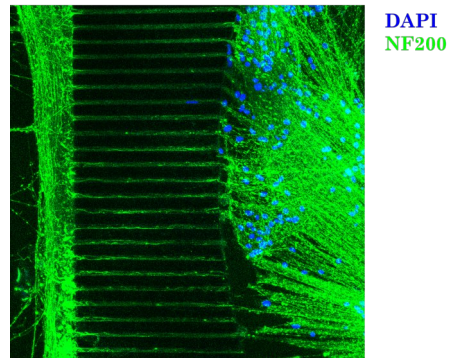


**Figure 4** Immunofluorescence staining of DRGO in the microfluidic platform, showing nuclei (in blue) and axons (in green).

# LivHeart: a platform for liver and heart compartmentalized culture

E. Ferrari<sup>1\*</sup>, R. Visone<sup>2\*</sup>, E. Monti<sup>1</sup>, P. Occhetta<sup>1,2</sup>, M. Rasponi<sup>1,2</sup>

<sup>1</sup>Dipartimento di Elettronica, Informazione e Bioingegneria (DEIB), Politecnico di Milano, Via Ponzio 34/5, 20133 Milano, Italy.

<sup>2</sup>BiomimX Srl, Via Giovanni Durando 38/A, 20158 Milano, Italy.

The drug discovery and development process is still long, costly and highly risky. The principal attrition factor is undetected toxicity, with hepatic and cardiac toxicities playing a critical role and being the main responsible of safety-related drug withdrawals from the market.<sup>[1]</sup>

Multi Organs-on-Chip (MOoC) represent a disruptive solution to study drug-related effects on several organs simultaneously and to efficiently predict drug toxicity in pre-clinical trials.<sup>[2]</sup>

Specifically focusing on drug safety, different technological features have been applied here to develop versatile MOoC platforms encompassing two culture chambers for generating and controlling the type of communication between a metabolically competent liver model and a functional 3D heart model. We thus developed the  $\mu$ Channels and Valve devices, where continuous and on/off communication between liver and heart chambers were respectively allowed. The liver compartment is based on the micropatterned co-culture (MPCC) functional model in a dual-chamber microfluidic platform, that we previously developed and successfully exploited to study the effects of liver-metabolized anticancer drugs on tumor cells. Compared to conventional 2D monolayers, in the MPCC model hepatocytes can maintain their characteristic cuboidal morphology (i.e., microscale 3D) and express high and stable functions (e.g., albumin and urea production). The heart compartment is composed of 3D neonatal rat cardiomyocytes (NRCM) laden fibrin gel. The administration of the drug Terfenadine, a cardiotoxic compound liver-metabolized into the non-cardiotoxic Fexofenadine, proved that liver metabolism and a fine

control over drug diffusion (i.e., on/off communication of the Valve device) are fundamental to elicit a physio-pathological cardiac response.

From these results, an optimized LivHeart platform was developed to house a liver model and a cardiac construct that can be mechanically trained to achieve a beating microtissue, whose electrophysiology can be directly and continuously recorded *in vitro*. The platform was proved able to predict off-target cardiotoxicity of Terfenadine after liver metabolism both in terms of cell viability and functionality. Concerning viability, NRCM viability was affected by the presence of Terfenadine without liver metabolism (TER, -11.76% viability compared to the control) whereas it was not affected by the incubation of pure Fexofenadine (FEX, +5.1% viability compared to the control), or Fexofenadine derived from MPCC-mediated metabolism (TER→FEX, -0.14% viability compared to the control). These results are consistent with data from literature.<sup>[3]</sup> From the recorded electrical signals, the field potential duration (FPD) which is the interval measured from the depolarization peak to the repolarization peak was recorded. The FPD increased only in the TER compared to the control ( $0.28 \pm 0.05$  sec vs  $0.19 \pm 0.04$  sec). For what concerns FEX and TER→FEX conditions, the FPD values were similar to the control ( $0.2 \pm 0.08$  sec vs  $0.21 \pm 0.05$  sec). Thus, compared to the control, the FPD increased of about 48%, 12% and 6% after the incubation of Terfenadine without liver metabolism, Terfenadine with liver metabolism and Fexofenadine, respectively. These results are consistent with the potassium channel blockage activity of Terfenadine.<sup>[4]</sup>

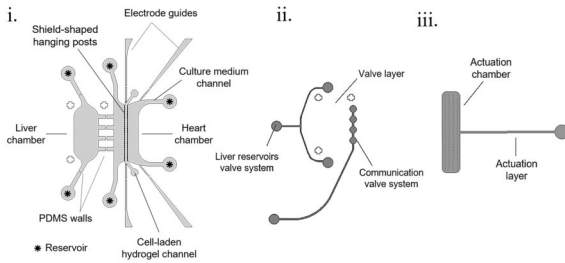
[1] N. Ferri et al. *Pharmacology & Therapeutics*, 138(3), 470–484 (2013).

[2] E. Ferrari et al., *APL Bioengineering*, 5, (2021).

[3] C. Oleaga et al., *Biomaterials*, 182, 176–190 (2018).

[4] C. Chen et al., *Drugs in R&D*, 8, 301–314 (2007).

## A LivHeart Layout



## B

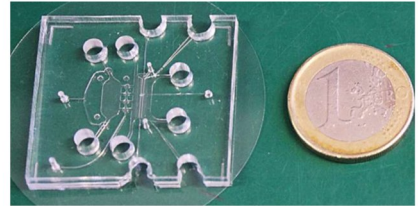
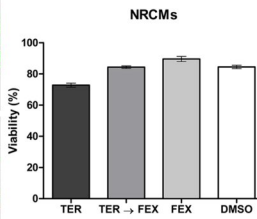
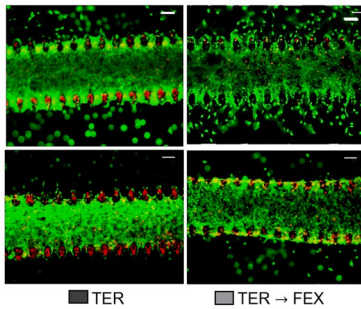


**Figure 1** Layout of the LivHeart device. (A) The LivHeart is composed by (i) a chambers layer for the liver and heart cultures, (ii) a valve layer comprising two valve systems (liver-reservoirs and communication valve systems) and (iii) an actuation layer which provides mechanical stimulus to the 3D cardiac microtissue. In the chambers layer, the 3D cardiac culture is confined between two parallel rows of shield-shaped hanging posts and a pair of PDMS walls is placed between the two compartment and between the liver chamber and the corresponding reservoirs. Guides for electrode's insertion needed for the cardiac signal monitoring are included in the design of the heart chamber. (B) Picture of the fabricated LivHeart device.

## A



## B

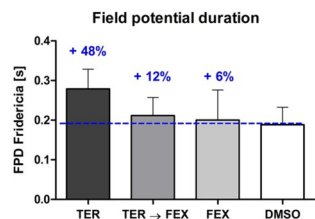


**Figure 2** Drug screening with Terfenadine in the LivHeart device. (A) Cell viability of cardiac models were monitored through Live/Dead assay. DMSO, vehicle control; TER, Terfenadine; FEX, Fexofenadine; TER → FEX, liver-metabolized Terfenadine. Scale bars of 250  $\mu\text{m}$  (i) and of 100  $\mu\text{m}$  (ii). (B) The electrical activity of the cardiac microtissue was monitored through the insertion of electrodes at the end of the construct. From the recorded signals the field potential duration (FPD) was measured. FPD mean values were corrected with Fridericia correction. In blue, mean values of conditions compared with the mean values of controls.

# 3D Liver-on-Chip with a perfusable physiologic-like vascular channel

E. Ferrari<sup>1\*</sup>, R. Visone<sup>2\*</sup>, Linda G. Griffith<sup>3</sup>, P. Occhetta<sup>1,2</sup>, M. Rasponi<sup>1,2</sup>

<sup>1</sup>Dipartimento di Elettronica, Informazione e Bioingegneria (DEIB), Politecnico di Milano, Via Ponzio 34/5, 20133 Milano, Italy.

<sup>2</sup>BiomimX Srl, Via Giovanni Durando 38/A, 20158 Milano, Italy.

<sup>3</sup>Massachusetts Institute of Technology, BE Department, Cambridge (MA), US.

The recapitulation of 3-dimensional (3D) architecture of native organs, including their vasculature, is paramount for the generation of functional *in vitro* models.<sup>[1]</sup>

Advanced Organs-on-Chip (OoC) platforms have been recently developed, able to provide both biochemical and physical stimulations to enhance tissue-specific functionality. However, these models present either separating membranes or scaffolds between the parenchyma and endothelial cells, introducing physical barriers absent in the native milieu. Moreover, they fail to recapitulate the intrinsic circularity of vascular channels, which is known to promote barrier functionality and cytoskeletal alignment of endothelial cells.<sup>[2,3]</sup>

To address these needs, we developed a method to generate on-chip a perfusable cylindrical endothelial channel embedded in a 3D construct without any physical separation. The device comprises two layers, namely (i) a culture chamber composed by a central channel for 3D cell-laden hydrogel confinement, flanked by two lateral channels for medium replenishment and (ii) a tank layer for cylindrical lumen obtainment. We implemented the method in a novel Liver-on-Chip platform, namely Direct-contact platform: primary human hepatocytes (PHH) were embedded in a hydrogel composed of 70% rat tail collagen I and 30% fibrin, generating a 3D construct surrounding an inner vascular channel, lined by human umbilical vein endothelial cells (HUVEC). Such hydrogel composition was chosen as it replicates the stiffness of a healthy liver ECM.<sup>[4]</sup> Liver functionality was assessed through albumin and enzymatic assays (e.g., CYP3A4) and immunofluorescence staining. Endothelial

Cells seeded in the lumen could generate a cylindrical channel displaying endothelial characteristic morphology and cellular junctions (e.g., CD-31, VE-CAD and ZO-1) at day 7 of culture. Additionally, barrier integrity was assessed by means of 4kDA FITC Dextran perfusion, showing HUVECs ability to retain dye in the lumen. From day 2 HUVECs are co-cultured with PHH under both static and dynamic (i.e., rocker platform) conditions. Bidirectional flow parameters were chosen so that the endothelial cells within the lumen can experience physiological shear stress.<sup>[5]</sup> LDH release showed higher cell mortality at days 1 and 3 of culture as expected, corresponding to PHHs and HUVECs respective seeding. Additionally, albumin production is enhanced when the endothelial phenotype is present in the system under dynamic conditions compared to static conditions or to when PHHs are cultured alone, thus better recapitulating functions and architecture of the liver sinusoid. For what concerns CYP3A4 activity, in the co-culture the enzymatic activity of hepatocytes is enhanced compared to PHH only conditions, with no statistical significance.

The device is in truth versatile and can be used for various purposes and to mimic different organ models where low seeding volumes are needed and modelling vasculature is pivotal, such as blood-brain-barrier and tumor microenvironment.

This methodology paves the way to numerous further uses of microfluidic technologies coupled to vascularized tissue models, for instance, the application of the immune system perfusion between different organ compartments of a MOoC platform.

[1] M. A. Polidoro et al., *Liver International*, 41(8), 1744–1761 (2021).

[2] K. J. Jang, et al., *Science Translational Medicine*, 11(517), (2019).

[3] B. F. L. Lai et al., *Advanced Functional Materials*, 27, 1–11 (2017).

[4] S. Mueller, *Hepatic Medicine: Evidence and Research*, 2, 49-67 (2010).

[5] Y. Du et al., *Lab on a Chip*, 17(5), 782-794 (2017).

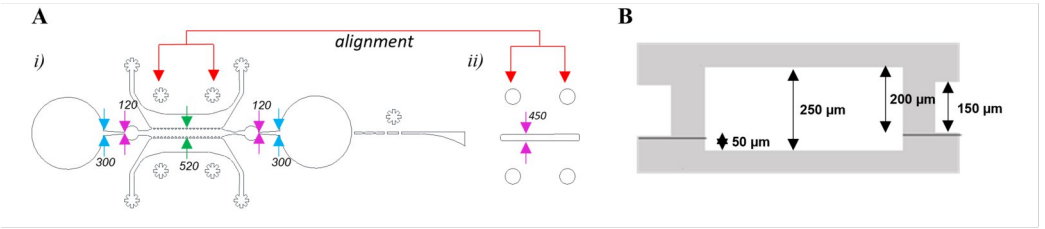


**Figure 1** Design and cross-sectional view of the Direct-contact platform. (A) design of the Direct-contact platform where (i) the microfluidic channel layer for cell culture and (ii) the tank layer for cell culture are presented with related dimensions in  $\mu\text{m}$ . (B) cross-section with dimensions of the Direct-contact platform. .

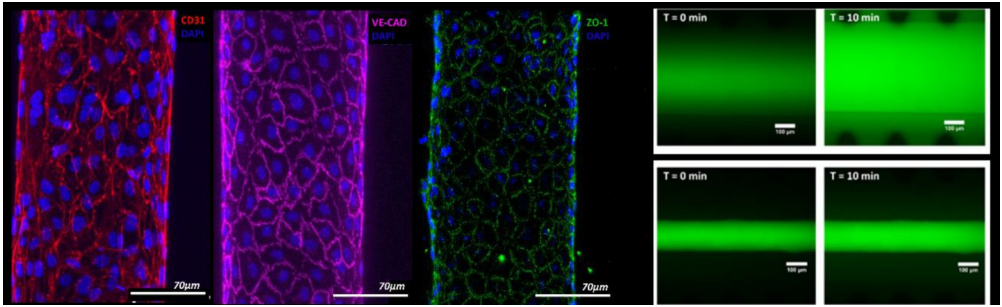


**Figure 2** HUVEC characterization: CD31, VE-CAD and ZO-1 expression; permeability experiments with 4kDa FITC-Dextran.

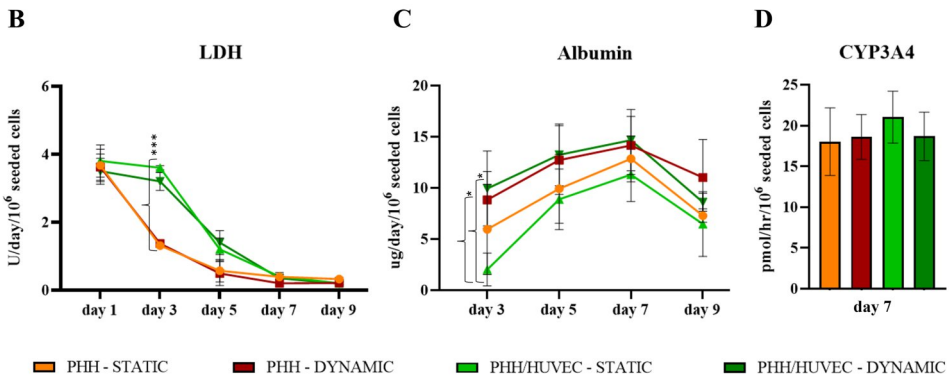


**Figure 3** Liver sinusoid model generated within the Direct-contact platform. (B) LDH release, (C) albumin production and (D) CYP3A4 activity in the four culture conditions (i.e., PHH only under static condition, PHH only under dynamic condition, PHH/HUVEC under static condition, PHH/HUVEC under dynamic condition). Statistical analysis was performed using analysis of variance (Anova) with Tukey correction: \*  $p = 0.033$ , \*\*\*  $p < 0.001$  ( $N=3$ ).

# Predicting human cardiac QT alterations and pro-arrhythmic effects of compounds with a 3D beating heart-on-chip platform

R. Visone<sup>1,2,\*</sup>, F. Lozano-Juan<sup>1,2,\*</sup>, S. Marzorati<sup>3</sup>, M. W. Rivolta<sup>4</sup>, E. Pesenti<sup>3</sup>, A. Redaelli<sup>1</sup>, R. Sassi<sup>4</sup>, M. Rasponi<sup>1</sup> and P. Occhetta<sup>1,2</sup>

<sup>1</sup>Dipartimento di Elettronica, Informazione e Bioingegneria (DEIB), Politecnico di Milano, Via Ponzio 34/5, 20133 Milano, Italy.

<sup>2</sup>BiomimX Srl, Via Giovanni Durando 38/A, 20158 Milano, Italy.

<sup>3</sup>Accelera Srl, Via Pasteur, 10, 20014 Nerviano, Italy.

<sup>4</sup>Dipartimento di Informatica, Università degli Studi di Milano, Via Giovanni Celoria 18, 20133 Milano, Italy.

Determining the potential cardiotoxicity and pro-arrhythmic effects of drug candidates remains one of the most relevant issues in the drug development pipeline<sup>[1]</sup>. New methods enabling to perform more representative preclinical *in vitro* studies by exploiting induced pluripotent stem cell-derived cardiomyocytes (iPSC-CM) are under investigation to increase the translational power of the outcomes. Here we present a pharmacological campaign conducted to evaluate the drug-induced QT alterations and arrhythmic events on uHeart, a 3D miniaturized *in-vitro* model of human myocardium encompassing iPSC-CM and dermal fibroblasts embedded in fibrin.

The 3D cardiac tissue was developed in a beating heart-on-chip<sup>[2]</sup> capable to provide a mechanical stimulation (uBeat® patented technology<sup>[3]</sup>) to a co-culture of induced pluripotent stem cells derived cardiomyocytes and dermal fibroblast mixed in a 3:1 proportion (75-125 x 10<sup>6</sup> cells/mL) in fibrin hydrogel. The tissue was subjected to a 10% uniaxial strain at 1Hz for seven days. The electrophysiological activity of the spontaneously beating cardiac culture was recorded by micro-electrodes inserted inside the heart-on-chip system ( $\mu$ ECG technology<sup>[4]</sup>). Drug cardiotoxicity was estimated by monitoring the electrical signal alterations (i.e. beating period-BP, field potential duration-FPD, spike amplitude-AMP) caused by 11 drugs (having high, medium, low risk of developing torsade de pointes ventricular tachycardia) added on the medium at incremental doses by means of a custom

made Matlab-based software.

Mechanically trained uHeart resulted in synchronously beating cardiac microtissues in one week, characterized by a clear field potential (FP) signal that was successfully recorded by means of the integrated electrical system. The drug screening protocol resulted compliant with the new International Council for Harmonisation of Technical Requirements for Pharmaceuticals for Human Use (ICH) guidelines<sup>[5]</sup>. The model allowed to predict with high sensitivity, specificity and accuracy how the drugs affected the cardiac BP, FPD, AMP and the stability of the electrical activity (i.e. arrhythmias), anticipating clinical outcomes. Specifically, uHeart showed a sensitivity of 83.3%, a specificity of 100% and an accuracy of 91.6% in predicting the drug-related QT prolongation. Cardiotoxic concentrations of drugs were notably detected in the range of the clinical highest blood drug concentration (C<sub>max</sub>).

uHeart was successfully qualified as a fit-for-purpose pre-clinical tool for cardiotoxicity studies. The software that we implemented allowed to validate the model and will be further developed to achieve the automatic detection and classifications of the arrhythmic events. Thanks to the fully human set-up, uHeart showed great potentiality to supplement and advance limited data currently provided by Ikr assay and telemetric studies on animal, better matching clinical outcomes in cardiac safety.

[1] L. Pang et al., *Circulation research*, 125(9), 855–867 (2019).

[2] A. Marsano et al., *Lab on a chip*, 16(3), 599-610 (2016).

[3] M. Rasponi, P. Occhetta and A. Redaelli, A microfluidic device for controlled generation and/or culture and/or maturation of three-dimensional cells and/or tissue constructs (2015).

[4] M. Rasponi, R. Visone and G.S. Ugolini, Microfluidic device for electrical measurement and/or stimulation (2018).

[5] ICH guideline E14/S7B: clinical and Nonclinical Evaluation of QT/QTc Interval Prolongation and Proarrhythmic Potential-questions and answers (2022).

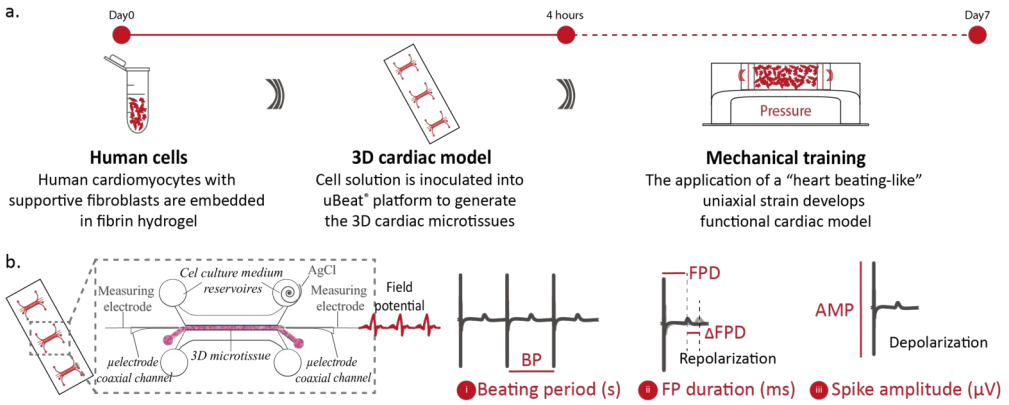


**Figure 1** Schematic representation of the experimental setup used to (A) develop the uHeart model and (B) to measure and evaluate the electrophysiological parameters of the cardiac microtissues (BP, FPD, FPD changes and AMP).

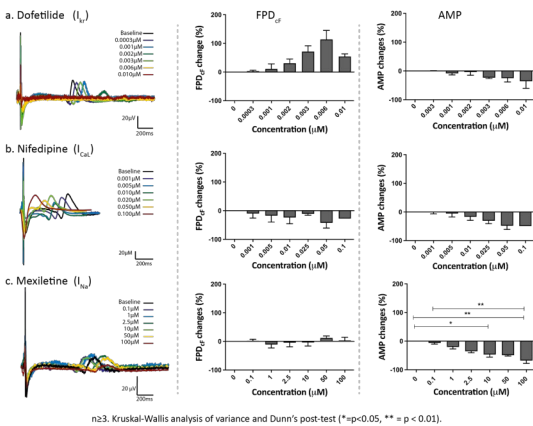


**Figure 2** Representative field potentials (FPs) and electrophysiological parameters (ie, BP and FP duration corrected with Fridericia methods) of uHeart microtissues subjected to drugs acting on single cardiac ion channels: (A) dofetilide, (B) nifedipine, and (C) mexiletine. Data are represented as mean with standard error.

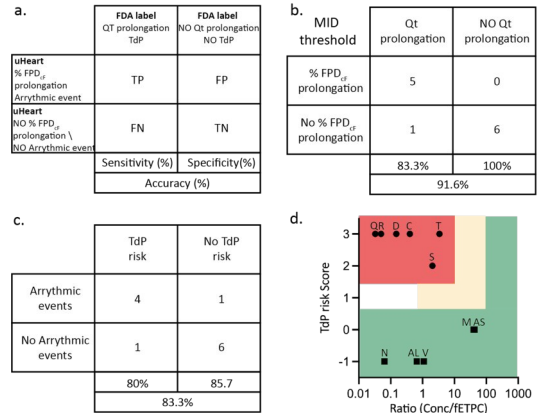


**Figure 3** A, Schematic representation of the concordance analyses and sensitivity, specificity, and accuracy parameters performed by comparing the results obtained in uHeart with the FDA drug labels. B, uHeart models is considered to show a field potential prolongation when the percentage changes in the FPD<sub>p</sub> is higher than the MID threshold. C, uHeart sensitivity, specificity and accuracy for detecting arrhythmic events, correlating with the risk of TdP onset. D, TdP Risk categorization depicted through two-dimensional map indicating high risk drugs in the top left area, intermediate risk drugs in the empty middle area and low risk drugs in the bottom and right area. The area not enclosed in rectangle indicates insufficient margins to categorize the compound (risk score 1, margin 1). Letters on the symbol indicate the first letter of each tested drug (for Alfuzosine-AL and Aspirine-AS).

## 3D PDMS micropatterned substrates to observe the cellular response to substrate stiffness

E. Bianchi, A. Pellegata, C. Crescioli, P. De Stefano, G. Dubini

$\mu$ FLUID LaBS, Dipartimento di Chimica, Materiali e Ingegneria Chimica "Giulio Natta", Politecnico di Milano, Piazza Leonardo da Vinci 32, 20133 Milano, Italy.

In their native environment cells are in contact with topographies ranging from macroscale to nanoscale. Macroscale topographies are reflected in tissue organization, microscale in the cellular level architecture and nanoscale in the subcellular architecture. Extracellular matrix (ECM) and/or neighbouring cells, act on cells by chemical and physical signals but also to mechanical stimuli, which affect various biological functions such as activation of signaling pathways, cell differentiation, migration and proliferation<sup>[1]</sup>. The increase in stiffness affects the cell-cell and cell-ECM adhesions as well as morphological changes, the ECM stiffening is typical in pathological conditions<sup>[2]</sup>. By means of the optimization of standard photolithography, to obtain SU8 molds, and PDMS molding (Dow Sylgard 184) we obtained different and reproducible micropillars substrates. Differently from silicon molds, SU8 enables the realization of micro pillars patterns on multilayered structures, of hundreds microns thickness, that are often useful in fabrication of microfluidic devices for cell culture and biological applications.

Micropillar arrays size has to allow single cells to spread on multiple pillars. Stiffness of pillars can be modulated by the shape of the pillar section, and the aspect ratio of the pillar the Young module of the material, that itself depends on PDMS concentration ratio pre-polymer to crosslinker, the curing temperature and curing time. First sets of micropillars pattern were fabricated showing a height range 2 to 5  $\mu\text{m}$ ,  $\varnothing$  3 to 4  $\mu\text{m}$  at spatial density of 4  $\mu\text{m}$  to 5.5  $\mu\text{m}$ .

Fabrication process involved the epoxy based negative SU-8 2005, double layer, spun 900 – 1800 rpm on silicon wafers and exposed under the maskless photolithography

writer Heidelberg MLA100. Optimization of exposure parameters is crucial. After the silanization (TCS) process, a PDMS solution is poured over the master mold. Then, the samples have been placed to cure in a furnace at 70°C or 80°C, for 15h, obtaining cured materials with different stiffness (Figure 1)

Since the actual height of the final PDMS structures depends on the thickness of the molds and on the efficacy of filling too, measurements on final PDMS structures are necessary to perform an effective optimization of the process.

The micron scale size, the translucent aspect and the electrical insulating properties of both PDMS and SU8 forced us to introduce some a step of surface metallization, to improve the visualization and characterization of samples under interferometry profilometer to investigate the homo-geneity, and the observation by SEM to characterized single structures (Figure 2-3). After plasma treatment, sterilization and protein coating, a cell sample (H5V murine endothelial cells) were seeded on PDMS micropatterned samples, in a 96-multiwell plate. As a preliminary result, cells were observed after 24h of incubation showing different grades of elongation on PDMS patterns of different stiffness (Figure 4). Further investigations and fabrication will be performed to widen the range of stiffness offered to cells and mimic defined physiological /pathological conditions.

This work is part of the Accelerator Award n° A26815: "Single-cell cancer evolution in the clinic" funded by Cancer Research UK and Fondazione AIRC (n° 22790).

[1] H. van Hoorn et al., Nano Letters, 14(8), 4257-4262 (2014).

[2] L. E. Dickinson et al., Journal of Biomedical Materials Research, 100(6), 1457-1466 (2012).

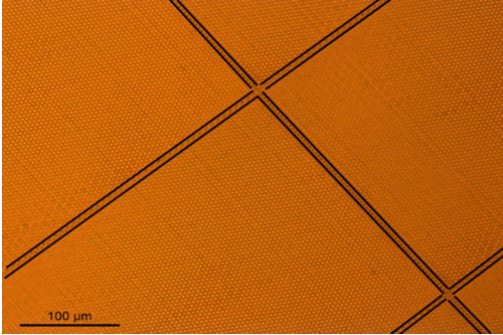


**Figure 1** PDMS micropatterned surface, (optical 10X – black lines define the stitching areas related to exposure mode of maskless photolithography).

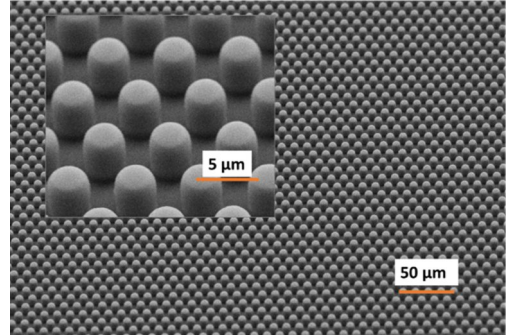


**Figure 2** PDMS micropatterned surface, SEM images with InLens detector, tilted 45°. 900 rpm – 5.5 μm spacing (center-center), 3,3 μm diameter, 3,7 μm height.

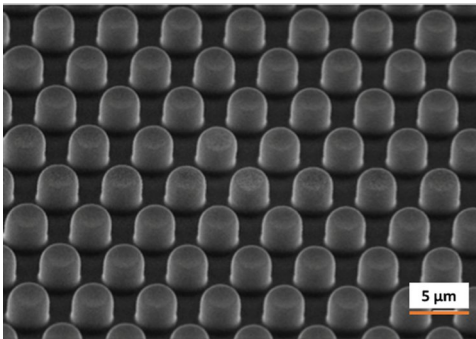


**Figure 3** PDMS micropatterned surface, SEM images with InLens detector, tilted 45°. 1800 rpm – 5.5 μm spacing (center-center), 3,3 μm diameter, 2,7 μm height.

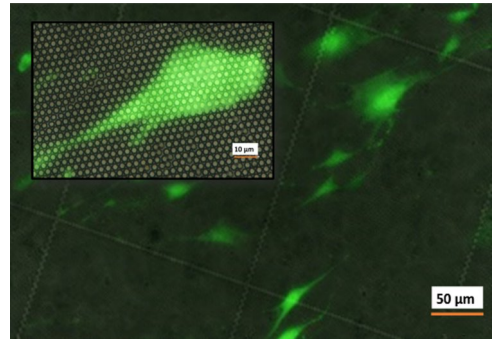


**Figure 4** Phase-contrast images in bright field of the micropillar substrate and a fluorescence image of H5V cells, merged (20X).

# PDMS Microstructures For Capillarity -Driven Filling In Open Microfluidic – Matrigel® and 3D cell cultures

E. Bianchi, P. De Stefano, P. Oldani, L. Leoni, M. Piergiovanni, G. Dubini

μFLUID LaBS, Dipartimento di Chimica, Materiali e Ingegneria Chimica "Giulio Natta", Politecnico di Milano, Piazza Leonardo da Vinci 32, 20133 Milano, Italy.

Matrigel®, a gold standard matrix for 3D cell culture, is hardly usable with high-throughput manual/automatic dispensing machines, due to its complex rheology and viscosity dependence from temperature and shear rate conditions. Therefore, we design an open microfluidic wire to generate 25 Matrigel® interconnected wells by exploiting the effect of capillary filling<sup>[1]</sup>.

25 x Ø3.4 mm wells were connected by open air microchannel, characterized by 300 μm in height/ 200 μm flow section. Capillary filling of simple wells was initially unsuccessful, leaving uncovered the surface in the middle of largest area. To solve this problem, we designed 3D structures on the bottom surfaces in order to drive Matrigel® to fill completely each well by capillarity. To enable capillary filling, internal surfaces of wells are selectively (by a PDMS mask) made hydrophilic by oxygen plasma treatment. Complete well filling occurs only in presence of 3D features (150 μm height). Wells are surrounded by a hydrophobic rim<sup>[2]</sup> (Figure 1), in order to enclose Matrigel® in the dome shape.

Microchip are made of PDMS molding it on a SU8 on a SU8 triple layers mold (SU82100 MicroChem) on silicon wafers, exposed under the maskless photolithography writer Heidelberg MLA100. Multilayered molds are obtained by three complete subsequent photolithography SU8 fabrications, just skipping the intermediate postbaking steps.

Three geometrical patterns of filling structures were designed: concentric structures, continue (CL), segmented (LL) or rotated (LP). They were evaluated by computational fluid dynamic models, comparing results to the experimental evidences.

Experiments on single well filling were

performed by manually pipetting 10 μl every 5 s in a well connected to the observed one while the filling of the 5x5 wells wire is given by the automatic dispensing of the matrix in the middle well, by means of a syringe pump (Figure 2). The presence of patterns in the wells allows Matrigel® completely filling to the creation of domes, as well as homogeneous distribution of cells. Moreover, from CFD analyses, CL pattern is the fastest, even if LL and LP show filling times of single wells. Filling strategy of the matrix and the role of the structures, as surfaces able to attract the matrix and keeping it in a slow but constant flow, able to homogeneously cover all the internal surface of the well, generating the dome (Figure 3-4). This validated CFD model may also provide data, such as shear stress or velocities, for further platform optimization.

A strategical design of 3D features allows the use of Matrigel® in a very performing microfluidic platform. CFD results are decisive in the definition of filling performances and parameters.

This work is part of the Accelerator Award n° A26815: "Single-cell cancer evolution in the clinic" funded by Cancer Research UK and Fondazione AIRC (n° 22790).

<sup>[1]</sup> E. Bianchi, et al., MICROTAS 2021, 10-14 October, Palm Springs, USA.

<sup>[2]</sup> O. Frey et al., Nature Communications, 5, 1–11 (2014).

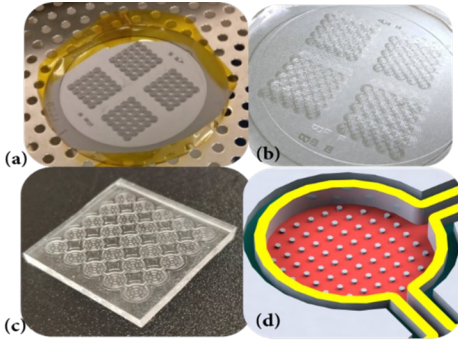


**Figure 1** (a) SU8 mold on a 4'' silicon wafer; (b) PMDS cured and detached from the mold; (c) 5x5 wells interconnected, filling microstructures are visible in the open wells; (d) design of the well: red is the hydrophilic surface with 3D filling structure (an example), yellow is the hydrophobic rim.

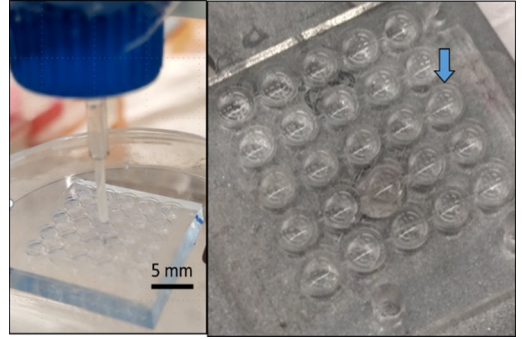


**Figure 2** Matrigel® deposited on the PDMS chip, filling the 25 wells starting from the center wells. On the right the final aspect of the domes inside/on the wells.

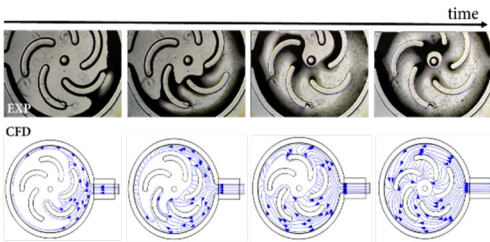


**Figure 3** Comparison between experimental and CFD filling results in 4 subsequent time steps (LP configuration). Arrows represent the presence and the direction of local flows of Matrigel®, filling the well along the structures.

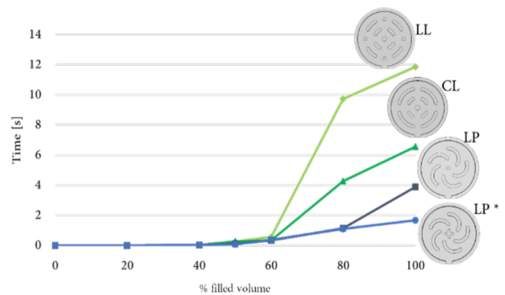


**Figure 4** Computational fluid dynamic results: filling time of single well with different microstructures. LP reach the 100% in 4s, a modification in the middle (LP\* configuration) improves the performance down to 2 s.

# Organic Biosensors

A. Kyndiah,<sup>1</sup> F. Viola,<sup>1</sup> F. Modena,<sup>1,2</sup> M. Caironi<sup>1</sup>

<sup>1</sup>Center for Nano Science and Technology @PoliMI, Istituto Italiano di Tecnologia, Via G. Pascoli 70/3, Milano, 20133 Italy.

<sup>2</sup>Dipartimento di Elettronica, Informazione e Bioingegneria (DEIB), Politecnico di Milano, Via Ponzio 34/5, 20133 Milano, Italy.

This activity aims at exploiting Electrolyte Gated Organic Transistor (EGOT) for Biosensing applications. EGOTs are three-terminal devices based on organic semiconductors, where an ionically conducting and electronically insulating solid or liquid electrolyte is employed as a gate insulator. The activity is structured along two main tasks: i) high sensitivity sensors arrays for biomarkers and ii) electrical recording of electrogenic cells.

In particular, research related to i) was performed within the European SiMBiT project (H2020 GA # 824946). SiMBiT aims to develop a matrix of 96 biosensors based on EGOTs structure, for the detection of both protein and genomic pancreatic cancer biomarkers, with a sensitivity that can reach the single-molecule level (zM in liquid). Part of SiMBiT devices are fabricated in PoliFAB: our activity in this facility is mostly related to the definition of the interdigitated source-drain electrodes (with channel width = 10 nm and channel length = 10  $\mu\text{m}$ ) by means of large-area (the 96 biosensors are distributed over an area of approximately 225  $\text{cm}^2$ ) optical lithography process (Figure 1). In particular, we use a photolithographic image reversal process (AZ5214E photoresist) for the definition of the layout of the interdigitated contacts on a transparent, plastic PEN substrate - 125  $\mu\text{m}$  thick - by using the 6" mask-aligner or the maskless aligner (Heidelberg MLA100), followed by thermal evaporation of chromium (2 nm) and gold (40 nm), and then lift-off in N-methyl-2-pyrrolidone.

EGOTs have also been recently employed as a bioelectronics recording platform for recording the electrical activity of electrogenic cells such as cardiac cells and neurons. To achieve this, in task ii), we are culturing cells directly on the

organic/carbon based semiconductor that is coated onto the source and drain electrodes of the transistor (Figure 2). The interdigitated source and drain electrodes are fabricated in PoliFab on glass or plastic substrates using the mask-less reverse lithography process (AZ5214 photoresist using MLA100 Heidelberg mask-less aligner) followed by thermal evaporation of chromium (2 nm)/ gold (15 nm) and lift-off in N-methyl-2-pyrrolidone. The design and geometry of the interdigitated electrodes is optimized by taking into consideration: (1) To achieve good electrical performance of the transistor (2) smaller area for local recording of few cells. One paper on this activity has been submitted in 2022.

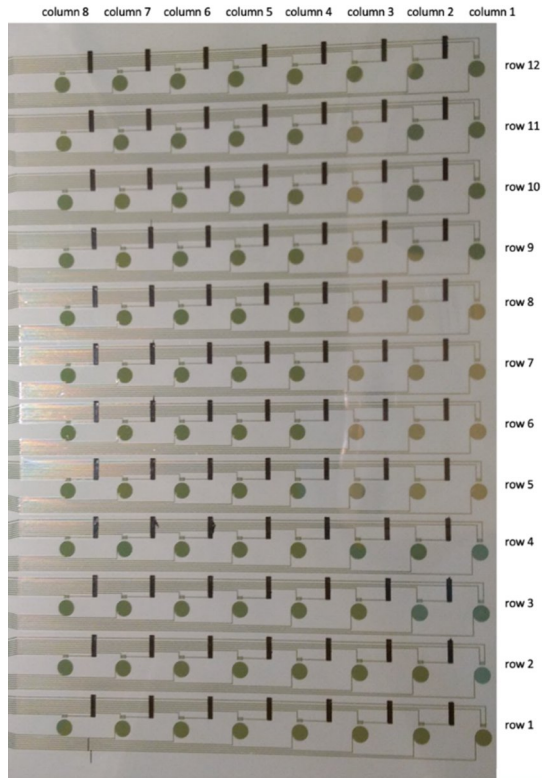


**Figure 1** 8x12 gold array patterned on PEN prior to coupling with an ELISA plate.



**Figure 2** Cardiomyocytes cultured on gold interdigitated structures.

# Patterning of microelectrodes for organic field-effect transistors

A. Luzio,<sup>1</sup> T. Losi,<sup>1,2</sup> S. Pecoraro,<sup>1,2</sup> M. Caironi<sup>1</sup>

<sup>1</sup>Center for Nano Science and Technology @Polimi, Istituto Italiano di Tecnologia, Via G. Pascoli 70/3, Milano, 20133 Italy;

<sup>2</sup>Dipartimento di Eletttronica, Informazione e Bioingegneria (DEIB), Politecnico di Milano, Via Ponzio 34/5, 20133 Milano, Italy.

This is an activity that serves the group needs for microelectrodes in reference organic field-effect transistors (OFETs) where to test new organic semiconductors, study device physics of such devices (charge transport and injection) and develop architectures for the operation of OFETs in the high frequency (HF), and in perspective in the ultra-high frequency regime (UHF). Such devices serve as important benchmark of fully printed devices, which is the general goal of the group.

The reference structures are either top-gate, bottom-contacts FETs (Figure 1) or bottom-gate, bottom-contacts FETs (Figure 2). Microelectrodes for source and drain contacts are typically made of gold, patterned with standard lift-off lithographic processes. Channel lengths are typically defined in the range from 2.5 to 50  $\mu\text{m}$ . Such structures are used to assess the electronic properties of several classes of organic semiconductors (conjugated small molecules, conjugated polymers and blends). They are also used to assess the properties of edible organic semiconductors, with the EU project ELFO (GA # 864299).

The activity serves also a specialized line of research in the group, dedicated to develop OFETs capable of operating at high frequency – a challenge considering the limited charge transport properties of solution-processable organic semiconductors. The development of OFETs working at high frequency aims at enable the application of organic electronics in fields like large area wearable electronics and IoT (Internet of Things). To measure the frequency of transition, determining the maximum operative frequency of OFETs, by means of S-parameters, a specific and

controlled metallic pattern is needed (Figure 3). Such pattern is defined by lift-off with gold thanks to the maskless aligner tool, defining channel lengths in the micron scale (1 – 5  $\mu\text{m}$ ). Thanks to the lithographic process, the device geometry is optimized by changing the critical dimensions of the transistors, including the channel length as well as the channel width and gate-to-source/drain overlap length, which are important for the final frequency performance.

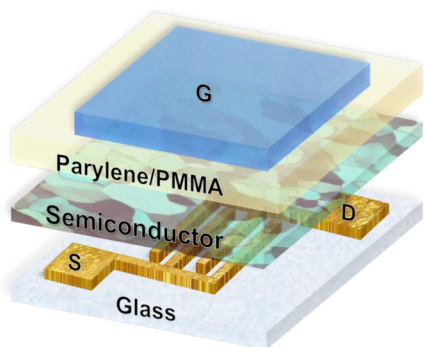


**Figure 1** Top-gate, Bottom-contacts OFET architecture.

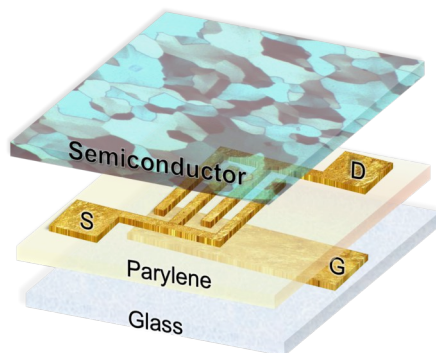


**Figure 2** Bottom-gate, Bottom-contacts OFET architecture.

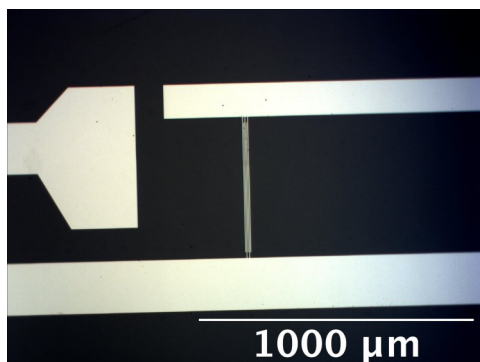


**Figure 3** Gold lithographic pattern for OFETs working at high frequency.

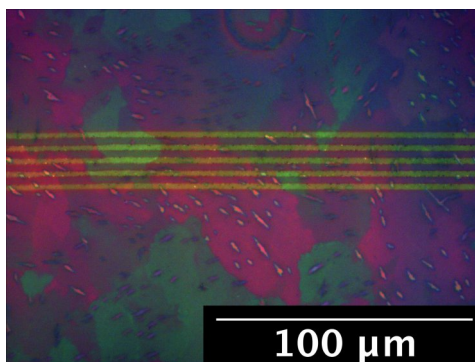


**Figure 4** Optical polarized microscope image of the transistor channel upon after deposition of the organic semiconductor.

# Integrated in-line visible light detector on Silicon nitride

C. De Vita,<sup>1</sup> F. Toso,<sup>1</sup> N. G. Pruiti,<sup>2</sup> C. Klitis,<sup>2</sup> G. Ferrari,<sup>4</sup> M. Sorel,<sup>2,3</sup> A. Melloni,<sup>1</sup> F. Morichetti<sup>1</sup>

<sup>1</sup>Dipartimento di Elettronica, Informazione e Bioingegneria (DEIB), Politecnico di Milano, Via Ponzio 34/5, 20133 Milano, Italy.

<sup>2</sup>University of Glasgow, Rankine Building, Oakfield Avenue, Glasgow G12 8LT, UK.

<sup>3</sup>Istituto TeCIP, Scuola Superiore Sant'Anna, 56124 Pisa, Italy.

<sup>4</sup>Dipartimento di Fisica, Politecnico di Milano, Piazza Leonardo da Vinci 32, 20133 Milano, Italy.

Visible-light integrated photonics is emerging as a promising technology for the realization of optical devices for applications in sensing, quantum information and communications, imaging, and displays. Among the existing photonic platforms, high-index-contrast silicon nitride ( $\text{Si}_3\text{N}_4$ ) waveguides offer broadband transparency in the visible spectral range and a high scale of integration. As the complexity of photonic integrated circuits (PICs) increases, on-chip detectors are required to monitor their working point for reconfiguration and stabilization operations. We propose to exploit the photoconductive properties of a-Si:H<sup>[1]</sup> by depositing a thin film on top of the waveguide and making the evanescent tail of the guided mode interact with a-Si, as schematized in Figure 1. The detector is integrated on a channel  $\text{Si}_3\text{N}_4$  waveguide with a core thickness of 200 nm cladded with a 600-nm thick layer of HSQ. The waveguide width  $w = 400$  nm guarantees single-mode propagation down to a wavelength of 630 nm. The HSQ layer is locally lowered to a thickness  $h_c = 200$  nm in order to guarantee the proper overlap of the optical mode with the a-Si:H top layer.

To selectively remove the HSQ cladding, direct laser writing (DLW) lithography on a AZ5214E photoresist was used to protect the HSQ upper cladding outside the trench area from the successive RIE process. Then, a 200-nm-thick a-Si:H film is deposited by PECVD with a substrate temperature of 300 °C. The film was then patterned with DLW technique followed by RIE to define an interaction region with the waveguide core of 50  $\mu\text{m}$ , ensuring a light absorption of 2 dB (37%).

The work is supported by the EC H2020 grant 829116 Super-Pixels in collaboration with JWNC at Glasgow University

[1] R. A. Street, Hydrogenated Amorphous Silicon, Cambridge University Press (1991). ISBN 9780511525247

[2] B. Desiatov et al., Applied Physics Letters, 115(12), 121108 (2019).

In Figure 2 some fabrication steps are represented while in Figure 3 a top view of the realized and measured device is presented.

The reference dark current is about 50 pA at  $V_e = 8$  V, corresponding to a resistance of 160 G $\Omega$  between the electrodes, limiting the device sensitivity to -45 dBm. Above the sensitivity threshold, we observe a change of the photocurrent versus the optical power  $P_d$  across a dynamic range of more than 20 dB, the maximum power of -25 dBm being limited by the loss of the experimental setup. Experimental results show that, when  $P_d = -30$  dBm ( $P_{abs} = 370$  nW), a photocurrent of 11 nA is measured for  $V_e = 8$  V, as plotted in Figure 4, resulting in a responsivity  $R_{ph}$  of about 30 mA/W, in line with similar devices<sup>[2]</sup>. We can estimate an increase of the a-Si conductivity to 0.68 mS/cm, that is more than four orders of magnitude larger with respect to the dark level value (18 nS/cm). The time-domain response of the a-Si photoconductor was assessed by detecting an intensity-modulated optical signal propagating in the  $\text{Si}_3\text{N}_4$  waveguide. A very fast response is observed in the first part of the transient, which is associated with the effective lifetime of free carriers  $\tau_{eff}$  and is expected to occur in a time scale of several ns.

Due to the well-assessed photogeneration properties of a-Si which extend across the entire visible-light range, the presented photoconductor concept can be extended to lower wavelengths. Finally, the additive CMOS-compatible fabrication process makes the device concept portable to any photonic platform for visible-light applications.

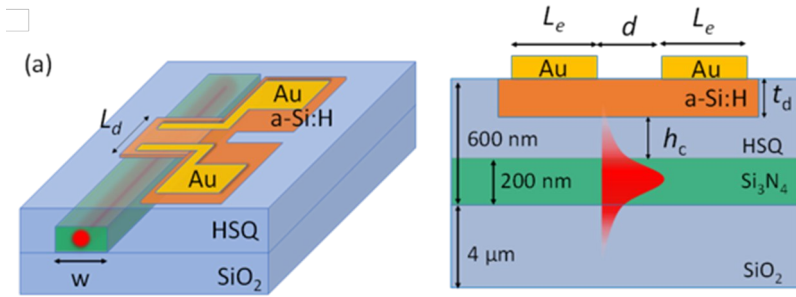


**Figure 1** Overview of the working principle.

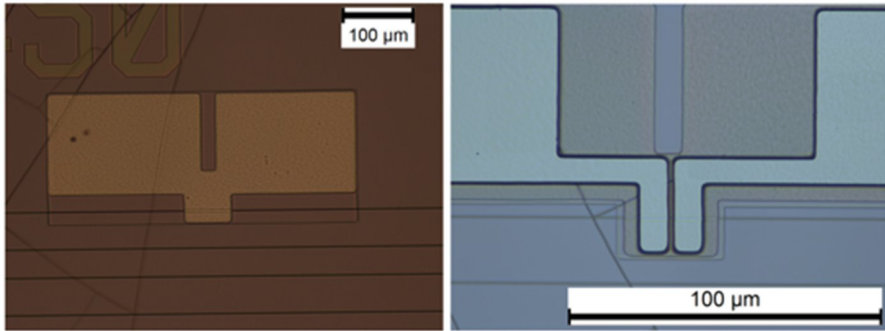


**Figure 2** Detail of the a-Si patterning and the pad lithography.

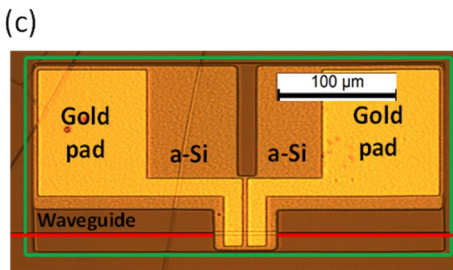


**Figure 3** Top view photograph of the realized device.

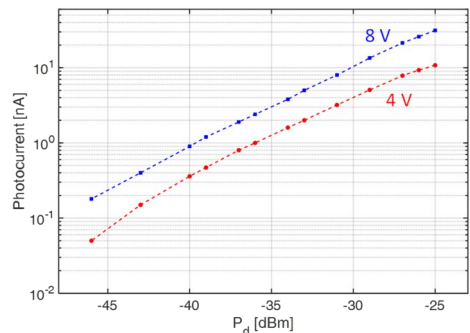


**Figure 4** Measured photocurrent vs optical power  $P_d$  reaching the detector when a DC bias of 4 V (red) or 8 V (blue) is applied.

# Antireflection coating in LWIR for TMOS performance improvement

C. De Vita<sup>1</sup>, F. Morichetti<sup>1</sup>, A. Melloni<sup>1</sup>, M. Asa<sup>2</sup>, C. Somaschini<sup>2</sup>, G. Bruno<sup>3</sup>, L. Castoldi<sup>3</sup>, G. Allegato<sup>3</sup>

<sup>1</sup>Dipartimento di Elettronica, Informazione e Bioingegneria (DEIB), Politecnico di Milano, Via Ponzio 34/5, 20133 Milano, Italy.

<sup>2</sup>Polifab, Politecnico di Milano, Via Colombo 81, 20133 Milano, Italy;

<sup>3</sup>STMICROELECTRONICS, Via Camillo Olivetti 2, 20864 Agrate Brianza, Italy.

A TMOS is an uncooled, thermally isolated, floating MOS transistor operating at subthreshold, that can be exploited to sense temperature changes induced by either a physical or a chemical phenomenon<sup>[1]</sup>. The sensor is based on a unique and innovative CMOS-SOI MEMS technology and is manufactured at STMICROELECTRONICS.

The device is composed by a 3-layer stack, with a bottom Silicon cap thick 150  $\mu\text{m}$ , a top cap of 130  $\mu\text{m}$  and the device encapsulated between the two caps for thermal isolation, as shown in Figure 1. The sensor operates at room temperature and above, corresponding to a radiation at a wavelength of about 10  $\mu\text{m}$ . A large part of the incoming radiation is reflected at the air-silicon interfaces because of the large silicon refractive index (3.4), reducing the sensitivity of the sensor. The scope of this work is to study and test an antireflection coating (ARC) layer to be deposited on the silicon top cap to increase the sensitivity by reducing the backreflection.

The antireflection is achieved with a quarter wavelength thick layer with a refractive index  $n_{\text{ARC}}=(n_{\text{air}}n_{\text{Si}})^{1/2}=1.86$ . Among the few available materials transparent at 10  $\mu\text{m}$ , ZnS is the one that is more suitable, both for its optical characteristics (highly transparent,  $n=2.27$ ) and the TMOS compatibility of the deposition process<sup>[3]</sup>.

The depositions of the ZnS films were performed with an Evatec BAK 640 machine at Polifab. Measurements showed that the ZnS film deposited on a silicon substrate at room temperature exhibits a very poor adhesion. Instead, with depositions at 200°C the film shows a compressive stress

higher than -200 MPa, corresponding to an excellent adhesion. Unfortunately, such a high temperature is not compatible with the TMOS process flow.

A successful strategy to increase the adhesion at room temperature consists in the addition of a very thin layer of another material between the silicon substrate and the ZnS film. We found that adding a 20-nm thick layer of  $\text{Al}_2\text{O}_3$  the adhesion problems are solved reducing the ZnS film stress to -240 MPa, compared to the -350 MPa without alumina, as shown in Figure 2. The simulated transmittance improvement is around 20% in case of a single ARC layer on top of the cap. Figure 3 reports the simulated transmission, reflection, and losses in case the ARC layer is deposited on both sides of the Silicon cap. The transmission increases by 66%. FTIR measurements on silicon bare wafers confirmed the results and a complete TMOS device has been realized with the ARC based cap. Sensitivity measurements made with a black body emitter demonstrated an improvement of 16% in the case of a single ARC deposited on the cap external surface and an 86% improvement with an ARC on both sides. Results are reported in Figure 4.

From the first trial wafers, more than 200 wafers have been processed. Further, TXRF analysis were carried out on each involved Polifab machine to test the contamination and the compatibility of the process with the STM production lines. The results have been successful, almost doubling the sensitivity of the final sensor. Further activities have been planned for the optimization of the TMOS towards other applications in a short future.

The work is performed within the Joint Research Centre “MEMS” and “STEAM” agreement between Politecnico di Milano and STMICROELECTRONICS.

[1] A. Zviagintsev et al., COMCAS, 1–5 (2015).

[2] L. Gitelman et al., Tmos novel uncooled sensors - theory and practice, COMCAS, 1–8 (2008).

[3] C. De Vita et al., Optical Materials Express, 12, 1 (2022).

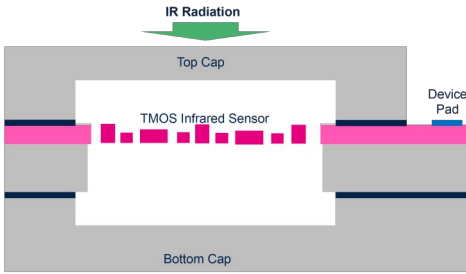


**Figure 1** TMOS stack in the ST process flow.

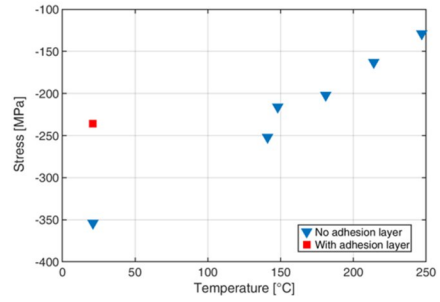


**Figure 2** Stress measurements with (red) and without (blue)  $Al_2O_3$  adhesion layer.

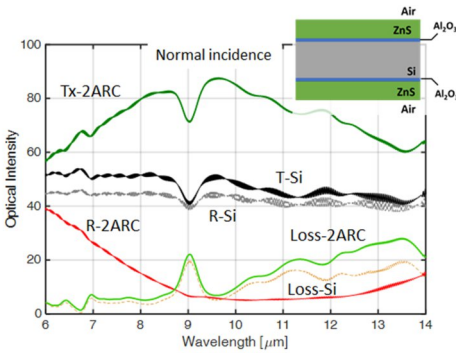


**Figure 3** Simulated Tx, Rx and Loss for bare Silicon and double ARC stack.

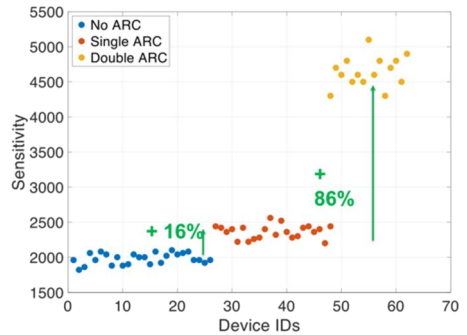


**Figure 4** Measured sensitivity for TMOS without ARC (blue), with single ARC (red) and with double ARC layer (yellow).

# Development of crosspoint memory arrays for neuromorphic computing

S. Ricci, P. Mannocci, M. Farronato, D. Ielmini

Dipartimento di Elettronica, Informazione e Bioingegneria (DEIB), Politecnico di Milano, Via Ponzio 34/5, 20133 Milano, Italy.

Resistive switching memory (ReRAM) is a novel memory class which is gaining a huge interest thanks to the capability of changing the electrical properties, as the resistance, according to different external voltage pulses. They rely on the local change of oxygen vacancy concentration to create and tune conductive paths with suitable conductances. The output current is proportional to the voltage applied and to the conductance, which can be programmed at analog grade. These devices can execute matrix-vector multiplication (MVM), the backbone of most machine learning and scientific computing algorithm, in parallel within the crosspoint array configuration, as in Figure 1a and Figure 1b, by summing the currents according to the Kirchhoff's law and multiplying voltage vector and conductance matrix by the Ohm's law in just one operation.

The worst limiting factor to the use of such components is the forming, the initial oxide breakdown process which initializes the RRAMs creating a conductive path in the device, which usually requires large voltages able to disturb and damage other devices in the passive crossbars. Figure 1c follows the optimization process adopted to reduce and even suppress the forming in Pt/HfO<sub>2</sub>/Ti stack, by thinning the oxide layer till a thickness comparable with the film roughness and exploiting the natural substoichiometric composition coming from the e-beam evaporation. Set and reset operations are thus possible after initialization, showing a butterfly-like hysteresis, in Figure 2a, which is increasingly wider with the compliance current (IC), maximum value the current can reach to prevent damages and possible short-circuits. The conductance values reached during the set transition, in Figure

2b, linearly depend on the ICC while the HRS is independent. The gradual behavior of the response during the reset suggests the possibility of controlling the device state by controlling the reset voltage during the sweep, as visible in Figure 1c, where the device is gradually reset and the hysteresis curves gradually move from the LRS to the HRS.

The tuning of the electrical properties and the possibility of performing MVMs in one step can be exploited to speedup mathematical operations, which massively rely on multiplication steps, as the power iteration, used to extract the matrix eigenvectors. Figure 3a sketches the equivalent circuit implementation of a fully memristive architecture for the power iteration. The output current of the MVM is converted in voltage amplitude through a proper gain of the transimpedance amplifier, and feed again the input. At each iteration the current values get closer to an asymptotic value link to the greatest eigenvector of the matrix, encoded in the conductances. This algorithm is particularly useful in the data science field, where huge amount of data must be clustered and organized. The Iris dataset, in Figure 3b for example, contains images of the Iris flowers categorized according to the sepal and petal lengths and widths. By extracting the eigenvectors of the covariance matrix, a matrix which represent the dataset and it is thus associated to the problem, it is possible to represent the data as linear combination of the extracted eigenvectors and thus distinguish the flowers, as in Figure 3c. The 98% accuracy, comparable with the software results, confirms the RRAMs as suitable elements for next generation of computing architectures, in-memory computing and hardware accelerator implementations.

<sup>[1]</sup> S. Ricci et al., Lecture Notes on Electrical Engineering, (2022). (To be published)

<sup>[2]</sup> S. Ricci et al., Advanced Intelligent Systems, 4, 2200053 (2022).

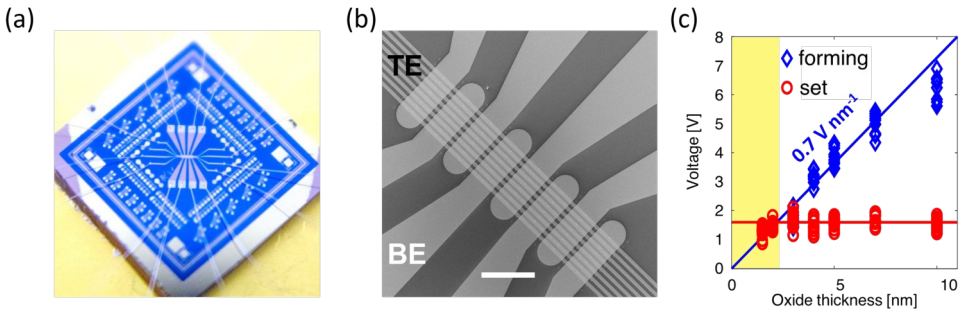


**Figure 1** Optimization of Non-Volatile Crossbar. a) Optical image of an 8x8 bonded crossbar. b) SEM image of an 8x8 crossbar optimized to reduce the line resistance and minimize the  $I$ - $R$  drop. c) Optimization process to suppress the forming voltage and achieve the forming-free condition.

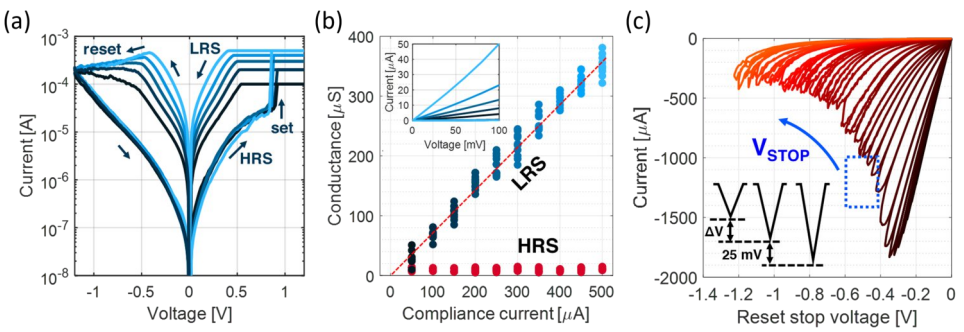


**Figure 2** Main electrical properties of non-volatile memories. a)  $I$ - $V$  sweeps with set and reset transitions at different compliance currents ( $I_C$ ), showing memristive hysteresis. b) Conductance levels achieved by tuning  $I_C$  during the set operation. c) Gradual reset sweep to decrease the device conductivity and come back to the HRS.

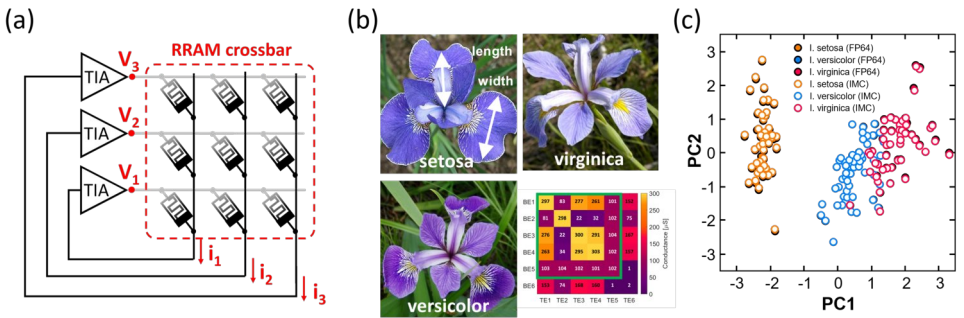


**Figure 3** RRAMs for in-memory computing applications. a) Equivalent circuit for power iteration and eigenvector extraction. The output currents of the MVM are converted in voltages and feed the circuit after proper scaling. As a result, the currents converge to asymptotic values associate to the eigenvector of the matrix. b) Iris dataset entries examples, with the three types of flowers classified according to length and width of sepals and petals, and the associated covariance matrix. c) Data clustering and comparison with software implementation. By using the first two eigenvectors to represent the dataset, data gives rise to three distinguishable groups, according to the flower properties.

# Memtransistor devices based on MoS<sub>2</sub> for memory and neuromorphic applications

M. Farronato<sup>1</sup>, P. Mannocci<sup>1</sup>, S. Ricci<sup>1</sup>, A. Bricalli<sup>2</sup>, M. Melegari<sup>1</sup>, C. Monzio Compagnoni<sup>1</sup> and D. Ielmini<sup>1</sup>

<sup>1</sup>Dipartimento di Elettronica, Informazione e Bioingegneria (DEIB) and IUNET, Politecnico di Milano, Via Ponzio 34/5, 20133 Milano, Italy.

<sup>2</sup>Weebit Nano, Hod Hasharon, Israel

In the last twenty years, a broad range of emerging memory technologies have been proposed as storage class memory (SCM) toward bridging the gap between high-performance memory and low-cost storage devices. Novel memory devices are also essential for developing low power, fast and accurate in-memory computing and neuromorphic engineering concepts that can compete with the conventional CMOS digital processors. 2D semiconductors, such as transition metal dichalcogenides (TMDs), provide a novel platform for advanced semiconductors, thanks to their atomic-scale thickness and their strong potential for 3D integration<sup>[1]</sup>. We present a three-terminal device called memtransistor, based on multilayer MoS<sub>2</sub> with ultra-short channel length. The device is a transistor with also a memristive characteristic. Depending on the channel length ( $L_{channel}$ ) and the physics mechanism exploited, the device can be used as a memory<sup>[2]</sup> or as a powerful computing device<sup>[3,4]</sup>.

Figure 1 shows the 3D sketch of the memtransistor, consisting of a three-terminal device with a back-gate structure. The MoS<sub>2</sub> is transferred by mechanical exfoliation on the CVD oxide. The thickness of the flakes is in the order of few atomic layers (Figure 2). Source and drain contacts are obtained by thermal evaporation of Ag after patterning by Electron Beam Lithography (EBL). Two types of devices are obtained depending on the distance between the two electrodes. When  $L_{channel}$  is below 50 nm, the device exhibits a switching characteristic thanks to the Ag cation migration between the two electrodes. This device is called ion-based memtransistor to distinguish it from the electron-based memtransistor in which charge trapping is exploited to obtain an

analog synaptic characteristic. The last device has a longer channel to avoid the ion migration between source and drain terminals. Figure 3 shows a Scanning Electron Microscopy (SEM) image of the channel region of an ion-based memtransistor with  $L_{channel} = 18$  nm.

Figure 4 shows the transcharacteristic of the memtransistor (both ion- and electron-based). The large hysteresis is due to the presence of trapping centers at the interface between the semiconductor and the oxide.

At relatively large  $V_{DS}$  values, the ion-based device shows a resistive switching (Figure 5). This event is attributed to the formation of a conductive filament (CF) on the surface of the MoS<sub>2</sub> channel. We provided an extensive study of the device physics and operations<sup>[2]</sup>. A demonstration of the implementation of a chain-type memory array (like NAND flash) entirely composed by ion-based memtransistors (Figure 6) pave the way for high density memory array based on 2D semiconductors.

The charge trapping is instead exploited to obtain the synaptic characteristics with electron-based memtransistors (Figure 7). Synaptic potentiation/depression are obtained moving the device threshold and analogically changing the channel conductance. The linearity of the characteristic makes the device extremely promising for the implementation of hardware neural network accelerators<sup>[3]</sup>. In addition, the dynamic characteristic of the device is exploited for the realization of the reservoir in a reservoir computing (RC) system for image recognition (Figure 8)<sup>[4]</sup>. The results make the memtransistors a promising technology for future high-density neuromorphic computing concepts.

[1] G. Fiori et al., Nature Nanotechnology, 9(10), 768–779 (2014).

[2] M. Farronato et al., Advanced Electronic Materials, 8, 2101161, (2022).

[3] M. Farronato et al., 2022 IEEE 4th AICAS, Incheon, Korea, (2022).

[4] M. Farronato et al., Advanced Materials, 2205381 (2022).

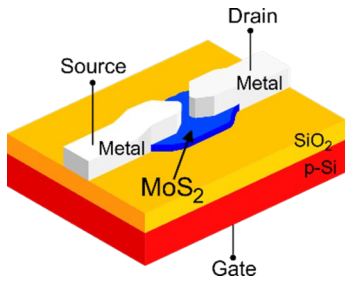


**Figure 1** Schematic of the memtransistor.

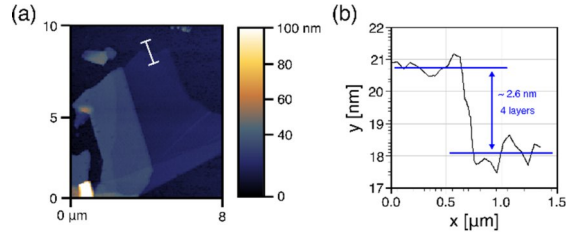


**Figure 2** (a) Atomic force microscopy (AFM) image of an exfoliated MoS<sub>2</sub> flake. (b) Profile across the trace in (a).

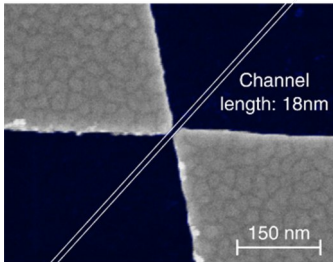


**Figure 3** SEM image of an ion-based memtransistor.

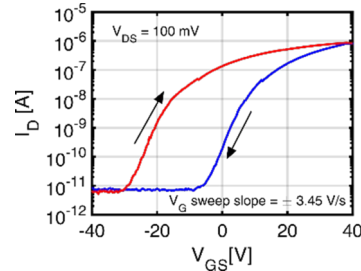


**Figure 4**  $I_D$ - $V_{GS}$  characteristic of memtransistors.

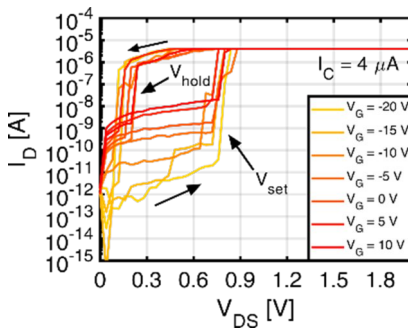


**Figure 5** Switching cycles of the ion-based memtransistor.

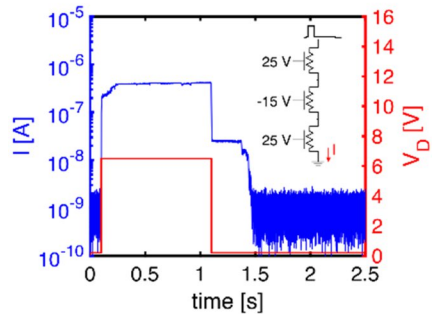


**Figure 6** Implementation of a chain-type memory array architecture with three ion-based memtransistors.

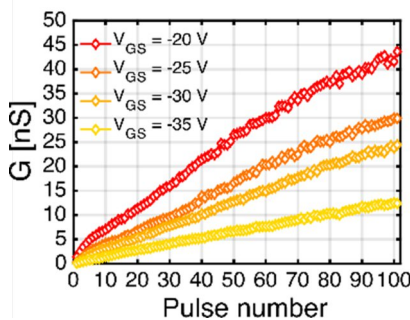


**Figure 7** Synaptic characteristics of an electron-based memtransistors.

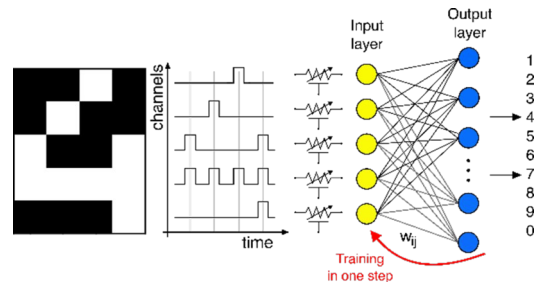


**Figure 8** Schematic of the reservoir computing system implemented using the electron-based memtransistor for pattern classification.

# SPOON – Silicon hyperuniform microfluidic channels

C. Barri<sup>1,2</sup>, P. Grassi<sup>2</sup>, L. Fagiani<sup>1,2</sup>, M. Bollani<sup>2</sup>

<sup>1</sup>Dipartimento di Fisica, Politecnico di Milano, piazza Leonardo da Vinci 32, 20133 Milano, Italy.

<sup>2</sup>Istituto di Fotonica e Nanotecnologie (IFN)-CNR, L-NESS, Via Anzani 42, 22100 Como, Italy.

The objective of our research activity in Polifab is to fabricate silicon microfluidic channels with a single and a double porosity patterned with a regular (homogeneous and heterogeneous) and a disorder hyperuniform morphology. The Environmental Fluid Mechanics laboratory (EFM) held by the professor P. De Anna (University of Lausanne), carries out the fluid transport analysis. The key objective is studying how the heterogeneity of the porous structure affects filtration processes of colloids. The data obtained will help the scientific community to model filtration processes embedding the heterogeneity of the pore space and to understand if a double porosity will increase the filtration properties of the structures.

The regular homogeneous and heterogenous design of the microfluidic channels has been studied by the EFM groups, instead the disorder hyperuniform (DHU) morphology has been obtained exploiting the instability of ultra-thin solid films during the research activity supported by the EU Project NARCISO. SiGe thin films have been epitaxially grown on ultrathin silicon on insulator. The desired DHU geometry characterized by transmitting pores and dead-end pores is obtained after the dewetting (annealing in an UHV environment) of the SiGe thin films (Figure 1)<sup>[1]</sup>.

The microfluidic designs, after an opportune scaling process, have been transferred to a physical hard-mask. Then, using the optical mask aligner Karl Süss MA56, they have been transferred on a Si wafer up to 4 inches. The structures are transferred by dry etching (Reactive Ion etching DP80 Plasmalab) to silicon. Since the microfluidic channels require a high aspect ratio to have enough fluid to be analyzed, the height of the channel must be at least 10  $\mu\text{m}$ . The channels obtained are characterized by a

single main porosity. Thanks to the lithographic facilities at Polifab we were able to obtain more appealing double porosity microfluidics channels. Such dual media are representative of several geological systems (from soil to carbonate rocks or karst) where fluids can move among the grains constituting the solid matrix of the system but also within the grains themselves that have a much smaller porous structure. The secondary porosity has been obtained by the combination of optical lithography and a reactive ion etching procedure. Opportune patterns of ordered disks, starting from the critical dimension diameter of 5  $\mu\text{m}$ , have been drawn on the photoresist using the maskless aligner (Heidelberg MLA100) and then they have been transferred in the Si surface by a RIE process. The thickness of the pillars is in the order of hundreds of nm (Figure 2 - Figure 3). The single and dual porosity of the microfluidic channels have been then covered by a PDMS flat chip with predrilled holes to let the inlet and outlet pipe reach the microfluidic channels (Figure 4).

Preliminary measurements on single porous channel have been performed. The EFM lab is able to collect the breakthrough curve of the colloids and we have proven the capability to observe the effect of the double porosity. Measurements of the double porous channels are being performed.

<sup>[1]</sup> M. Salvalaglio et al., Physical Review Letters, 125(12), 126101 (2020).

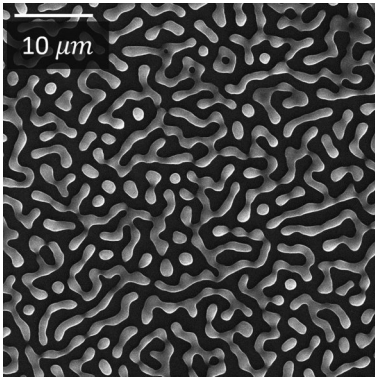


**Figure 1** Scanning electron microscope image (planar view) of a SiGe 150 nm dewetted structures. After an opportune scaling process the design has been transferred to a physical hard-mask to obtain the DHU microfluidic channels.

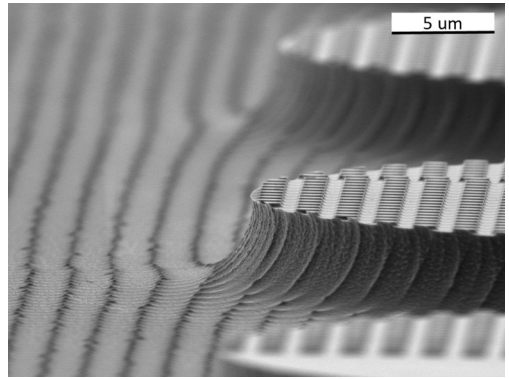


**Figure 2** Scanning electron microscope image (tilt view 60°) of a silicon homogeneous microfluidic channel characterized by dual porosity.

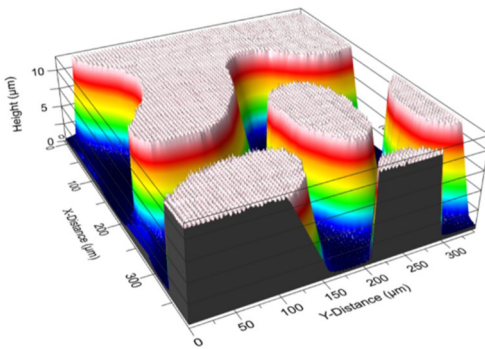


**Figure 3** Filmetrics Profil3D characterization of one disorder hyperuniform silicon microfluidic channel characterized by a dual porosity.

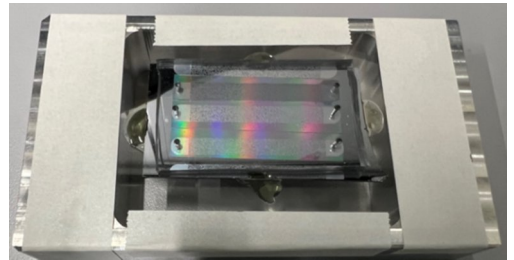


**Figure 4** Three microfluidic channels covered by a predrilled plasma bond flat PDMS chip placed on the microscope stage adapted for the microfluidic analysis.

# Fabrication of erbium-doped diode on a silicon-on-insulator (SOI) platform

G. Tavani, C. Barri, M. Bollani

L-NESS, Dipartimento di Fisica, Politecnico di Milano, Via Anzani 42, 22100 Como, Italy.

Quantum communication is expected to cover several market needs in the years to come<sup>[1]</sup>. For this reason, quantum key distribution (QKD) protocols have been implemented using both single photon sources and attenuated laser pulses, towards the integration on photonic chips<sup>[2]</sup>. Recent works on the security bounds for decoy-state QKD have opened new opportunities to use silicon light sources with an arbitrary photon emission statistic, including weak sources based on multiple emitters<sup>[3]</sup>.

In our work, we carried out the fabrication and a first optical characterization of a silicon diode doped with erbium that behaves like such a weak photon source, compatible with the emission of light at telecom wavelength at 1550 nm directly in a silicon chip<sup>[4]</sup>.

The device consists in a silicon planar junction with a central region, nearby the p-n depletion area, doped with erbium and oxygen atoms. Upon setting a potential difference between the p-n regions, photons are created by the electroluminescence of erbium ions (Figure 1). The expected advantages of this kind of device are its emission centered in the third telecommunication window (1520 nm – 1550 nm), its working range of temperature between 77 K and 300 K. To increase the erbium luminescence yield at room temperature, an oxygen co-doping has been introduced<sup>[5]</sup>.

Three samples were fabricated and characterized, they differ from each other by the size of the erbium doped area: in the first device it is equal to  $1\ \mu\text{m} \times 1\ \mu\text{m}$  (Figure 1), in the second one to  $15\ \mu\text{m} \times 15\ \mu\text{m}$  and in the last one to  $50\ \mu\text{m} \times 50\ \mu\text{m}$ .

The devices were fabricated through a top-down process performed by a combination of electron beam lithography, reactive ions etching, electron beam physical vapor deposition and ion implantation starting. The entire process was performed on a 220 nm thick Si layer on a  $2\ \mu\text{m}$  thick  $\text{SiO}_2$  buried oxide layer. The first step was the definition of the mesa structure, followed by the doping of the n area with phosphorus, of the p area with boron as well as of the optically active zone, in the center of the device, with erbium and oxygen. All the dopants were introduced by ion implantation and activated with a rapid thermal annealing processes. The final step was the definition of the two gold contacts on top of the n and p regions (Figure 2).

The correct electrical and optical behavior of the diodes depends on the doping process that is made of three steps. First, the left pad is doped with phosphorous, then the right pad is doped with boron and finally, the central region is co-doped with erbium and oxygen. It is crucial that the doping is introduced only in the right region, protecting the rest. This was carried out evaporating a 100 nm-thick  $\text{SiO}_2$  layer over all the device except the region to be doped. (Figure 3). The doping was performed by using a 400 kV High Voltage Engineering ion implanter. The  $\text{SiO}_2$  was then removed with an HF bath.

In conclusion, we presented the design and fabrication of an erbium-doped diode on a SOI platform.

[1] F. Cavaliere et al., *Quantum Reports*, 2(1), 80-106 (2020).

[2] M. Avesani et al., *npj Quantum Information*, 7(1), 1-8 (2021).

[3] G. Foletto et al., *Physical Review A*, 105(1), 012603 (2022).

[4] M. Di Giancamillo et al., *EPJ Web of Conferences* 255, EOSAM21 (2021).

[5] F. Priolo et al., *Physical Review B*, 57(8), 4443 (1998).

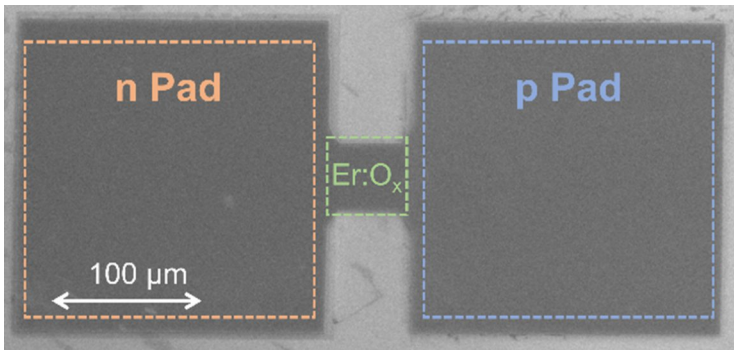


**Figure 1** A scanning electron microscope image (SEM) of one of the fabricated devices. In this device, the erbium-doped central area is 50 μm × 50 μm.

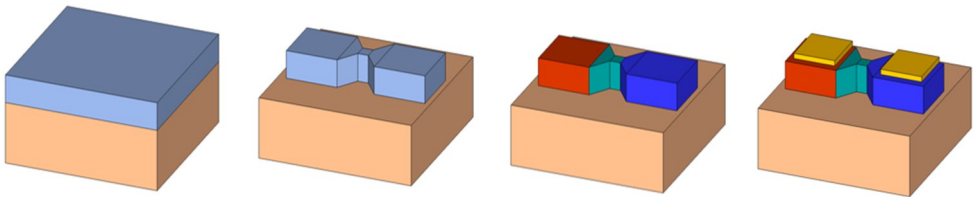


**Figure 2** Fabrication flow of the device. In red, the p-area doped with boron. In blue, the ones doped with phosphorous and in green, the region co-doped with erbium and oxygen. The electrical contacts made of titanium and gold and they are sketched in yellow.

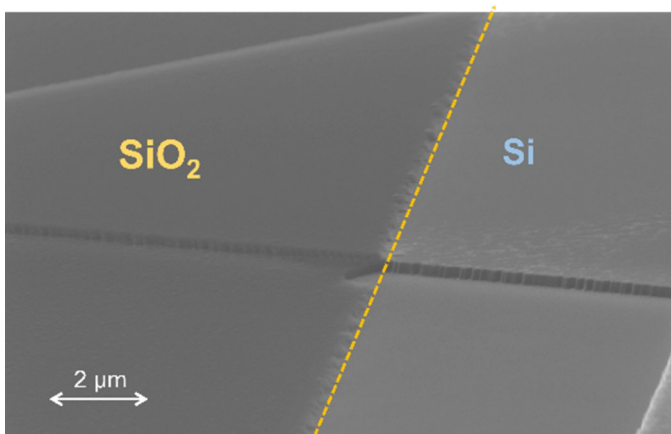


**Figure 3** SEM tilted view of the 100 nm SiO<sub>2</sub> protecting layer used during the doping procedure. The left part is covered with SiO<sub>2</sub> so dopants will not be implanted in the Si beneath. The right part is left uncovered and it will be doped.

# Impact of substrate doping on the performance of vertically illuminated Ge-on-Si photodetectors

R. Giani, S. Calcaterra, A. Barzaghi, A. Ballabio, J. Frigerio and G. Isella

L-NESS, Dipartimento di Fisica, Politecnico di Milano, Via Anzani 42, 22100 Como, Italy.

Germanium on silicon photodiodes have been studied for more than twenty years, mainly for integrated photonics in a waveguide configuration.<sup>[1]</sup>

These devices tolerate fairly high dark current densities since the small volume and high optical power results in a sufficiently large signal to noise ratio.

Vertically illuminated photodetectors are instead required for imaging applications of interest in the automotive and biomedical areas. In this case, a sufficiently low dark current density is required for the fabrication of multipixel devices.<sup>[2,3]</sup>

In recent years the reduction of threading dislocations<sup>[4]</sup> and the implementation of surface passivation<sup>[5]</sup> strategies have been investigated in order to reduce the dark current density. Instead, the effect of doping in the silicon-germanium heterostructure on the dark current has been not fully analyzed.

In order to evaluate the impact of silicon substrate doping on dark current and photoresponse, a set of germanium photodiodes were grown by LEPECVD and microfabricated by optical lithography (Figure 1).

All the investigated photodiodes feature a 1500 nm thick, nominally intrinsic germanium layer and a heavily doped germanium top contact layer with a thickness of 100 nm. The silicon substrates doping has been varied from  $10^{14} \text{ cm}^{-3}$  to  $10^{19} \text{ cm}^{-3}$ .

Current/voltage measurements have been performed on devices featuring different diameters to obtain the bulk and surface contribution to the total dark current

density.

Temperature dependent current/voltage and capacitance/voltage measurements have been performed to highlight the relative weight of the different physical mechanisms giving rise to the dark current such as diffusion, generation-recombination and trap-assisted tunnelling.

To characterize the photoresponse of the photodetectors, the responsivity and the specific detectivity were measured for photodiodes at the interesting wavelengths (1000-1700  $\mu\text{m}$ ) and for different negative biases.

We have observed a monotonic dependence of photodiodes performance as a function of substrate doping, highlighting the relevant role of substrate resistivity in Ge on Si devices.

[1] J. Michel et al., *Nature Photonics*, 4, 527 (2010).

[2] R. Kaufmann et al., *Journal of Applied Physics*, 110, 023107 (2011).

[3] G. Xu et al., *IEEE Photonics Technology Letters*, 34(10), 517-520 (2022).

[4] H. Tetzner et al., *Applied Physics Letters*, 119, 153504 (2021).

[5] J. Isometsa et al., *APL Materials*, 9, 1111113 (2021).

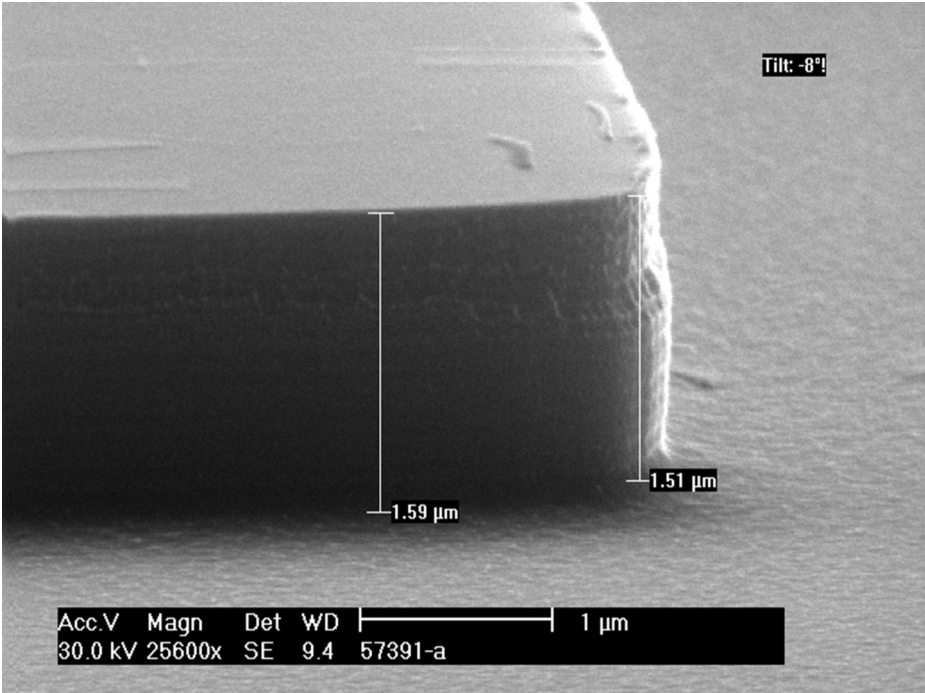


**Figure 1** SEM image of the germanium MESA structure obtained by Microlithography and Reactive Ion Etching

# SiGe waveguides for mid-infrared nonlinear photonics

*J. Frigerio, V. Falcone, A. Barzaghi, S. Calcaterra, R. Giani*

L-NESS, Dipartimento di Fisica, Politecnico di Milano, Via Anzani 42, 22100 Como, Italy.

In recent years, mid-infrared integrated photonics has raised an increasing interest due to the envisioned applications in molecular sensing, environmental monitoring and security. The Silicon-on-insulator (SOI) based technology, operating at wavelengths  $\lambda < 3.2 \mu\text{m}$  has already reached a significant technology readiness level. By leveraging the maturity of the SOI technology and taking advantage of the high index contrast between Si and  $\text{SiO}_2$  many functionalities such as low-loss waveguiding, modulation and frequency comb generation have already been demonstrated. Nevertheless, extending the operational wavelengths toward the long-wave infrared region (LWIR) ( $8 \mu\text{m} - 12 \mu\text{m}$ ) present many challenges. In this context the SiGe-on-Si material platform seems particularly promising. First of all, by taking advantage of the wide transparency range of Ge, low-loss waveguides operating up to  $\lambda = 11 \mu\text{m}$  have been recently demonstrated, as well as a whole set of passive photonic components including Mach-Zehnder interferometers, resonators and spectrometers. Also electro-optic modulation based on plasma effect has been recently reported. Nevertheless, key functionalities such as wavelength conversion, photodetection and high speed optical modulation are still missing. In this framework, Ge/SiGe quantum wells could be exploited to fill this gap. Intersubband optical transitions in the valence band of such heterostructures can be used for light detection, for high-speed modulation through the quantum confined Stark effect (QCSE), and for wavelength conversion through second harmonic generation. Ge/SiGe QWs can be easily grown on top of SiGe buffers, making them fully compatible with the existing SiGe-on-Si material platform. We recently demonstrated mid-infrared second harmonic generation in

prism-cut Ge/SiGe QWs<sup>[1]</sup> and we are now moving toward waveguide integration, that requires the development of a fabrication procedure suitable to process rib waveguides with an height of  $6 \mu\text{m}$ .

In Figure 1 it is shown a section of a rib waveguide with an height of  $6 \mu\text{m}$  and a width of  $10 \mu\text{m}$ . A careful optimization of the etching protocol has been carried out in order to obtain vertical sidewalls with a very low roughness, which is crucial to minimize the propagation losses.

[1] J. Frigerio et al., ACS Photonics, 8(12), 3573-3582 (2021).

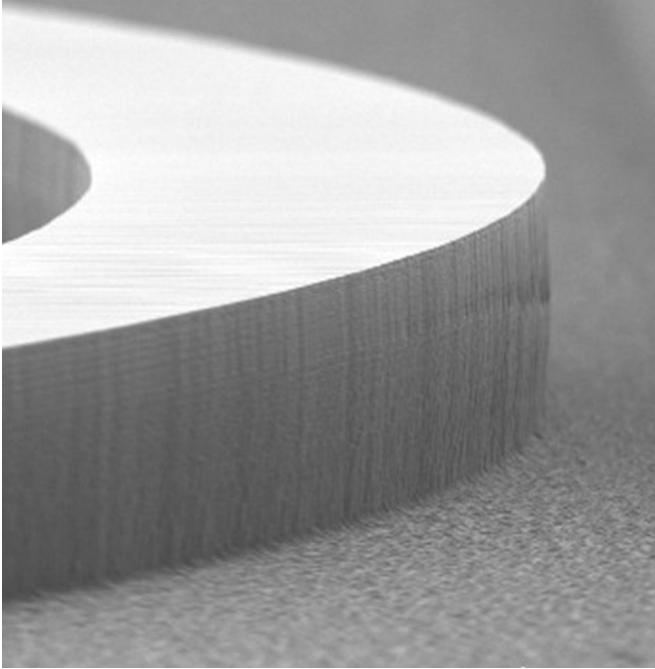


**Figure 1** *SiGe waveguide with embedded quantum wells.*

# Thermal phase shifters for femtosecond-laser-written universal photonic processors

M. Gardina<sup>1</sup>, C. Pentangelo<sup>2,1</sup>, F. Ceccarelli<sup>1</sup>, R. Osellame<sup>1</sup>

<sup>1</sup>Istituto di Fotonica e Nanotecnologie (IFN)-CNR, piazza Leonardo da Vinci 32, 20133 Milano, Italy.

<sup>2</sup>Dipartimento di Fisica, Politecnico di Milano, piazza Leonardo da Vinci 32, 20133 Milano, Italy.

Programmable photonic integrated circuits (PICs) are a leading platform for classical and quantum information processing and computing. Among programmable PICs, universal photonic processors (UPPs) are of particular interest because they can implement any unitary transformation among  $N$  input/output optical signals. UPPs are typically implemented by a mesh of programmable Mach-Zehnder interferometer (MZI) cells, in which reconfigurability can be achieved by means of thermal phase shifters, i.e. resistive micro-heaters able to tune the optical properties of the circuit by exploiting the thermo-optic effect.

Among the many available technological platforms, femtosecond laser writing (FLW) of glass substrates displays excellent features for quantum applications. As an example, the rapid and cost-effective prototyping enabled by FLW allows the development of complex 3D waveguide layouts. However, the complexity of FLW-UPPs is limited to six optical modes<sup>[1]</sup> by the phase-shifter fabrication technology, currently based on the laser ablation of a single metal film for both micro-heaters and interconnections.

A novel thermal phase shifter fabrication process is here briefly presented. Chromium and copper are employed as high and low resistivity metals for micro-heaters and interconnections, respectively.

Photolithography is performed via a maskless aligner on a dry-film photoresist, which provides a uniform coverage of the deep trenches used to provide thermal isolation (Figure 1a). Chromium is first evaporated and etched, after the first lithography step, with a dedicated commercial mixture (Figure 1a). Copper is evaporated once the chromium features are

patterned with a thin titanium adhesion layer and etched with a custom acid solution (Figure 1b).

The process is completed with a vacuum annealing at 400°C for one hour in order to prevent the downward drift of the electrical resistance in the long-term operation. On the other hand, a silicon nitride passivation layer is needed to prevent the metal oxidation and the consequent upward drift of the micro-heater resistance. The packaging finalizes the UPP fabrication process: the glass chip is mounted on an aluminum heat sink along with electrical printed circuit boards, to which copper pads are electrically connected via wire-bonding.

The double-metal structure ensured a parasitic resistance lower than 1%. The electrical resistance stability was assessed at different operation powers and variations were reported to be below 0.02% over 10 hours of continuous operation. The process here described has been exploited for the assessment of compact geometries of the MZI unit cell on the basis of power dissipation (Figure 2a), thermal crosstalk (Figure 2b) and dynamic response. Thanks to these results, the MZI cell length was reduced from 9.93 mm to 5.92 mm<sup>[2]</sup>.

The fine optimization of the process variables allowed the achievement of a process resolution equal to the nominal photoresist one, i.e. 20  $\mu\text{m}$  (Figure 3). Such remarkable result enabled the use of a more compact implementation of the programmable MZI cell, encompassing the fabrication of micro-heaters on both the arms, thus opening the perspective of a 20-mode UPP within a 12 cm chip.

[1] C. Pentangelo et al., Proceedings of SPIE 12004, Integrated Optics: Devices, Materials, and Technologies XXVI, 120040B (2022).

[2] R. Albiero et al., Micromachines, 13 (7), 1145 (2022). Images used under CC License v4.0 <https://creativecommons.org/licenses/by/4.0/>

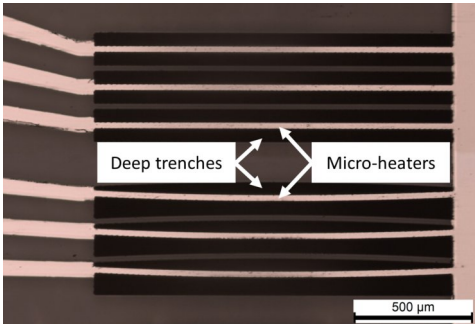


**Figure 1a** Chromium features patterned on different geometries of the thermal isolation structures. Picture from [2].

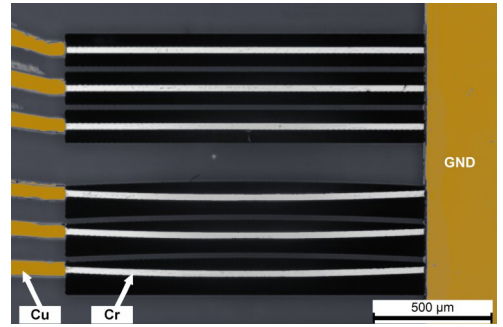


**Figure 1b** Chromium features patterned on different geometries of the thermal isolation structures. Picture from [2].

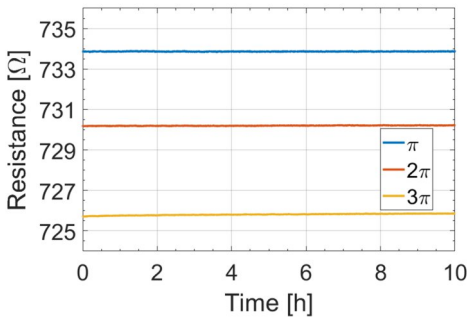


**Figure 2a** Electrical stability measurement at different optical power levels. Plot from [2].

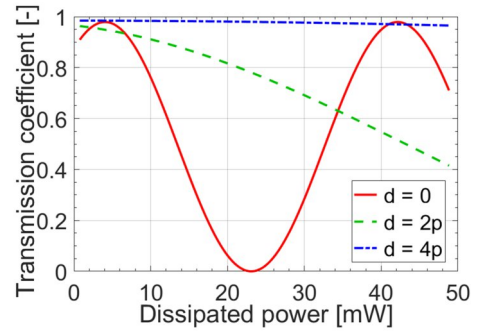


**Figure 2b** First ( $d=2p$ ) and second ( $d=4p$ ) neighbour thermal crosstalk compared with the transmission reconfiguration obtained on the target MZI. Plot from [2].

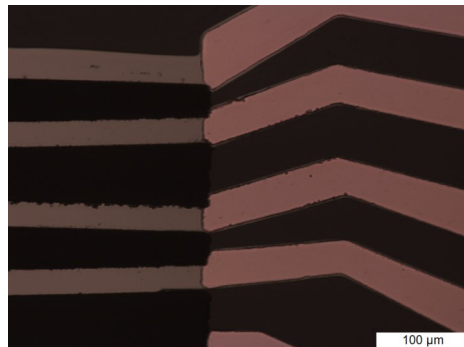


**Figure 3** Micro-heaters fabricated on each MZI arm with respective interconnections at a distance of 20 μm.

## Flat optics for light engineering

M. Almeida De Oliveira<sup>1,2</sup>, M. Piccardo<sup>1</sup>, G. Venturi<sup>1,2</sup>, A. Ambrosio<sup>1</sup>

<sup>1</sup>Center for Nano Science and Technology, Istituto Italiano di Tecnologia, Via G. Pascoli 70/3, Milano, 20133 Italy.

<sup>2</sup>Dipartimento di Fisica, Politecnico di Milano, piazza Leonardo da Vinci 32, 20133 Milano, Italy.

The research activity of the *Vectorial Nano-imaging* Research Line at the Fondazione Istituto Italiano di Tecnologia is devoted to engineering light in all the degrees of freedom: amplitude; phase; polarization.

The implemented platforms range from diffractive optical elements to semiconductive 2D materials, from metasurfaces to implanted quantum emitters. Common to all these approaches is the development of flat optical devices (with sub-wavelength thickness). Most of our work requires the use of clean room fabrication and characterization techniques, including Electron beam Lithography, Reactive Ion Etching, Thermal Annealing, Photolithography.

In 2022, we developed a structured light laser capable of producing vortex laser arrays with actively tunable topologies and non-local coupling dictated by the array's topology. The gain medium of our laser has a large transverse cross-section supporting many transverse modes, which we forced to be organized and form a lattice of a hundred laser beams by inserting a metasurface mask that modulates the phase and amplitude of the field. More specifically, the phase profile was designed to produce vortex beams with an annular intensity profile, useful for communication, microscopy, and lithography applications. Importantly, in our new laser arrays, the coupling network is not limited to the nearest neighbours, as for arrays of Gaussian lasers with no topological charge, but instead can be tailored to mix vortices that are widely separated in the lattice. Although several methods for generating a single vortex in a cavity have already been demonstrated, we have showed the conditions for generating vortex laser arrays in a single cavity, realizing a

platform to explore complex topological transformations and collective vortex effects at the source.

Solid-state quantum emitters provide a valuable avenue for quantum technologies. The engineering and control of single-photon emitters (SPEs) in diamond and silicon carbide serve as benchmarks for quantum emission from crystals. However, their 3D nature limits some of their applications. 2D materials can circumvent this problem, and they can also be integrated into standard CMOS technology. In this framework, wide bandgap hexagonal 2D boron nitride (hBN) SPEs have many advantageous properties, including high brightness, photostability, and most importantly, room temperature operation. Different forms of hBN have been studied, from bulk crystals epitaxial films to nanocrystals, and several techniques have been exploited to induce quantum emitting crystal imperfections.

In another experiment, we then characterized the efficacy of ion irradiation to generate emitters in hBN. We compared the throughput of different ions (Ne, Ga, C) in producing the largest number of defects within target hBN flakes. We also succeeded to tune the ion energy to address a specific penetration depth inside the mechanically exfoliated hBN. Additionally, the ion fluence was also spanned across a wide range. We conclude that boron atoms are displaced from lattice sites, creating boron vacancies. These become negatively charged and lead to emission in the NIR region.

M. Piccardo et al., *Nature Photonics*, 16, 359 -365 (2022).

S. Chiodini et al., *ACS Nano*, 16, 7589 – 7604 (2022).

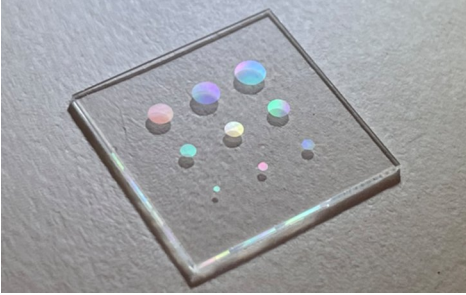


**Figure 1** Flat lenses on glass.

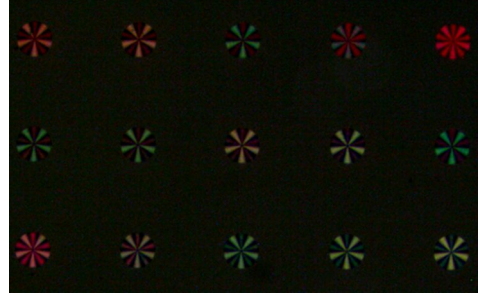


**Figure 2** Light from an array of dielectric metasurfaces.

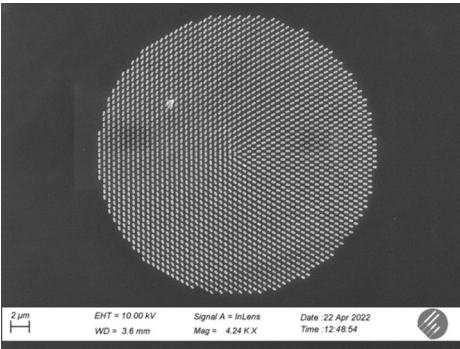


**Figure 3** SEM micrograph of a dielectric metasurface.

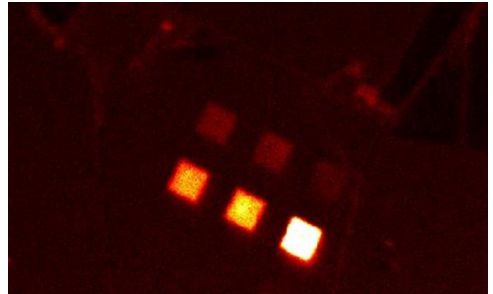


**Figure 4** Light from implanted defects in hexagonal Boron Nitride thin flake.

# Characterization of ferroelectric and state-change tunable materials for mm-wave applications

G. G. Gentili<sup>1</sup>, M. Khosronejad<sup>1</sup>, L. Codecasa<sup>1</sup>, U. Spagnolini<sup>1</sup>, L. Draghi<sup>1</sup>, L. Nobili<sup>1</sup>, L. Squillantini<sup>1</sup>, B. Marino<sup>1</sup>, G. Dotelli<sup>1</sup>, M. Cametti<sup>1</sup>, C. Mazzucco<sup>2</sup>, L. Resteghini<sup>2</sup>, A. Milani<sup>2</sup>

<sup>1</sup>Dipartimento di Elettronica, Informazione e Bioingegneria (DEIB), Politecnico di Milano, Via Ponzio 34/5, 20133 Milano, Italy & Dipartimento di Chimica, Materiali e Ingegneria Chimica "Giulio Natta" (CMIC), Politecnico di Milano, Piazza Leonardo da Vinci 32, 20133 Milano, Italy.

<sup>2</sup>Huawei Technology Italia Srl, Via Andrea Verrocchio 2, 20129 Milano, Italy.

Tunable materials offer a wide range of possible applications at mm-waves. Phase shifters, Tunable Intelligent Reflecting Surfaces, Variable capacitors are examples of devices for which tunable material offer a low-cost alternative with respect to PIN diodes, Varactors and MEMS.

An extensive test campaign was carried out at Polifab, DEIB (Dipartimento di Elettronica, Informazione e Bioingegneria) and CMIC (Dipartimento di Chimica) trying to explore the realizability (accuracy and repeatability) and the performances of BST ( $\text{Ba}_{1-x}\text{Sr}_x\text{TiO}_3$ , Barium, Strontium, Titanate) and GST ( $\text{GeSbTe}$  (germanium-antimony-tellurium) materials at mm-waves.

Test circuits in coplanar waveguide have been designed with the purpose of characterizing the material at RF with TRL calibration technique. Coplanar waveguide offer the best compromise in terms of accuracy and capability to apply a DC voltage to the material by the Bias-Tee functionality of the VNA. DC voltage is the control signal that is used to change the RF permittivity of the material itself.

BST and GST have been deposited on the waver substrate and as a subsequent step metalizations have been realized. Tunable materials with 1 mm x 1 mm total area and thin thickness of the order of few hundreds of nm have been with Physical Vapour Deposition (PVD) via magnetron sputtering. PVD is traditionally applied to standard photolithographic processes, and for this category of materials

to be tested and lift-off process was the straightforward choice used to obtain the desired features. Optimization of processing parameters, however, was required especially in consideration that a bias was imposed on the substrate with the aim to

better control the microstructure of the thin film. To support high temperature treatment of as deposited materials, required for BST to acquire the effective crystalline structure, fused silica wafers were used for lithography and deposition. Moreover, as the dielectric properties of BST films depend critically on the elemental composition, to preliminary evaluate the influence on the tunability, three largely different barium /strontium ratios, namely 70:30, 50:50 and 30:70, were prepared and characterized.

Results have been obtained by a multi-step inversion algorithm in which we first derived the permittivity of the glass, then the complex permittivity of the BST/GST with no Bias and finally the complex permittivity of the biased materials. Because of the intrinsic non-linear behavior of the material in terms of voltage-field curve, the inversion must necessarily account for all applied voltages in the inversion process. The final curve is a relationship field-permittivity that provides the basis for further deisgn of mm-wave components.

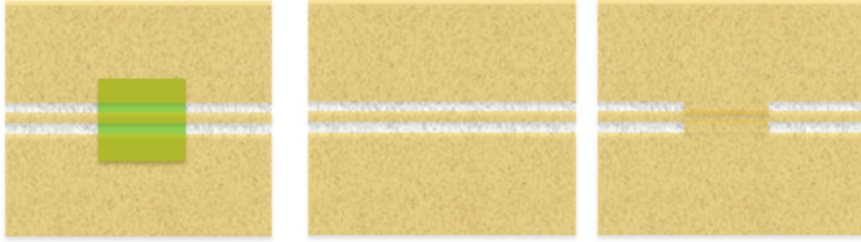


**Figure 1** TRL circuit in coplanar waveguide.

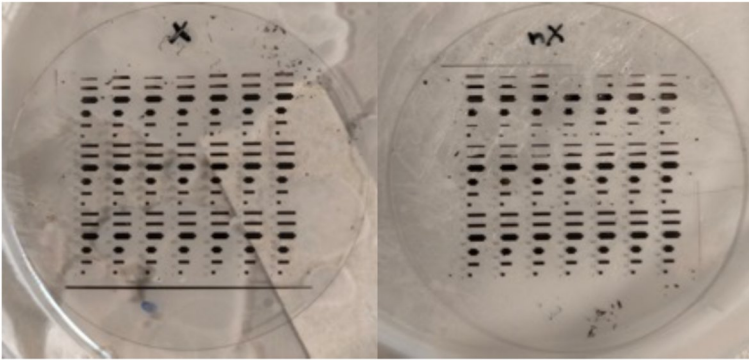


**Figure 2** Thermally treated and untreated GST material.

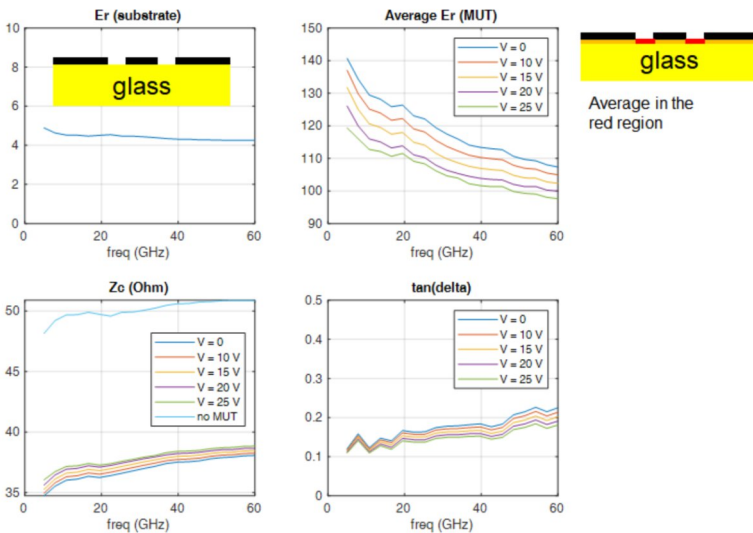


**Figure 3**

## Research Activity of PhyND group

*D. Girardi, V. Levati, M. Vitali, N. Pellizzi, M. Panzeri, I. Biancardi, E. Materassi, D. Petti, E. Albisetti*  
Dipartimento di Fisica, Politecnico di Milano, piazza Leonardo da Vinci 32, 20133 Milano, Italy.

The research activity carried out at Polifab has been focused mainly on three activities.

### **Synthetic Antiferromagnet (SAF) Microstructures for 3D magnonics.**

Scope of this activity was the optimization of magnetic structures for the nanoscale time-resolved imaging of propagating spin waves in three dimensions, using the recently developed time-resolved soft X-ray laminography (tr-SoXL) technique. Microstructures were patterned on top of  $\text{Si}_3\text{N}_4$  membranes at the Paul Scherrer Institute (PSI). Then, a Ru(4) / NiFe(40) / Ru(0.5) / CoFeB(50) (thickness in nm) multilayer was grown via DC (Ru, NiFe) and RF (CoFeB) magnetron sputtering in an AJA Orion 8 System, with a base pressure below  $1 \times 10^{-8}$  Torr. The layer thicknesses and growth conditions were optimized in order to obtain at remanence, i.e. at 0 external magnetic field, an antiparallel coupling of the magnetization of the NiFe and CoFeB layers. Following the deposition of the SAF layers, the unexposed resist was lifted off by immersion of the samples in pure acetone. On top of the structures, a Cu antenna was fabricated in order to excite spin waves within the structure.

Via tr-SoXL, we imaged in three-dimensions the precession of the magnetization vector associated with spin-wave propagation in the SAF, with nanoscale spatial resolution (Figure 1). By mapping the spin-wave amplitude in the film thickness, we imaged the spatial localization of the spin-wave, as expected for an uncompensated SAF structure. We found that this non-uniform spin-wave amplitude leads to intrinsically three-dimensional spin-wave interference figures, which we reveal experimentally and confirm with simulations.

### **Direct Laser Patterning of magnonic crystals in YIG.**

Scope of this activity was the demonstration of a new patterning approach, called “phase micro- and nano-engineering”, on magnetic materials for magnonics. We used the laser of the NanoFrazor Explore of Polifab for locally modifying the structural and magnetic properties of 1  $\mu\text{m}$  and 100 nm thick Yttrium Iron Garnet (YIG) crystals. We then performed magnetic force microscope (MFM, Figure 2), micro-Kerr and micro-Raman characterization (in collaboration with V. Russo and A. Li Bassi, POLIMI). We found that, by inducing small changes in the structural/chemical properties of YIG, it was possible to obtain a modulation of the magnetic anisotropy and saturation magnetization. We exploit this condition, to fabricate magnonic crystals based on patterned dot lattices. By micro-Brillouin Light Scattering measurements (in collaboration with Perugia University), we demonstrate that these crystals can modify the dispersion and localization of the spin waves<sup>[2]</sup>.

### **Tam-SPL for skyrmion crystals.**

We used the NanoFrazor Explore to demonstrate the Thermally assisted magnetic Scanning Probe Lithography<sup>[3]</sup> on Py/IrMn multilayers (in collaboration with O. Boulle, SPINTEC). Via tam-SPL we were able to pattern with nanoscale resolution domains, chiral domain walls and skyrmions, which we imaged via MFM (Figure 3). We are now using this approach to fabricate skyrmion crystals for magnonic applications.

<sup>[1]</sup> D. Girardi et al. (submitted).

<sup>[2]</sup> V. Levati, M. Vitali et al. (in preparation).

<sup>[3]</sup> E. Albisetti et al., *Nature Nanotechnology*, 11, 545-551 (2016).

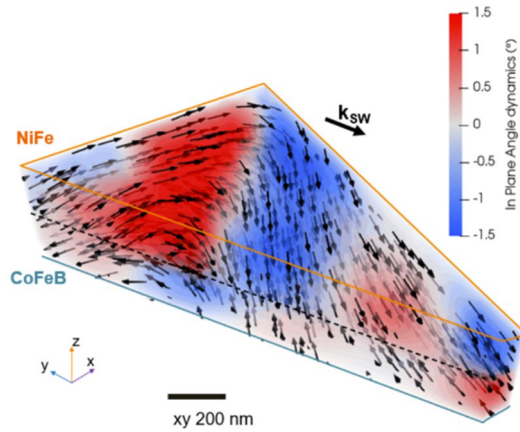


**Figure 1** Experimental 3D reconstruction of the spin waves propagating in the synthetic antiferromagnetic system. The black arrows represent the dynamic magnetization vector, while the color-code is the in plane component of the dynamic magnetization.

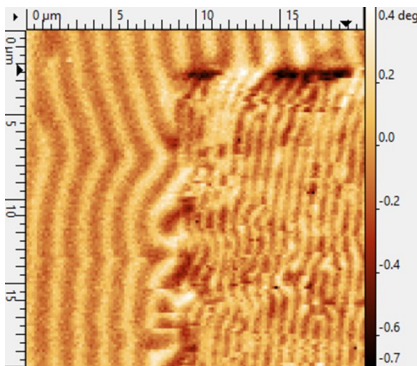


**Figure 2** Magnetic force microscope image of a square  $50 \times 50 \mu\text{m}^2$  patterned via direct laser writing on a  $1 \mu\text{m}$ -thick YIG crystal. Stripe domains are visible both inside and outside the pattern, with a sizable change (halving) of the dimension of the pitch of the domains.

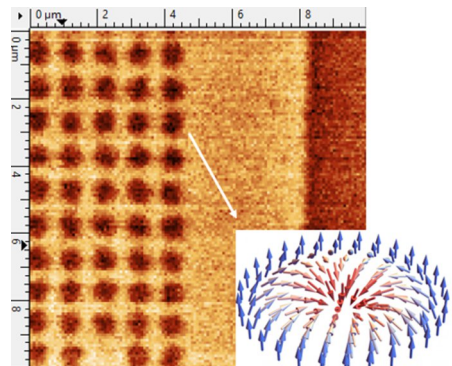


**Figure 3** Artificial skyrmion crystal patterned via thermally assisted magnetic scanning probe lithography on an out-of-plane magnetized magnetic multilayer.







## Publications citing Polifab

E. Bianchi et al. "Matrigel capillarity-driven filling in open microfluidics for high-throughput drug screening on 3D patient derived organoids cultures", MICROTAS 2021, 10-14 October, Palm Springs, USA.

C. De Vita et al. "Room-temperature deposition of ZnS antireflection coatings for MIR-LWIR applications," Opt. Mater. Express 12, 272-283 (2022).

M. Farronato et al. "Memtransistor Devices Based on MoS<sub>2</sub> Multilayers with Volatile Switching due to Ag Cation Migration", Adv. Electron. Mater., 8, 2101161 (2022).

M. Calvarese et al. "Strategies for improved temporal response of glass-based optical switches", Scientific Reports 12.1: 1-9 (2022).

G. Milano et al. "In materia reservoir computing with a fully memristive architecture based on self-organizing nanowire networks", Nat. Mater. 21, 195-202 (2022).

S. Pecorario et al. "Stable and Solution-Processable Cumulenic sp-Carbon Wires: A New Paradigm for Organic Electronics", Advanced Materials 34 (15), 2110468 (2022).

P. Cataldi et al. "An Electrically Conductive Oleogel Paste for Edible Electronics", Advanced Functional Materials, 2113417 (2022).

L. Sarcina et al. "A large-area organic transistor with 3D-printed sensing gate for noninvasive single-molecule detection of pancreatic mucinous cyst markers", Analytical and Bioanalytical Chemistry, 1-13 (2022).

V. Falcone et al. "Graphene/Ge microcrystal photodetectors with enhanced infrared responsivity", APL Photonics, vol. 7, no. 4, p. 046106 (2022).

C. De Vita et al. "Amorphous-silicon visible-light detector integrated on silicon nitride waveguides", Optics Letters 47(10): 2598-2601 (2022).

P. Borga et al, "Active Opto-Magnetic Biosensing with Silicon Microring Resonators", Sensors, 22(9):3292 (2022).

F. Hoch et al. "Reconfigurable continuously-coupled 3D photonic circuit for Boson Sampling experiments", *npj Quantum Information* 8.1: 1-7 (2022).

S. Ricci et al. "Forming-Free Resistive Switching Memory Crosspoint Arrays for In-Memory Machine Learning", *Adv. Intell. Syst.*, 4: 2200053 (2022).

M. Spagnolo et al. "Experimental photonic quantum memristor", *Nature Photonics* 16.4: 318-323 (2022).

R. Albiero et al. "Toward higher integration density in femtosecond-laser-written programmable photonic circuits", *Micromachines* 13.7: 1145 (2022).

J. Ahmadi-Farsani et al. "A CMOS-memristor hybrid system for implementing stochastic binary spike timing-dependent plasticity", *Philos. Trans. A Math. Phys. Eng. Sci.*;380(2228): 20210018 (2022).

M. Milanizadeh et al. "Separating arbitrary free-space beams with an integrated photonic processor", *Light. Sci. Appl.*, 11(1): 197 (2022).

C. Pentangelo et al. "Low-power programmable integrated photonic circuits fabricated by femtosecond laser micromachining", *Il Nuovo Cimento C* 45.6: 1-4 (2022).

M. Calvarese et al. "Integrated optical device for Structured Illumination Microscopy", *Optics Express* 30.17: 30246-30259 (2022).

M. Pont et al. "Quantifying n-photon indistinguishability with a cyclic integrated interferometer", *Physical Review X* 12.3: 031033 (2022).

S. Pecorario et al. "Effects of Molecular Encapsulation on the Photophysical and Charge Transport Properties of a Naphthalene Diimide Bithiophene Copolymer", *Chemistry of Materials* 34 (18), 8324-8335 (2022).

F. A. Viola et al. "A n-type, Stable Electrolyte Gated Organic Transistor Based on a Printed Polymer", *Advanced Electronic Materials*, 2200573.

M. Farronato et al. "Low-current, highly linear synaptic memory device based on MoS<sub>2</sub> transistors for online training and inference," 2022 IEEE 4th International Conference on Artificial Intelligence Circuits and Systems (AICAS), Incheon, Republic of Korea, pp. 1-4 (2022).

R. Visone et al. "Predicting human cardiac QT alterations and pro-arrhythmic effects of compounds with a 3D beating heart-on-chip platform", *Toxicological Sciences*, kfac108 (2022).

L. Lamanna, et al. "Monitoring of Drug Release via Intra Body Communication with an Edible Pill", *Advanced Materials Technologies*, 2200731 (2022).

M. Farronato et al. "Reservoir Computing with Charge-Trap Memory Based on a MoS<sub>2</sub> Channel for Neuromorphic Engineering", *Adv. Mater.*, 2205381 (2022).

M. Petrini et al. "Spectral Classification and Cloning of Photonic Integrated Filters for Volume Testing", *Journal of Lightwave Technology*, 41(2): 645-652 (2022).

A. Kumar et al. "Low-temperature solution-processed high-capacitance AlOx dielectrics for low-voltage carbon-based transistors", *Organic Electronics* 110, 106636 (2022).

M. Hassan et al. "Thin-Film Heterostructures Based on Co/Ni Synthetic Antiferromagnets on Polymer Tapes: Toward Sustainable Flexible Spintronics", *ACS Appl. Mater. Interfaces* 14, 51496 (2022).

M. Kazemian et al. "X-ray absorption spectromicroscopy gives access to Li<sub>1+x</sub>Al<sub>x</sub>Ge<sub>2-x</sub>(PO<sub>4</sub>)<sub>3</sub> (LAGP) local degradation at the anode-electrolyte interface", *Journal of Power Sources Advances*, 17-18, 100106 (2022).

G. Protopapa et al. "A new microfluidic platform for the highly reproducible preparation of non-viral gene delivery complexes", *Lab on a Chip* 23.1: 136-145 (2023).

B. J. Green et al. "PillarX: A Microfluidic Device to Profile Circulating Tumor Cell Clusters Based on Geometry, Deformability, and Epithelial State". *Small* 18.17: 2106097 (2022).

S. Ricci et al. "Decision Making by a Neuromorphic Network of Volatile Resistive Switching Memories", *IEEE ICECS 2022*.

F. Morichetti, A. Melloni, DOM de Aguiar, "Optical system comprising a reconfigurable device and optical system control method", US Patent App. 17/775,408.

R. Bertacco, A. I. Melloni, P. P. Sharma, N. Peserico, "Opto-magnetic sensor device and molecular recognition system", US Patent 11,313,793.

A. Melloni, D. Melati "Optical delay method and system", US Patent 10,890,717.

A. Melloni, M. Sampietro, S. Grillanda, F. Morichetti, M. Carminati, G. Ferrari, "Optical radiation detection system comprising an electric parameter measuring circuit", US Patent 9,722,124.

R. Bertacco, D. Petti, E. Albisetti, G. Ferrari, M. Giacometti, "Device and Method for the Quantification of Corpusculated and Non-Corpusculated Blood Components", in Europa (n. EP3655773 A1), negli Stati Uniti (n. US2021/0086182 A1), in Cina (n. 102017000082112) e India (n. IN202017005991).

R. Bertacco, G. B. Fiore, G. Ferrari, M. Giacometti, F. Milesi, L. Coppadoro, E. Giuliani, "Apparatus for the quantification of biological components dispersed in a fluid", PCT n. WO2020/148718.

M. Giacometti, M. Carminati, S. Chiodini, M. Sampietro, G. Ferrari, "Device and method for detecting nonelectrolyte particles in two flows of liquid solutions containing an electrolyte", PCT n. WO 2017/187252 A1.

G. Ferrari, G. Gervasoni, M. Carminati, F. Campoli, "Electric quantity measuring device comprising an analog-digital converter", US Patent 10,511,317.

F. Maspero, P. Pirro, R. Bertacco, "Integrated Magnonic Device", PCT Patent application code PCT/IB2022/060130.

J. Frigerio, G. Isella, A. Ballabio, A. De Iacovo, L. Colace, "Electromagnetic radiation spectrum detection system" WO WO2022024021A1.

J. Frigerio, G. Isella, A. Ballabio, A. De Iacovo, L. Colace, "Double photodiode electromagnetic radiation sensor device" WO WO2022024025A1.



PoliFAB - Politecnico di Milano  
via Giuseppe Colombo 81  
20133 Milano - Italy  
<https://www.polifab.polimi.it/>  
[infopolifab@polimi.it](mailto:infopolifab@polimi.it)